MAGNETIC FIELD RESISTIVITY OF SUPERCONDUCTING BISMUTH OXIDES

BY

THOMAS WALTER KRAUSE, M.Sc.

A Thesis

Submitted to the School of Graduate Studies

in Partial Fulfilment of the Requirements

for the Degree

Doctor of Philosophy

McMaster University

MAGNETIC FIELD RESISTIVITY OF SUPERCONDUCTING BISMUTH OXIDES

DOCTOR OF PHILOSOPHY (1992)
(Physics)

McMASTER UNIVERSITY
Hamilton, Ontario

TITLE: Magnetic Field Resistivity of Supercondcting Bismuth Oxides

AUTHOR: Thomas Walter Krause, B.Sc. (University of Calgary)

M.Sc. (McMaster University)

SUPERVISOR: Professor W. R. Datars

NUMBER OF PAGES: xiv, 117

ABSTRACT

The superconducting transition in the magnetic resistance of members of the family of bismuth based high temperature superconductors was investigated. Measurements were performed in magnetic fields up to 1.7 T. Small current densities ranging from 0.03 A/cm^2 to 3.0 A/cm^2 were applied. The resistivity of $Bi_2Sr_2CaCu_2O_x$ single crystals was analyzed in terms of the thermally activated flux flow expression, $\rho=\rho_o U/T \exp(-U/T)$ where T is the temperature. It was found that the activation energy was given by $U\propto(H\sin\theta)^{-\alpha}$ where $\alpha\approx 1/3$ and that the prefactor had the form, $\rho_o\propto H\sin\theta$, where H was the applied field and θ the angle of the field with respect to the CuO_2 planes. Results demonstrated that dissipation could be accounted for by the motion of two-dimensional vortices whose density is given by the field, $H\sin\theta$, projected on the CuO_2 planes.

Measurements of the resistivity and current dependent resistivity were performed with two Sn-doped and two Sb-doped polycrystalline $Bi_{1.7}Pb_{0.3}Sr_2Ca_2Cu_3O_y$ samples. Features in the temperature derivative of the resistivity curves were associated with the presence of a superconducting transition between superconducting grains, coupled by weak links with a distribution of critical currents and critical temperatures,

and the superconducting transition within grains. The transition between grains was more strongly suppressed in temperature with the application of a magnetic field in samples with weaker coupling between grains. The presence of a transition in a magnetic field due to weak links between grains was verified at 77 K by the observation of a current dependent resistivity in a magnetic field.

Measurements of a $Bi_2Sr_2CaCu_2O_x$ diffusion grown thick film ring were done. The transverse voltage, the voltage at the centre of a 120 μm thick branch with respect to the centre of a 76 μm thick branch, was measured. A higher critical temperature from the presence of more texturing in the 76 μm branch as determined by separate resistivity, x-ray and scanning electron microscopy measurements was consistent with the measurement of a crossover from a negative to positive transverse voltage as the temperature of the sample went through its superconducting transition.

ACKNOWLEDGEMENTS

I wish to thank my supervisor, Dr. W. R. Datars for his guidance throughout the course of this research and for his constructive criticisms which were a considerable aid in the completion of this thesis. I would like to thank Dr. Robert Nkum for frequent discussions and for supplying the Sn and Sb doped $Bi_{1.7}Pb_{0.3}Sr_2Ca_2Cu_3O_y$ samples. For discussions concerning flux motion in $Bi_2Sr_2CaCu_2O_y$ crystals I would like to thank Dr. An-Chang Shi. For teaching me how to prepare the $Bi_2Sr_2CaCu_2O_y$ crystals and the diffusion grown $Bi_2Sr_2CaCu_2O_y$ thick film I would like to thank Dr. Pash Ummat. For involving me in his project and getting me started on high temperature superconductors, I would like to thank Dr. Vladimir Gridin. I would also like to thank my wife, Karen, for her support and understanding throughout my studies and my daughter Megan for spending long and probably tedious hours in the lab while daddy did his research.

This research was supported by a grant from the Natural Sciences and Engineering Research Council of Canada.

TABLE OF CONTENTS

LIST OF ILLUSTRATIONS

LIST OF TABLES

CHAPTER I

INTRODUCTION

Superconductivity between 7 and 22 K was discovered in the Bi-Sr-Ca-Cu-O system in May 1987 by Michel *et al.* (1987). In January 1988 Maeda *et al.* (1988) and Chu *et al.* (1988) independently produced samples that were superconducting above liquid nitrogen by adding Ca to the Bi-Sr-Cu-O system. Three superconducting phases have been identified (Beyers and Shaw, 1989, p. 135). These are $Bi_2Sr_2CuO_{6+x}$ (Bi:2201), $Bi_2Sr_2CaCu_2O_{8+x}$ (Bi:2212) and $Bi_2Sr_2Ca_2Cu_3O_{10+x}$ (Bi:2223). The latter two have transition temperatures of about 85 K and 110 K, respectively. Their structures consist of perovskite-like units containing one, two or three CuO_2 planes, respectively, sandwiched between Bi-O layers as shown in figure 1.

From experimental values of H_{C2} Batlogg *et al.* (1988) and Mandal *et al.* (1990) have obtained the Ginzburg-Landau coherence lengths parallel, $\xi_{ab}(0)$, and perpendicular, $\xi_c(0)$, to the CuO_2 planes for $Bi_2Sr_2CaCu_2O_{8+x}$ with values of 30.1 Å and 5.7 Å for $\xi_{ab}(0)$ and $\xi_c(0)$, respectively. $\xi_C(0)$ is clearly smaller than the interplanar spacing of 30.7 Å (Tarascon *et al.* 1988) along the c axis for $Bi_2Sr_2CaCu_2O_y$. The critical field of $Bi_2Sr_2CaCu_2O_{8+x}$ along the c axis is 40 T (Kim *et al.*

Figure 1

Chemical structure of (a) Bi:2201, (b) Bi:2212 and (c) Bi:2223 consisting of Bi(○), Ca(⊙), Sr(⊜), Cu(●) and O(•) (Beyers and Shaw, 1989, p. 135).

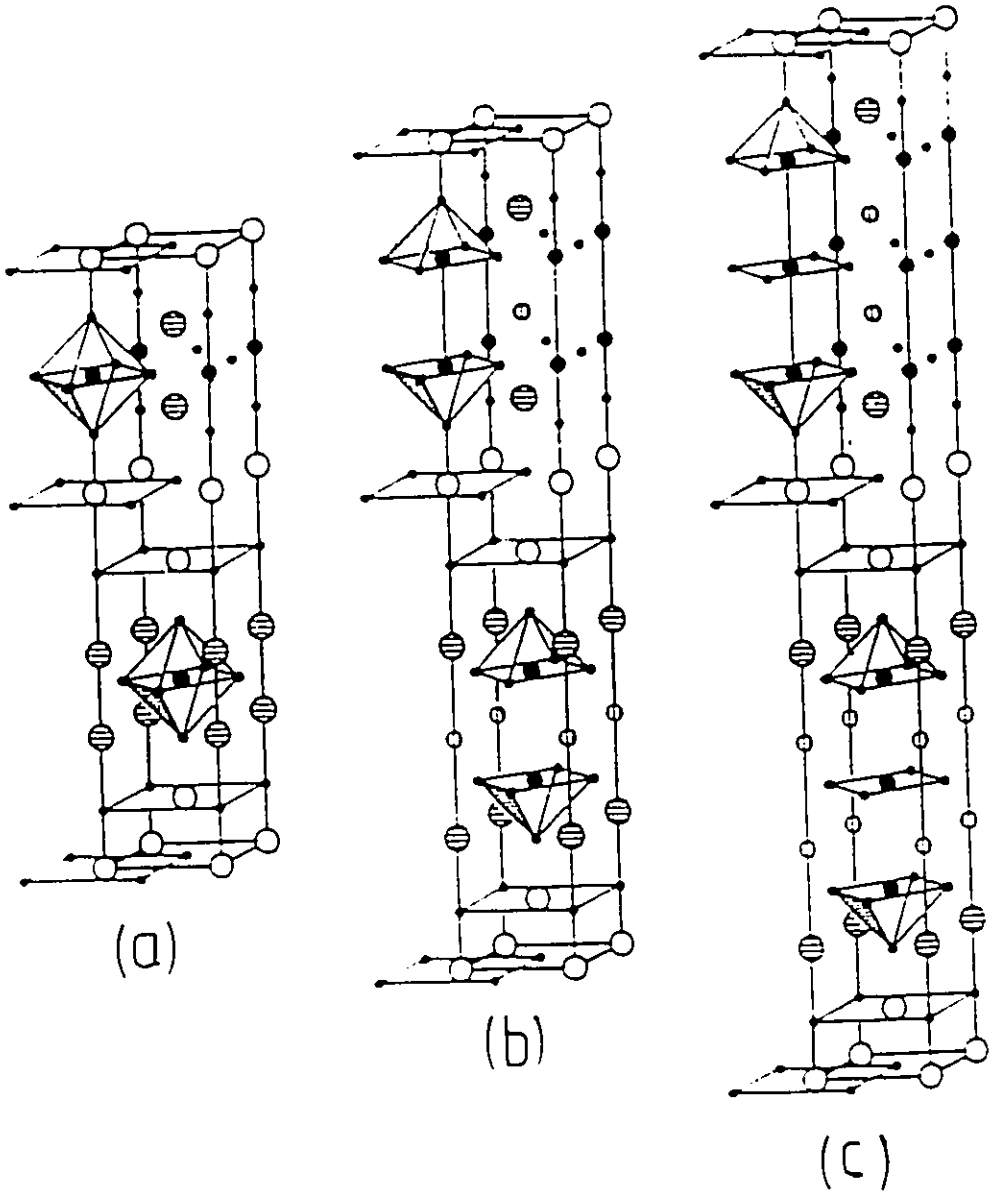

Figure 1

1991). The penetration depth in the CuO_2 planes of $Bi_2Sr_2CaCu_2O_y$, $\lambda_{ab}(0)$, is 2300 Å, demonstrating the extreme type II nature of this material (Kim *et al.*, 1991).

The broadening of the superconducting transition in the resistance of high temperature superconductors in a magnetic field is important from the perspective of material applications. In response to this, considerable work has been done with this property of the bismuth based superconductors (Palstra *et al.* 1988, 1989 and Kim *et al.* 1991). The resistive broadening of the superconducting transition is anisotropic in a magnetic field. This is indicated by a larger width of the transition with the magnetic field perpendicular to the CuO_2 planes than with it parallel to the planes (Palstra *et al.* 1988). Furthermore, angular dependence measurements of the resistivity indicate that for angles not too close to the ab plane the dissipation observed can be described by the field projected on to the CuO_2 planes (Kes *et al.* 1990). This supports a picture of 2-dimensional (2D) vortex "pancakes" as first proposed by Clem (1991) since the field perpendicular to the layers corresponds to the total density of 2D vortices per layer. As well, decoration experiments (Bolle *et al.* 1991) indicate that the average density of vortices in the CuO_2 layers is proportional to the field component perpendicular to the layers.

Several factors contribute to the resistive broadening observed in these materials. These are, i) the short Ginzburg-Landau coherence lengths, ii) the weak coupling between layers in these layered compounds which results in their large anisotropy, and iii) the high temperatures, compared to conventional superconductors, at which the superconductivity exists. That broadening of the resistive transition is associated with the weak coupling between layers in these materials, has been clearly demonstrated by Antognazza *et al.* (1991) for transport measurements on superconducting-insulating 24Å-$YBa2Cu_3O_7$/96Å-$PrBa_2Cu_3O_7$ superlattices.

Weak coupling between superconducting layers implies the presence of 2D vortices. Therefore, pinning occurs only in the CuO_2 planes (Kes, 1991) and the pinning is weaker than that for 3D vortex lines. These factors along with the high temperatures at which superconductivity occurs imply that thermal fluctuations play a much larger role in the high temperature superconductors than in the conventional superconductors. As well as verifying the short coherence lengths, measurements of the superconducting fluctuations above the critical temperature, T_c, verify the two dimensionality of the system (Mandal *et al.* 1990). Observations of a Kosterlitz-Thouless transition (Kosterlitz

and Thouless, 1973), the dissociation of vortex-antivortex pairs, immediately below T_C (Martin *et al.* 1989) also confirm the two dimensionality of the system. Farrell *et al.* (1989) performed torque measurements demonstrating the extreme anisotropy of Bi:2212 with values of the mass enhancement factor of $\Gamma \equiv m_c/m \approx 3000$ where m_c and m are the Ginzburg-Landau superconducting effective masses of charge carriers along the c axis and in the ab plane, respectively. Values an order of magnitude larger than this have been obtained by Okuda *et al.* (1991).

Coupling between vortices in adjacent CuO_2 layers becomes negligible for magnetic fields above a crossover field given by $B_{2D} \equiv \Phi_o/\Gamma d^2 \approx 0.3$ T for Bi:2212 (van der Beek and Kes, 1991). At this point the pinning and creep of the vortex lattice should be described by isolated films of thickness d, the spacing between double CuO_2 layers. The decoupling of the CuO_2 planes is supported by measurements made by Briceno *et al.* (1991) who applied magnetic fields parallel to the c axis and measured the resistivity parallel to the c axis. Considerable shifts of the superconducting transition imply a decoupling of the Josephson coupled planes.

Considerable broadening of the resistive transition in a magnetic field is observed in *polycrystalline* bismuth based high temperature superconductors as well. For samples where

the orientation of the grains is not random, texturing occurs and an angular dependence in the resistivity with respect to a fixed magnetic field is observed. Samples with randomly oriented grains demonstrate no angular dependence for a fixed magnetic field. Again it is the short coherence length that plays the decisive role with respect to resistive broadening in a magnetic field for polycrystalline high temperature superconductors. Because of the short Ginzburg-Landau coherence length the superconductivity between the grains is considerably suppressed (Deutscher, 1988). The system can therefore be modeled as a system of 3-dimensional Josephson weak links (Tinkham and Lobb, 1989, p.91). As demonstrated experimentally by Pureur *et al.* (1991) this system may be described in terms of a percolation system where different Josephson junctions have associated with them their own critical currents. On increasing the applied current some of the critical currents in these junctions are exceeded and a branch of the percolation path can no longer contribute nondissipatively. Just as the application of a magnetic field suppresses the superconducting order parameter between planes and decouples them, so too are grains in a polycrystalline material decoupled with the application of a magnetic field. In a magnetic field dissipation due to the motion of Josephson vortices also occurs (Jones et al. 1991 and Fehrenbacher *et al.* 1992). Dissipation and broadening of the resistive

transition in a magnetic field in polycrystalline materials may therefore be attributed to two sources: Dissipation at grain boundaries due to a suppressed order parameter and intrinsic dissipation as observed in single crystal studies.

In this thesis measurements are reported on two single Bi:2212 crystals with critical temperatures of 87 K and 84 K respectively, two Sb and two Sn doped $Bi_{1.7}Pb_{0.3}Sr_2Ca_2Cu_3O_{10+x}$ polycrystalline 110 K superconductors, and textured thick films of Bi:2212. Voltage versus current characteristics in the small current density regime were performed on all samples in fields up to 1.6 Tesla applied perpendicular to the transport current in the temperature range of their respective superconducting transitions.

For both Bi:2212 crystals measurements were made with the magnetic field oriented parallel to the crystallographic c axis. For the second of the two samples the angular dependence, from 5° to 90° with respect to the CuO_2 layers, of the resistivity in a constant field of 1.6 T was also measured.

The single crystal measurements were analyzed in terms of thermally activated flux flow (TAFF) (Dew-Hughes, 1988 and Brandt, 1991). Resulting values for the activation energy and resistivity prefactor indicated that only the magnetic field projected on to the CuO_2 planes causes broadening of the resistive transition. Therefore, dissipation in Bi:2212

crystals can be attributed to the thermally activated motion of 2D vortices. The magnetic field behaviour of the resistivity prefactor can be understood in terms of the simple Bardeen and Stephen (1965) model for the flux flow resistivity in a magnetic field.

The magnetic field dependence of the resistivity was obtained for two Sb doped and two Sn doped $Bi_{1.6}Pb_{0.4}Sr_2Ca_2Cu_3O_{10+x}$ polycrystalline samples. These results were interpreted in terms of dual superconducting transitions due first, to the intrinsic superconducting transition within the grains and secondly, to the superconducting transition between grains. A broad maximum, was visible for fields of 1 T or less in the $d\rho/dT$ as a function of temperature curves for three of the samples. This broad maximum was attributed to the superconducting transition between superconducting grains. Current dependence of the resistivity as a function of temperature in zero field and as a function of field up to 1.7 T at 77 K was also investigated in three of the samples.

A set of measurements was performed on a textured Bi:2212 thick film in the shape of a ring. The potentiometric voltage, the voltage of the centre of one branch of the ring with respect to the centre of the other branch, was measured as the sample went through its superconducting transition. The results are interpreted in terms of small differences in critical temperature and differences of the resistive

broadening in a magnetic field of the differentially textured branches. A magnetic field oriented parallel and perpendicular to the film's substrate demonstrated differential texturing between the two branches of the sample.

CHAPTER II

THEORY

A. INTRAGRAIN SUPERCONDUCTIVITY

Resistive dissipation in superconductors in an applied magnetic field below T_C is primarily associated with the motion of vortices. The dissipation of energy is due to i) eddy currents induced by a moving flux line that also flow through the normal conducting core and ii) from the relaxation of the superconducting order parameter along the path of the vortex core (Tinkham, 1988).

Bardeen and Stephen (1965) have obtained a simple result for the dissipation of moving flux lines in a magnetic field. This flux flow resistivity is given by the density of flux lines in the superconductor and may be expressed as:

$$\rho_{FF} = B\ \rho_n/H_{c2}(T), \qquad (1)$$

where B is the magnetic induction within the sample, $H_{c2}(T)$ is the upper critical field and ρ_n is the normal state resistivity. Gor'kov and Kopnin (1976) have considered this problem for various field, temperature and impurity ranges; however, the general form of the result remains the same.

The motion of vortices and, therefore, the presence of dissipation in the high temperature superconductors, is greatly enhanced over that in conventional superconductors by

several intrinsic factors. These include the presence of short coherence lengths, large penetration depths, considerable anisotropy, and thermal fluctuations due to high temperatures. These effects combine to lead to thermal energies comparable to the energies that pin flux lines.

Flux creep is an important dissipative mechanism because of the large thermal energies in the high temperature superconductors. Anderson's flux creep model (Anderson, 1962, and Anderson and Kim, 1964) assumes thermally activated jumps of pinned flux line bundles. In the presence of a transport current or flux gradient these flux lines are induced to hop preferentially in one direction. Since the available thermal energy k_BT in high temperature superconductors is an order of magnitude larger than in conventional superconductors, the Anderson flux creep theory must be extended to include reverse hopping in the low driving force limit (Dew-Hughes, 1988 and Kes *et al.* 1989). The hopping frequencies with and against the Lorentz force are denoted by ν_+ and ν_-, respectively. The total hopping frequency is given by their difference

$$\nu = \nu_+ - \nu_- = 2\nu_o \exp(-U/k_BT)\sinh(W/k_BT), \qquad (2)$$

where ν_o is the attempt frequency, k_B is the Boltzmann constant, T is the temperature and U(B,T) is the activation energy for a bundle to overcome its pinning barrier. W is the reduction of the barrier or the work done during one forward

jump. W is given by $W = JBV_c l$ where V_c is the correlated jump volume and l is the hopping distance. The resulting electrical field for flux jumps may be written in terms of phenomenological parameters; $J_C(B)$ the critical current density at T=0, $W=JU/J_C$, and $\rho_C(B,T)$ the resistivity at $J=J_C$,

$$E(J)=\rho J=vB=(\nu_+-\nu_-)lB$$
$$=2\rho_C J_C \exp(-U/k_BT)\sinh(JU/J_c k_B T). \qquad (3)$$

With an increasing Lorentz force the flux bundles move up in their pin potentials, until they eventually break away, entering the flux-flow regime. At small current densities $J<<J_o=J_C k_B T/U$ the above equation can be linearized (Brandt, 1991) and one obtains the ohmic regime of thermally activated flux flow as first described by Dew-Hughes. At larger currents, E(J) becomes nonlinear (flux creep regime) and goes over into the usual flux flow at $J>>J_c$. These three resistivity regimes can be summarized as

$$\rho \approx 2\rho_C U/k_B T \exp(-U/k_B T) \qquad J<<J_o \qquad (4)$$

$$\rho \propto \exp(J/J_o) \qquad J \approx J_C \qquad (5)$$

$$\rho \approx \rho_{FF}(1-J_c^2/J^2)^{1/2} \approx \rho_{FF} \qquad J>>J_C. \qquad (6)$$

Kes and van den Berg (1990) considered the attempt frequency of the form $\nu_o = \alpha_L/2\ \eta$, where η is the viscosity of the flux line lattice (FLL) and α_L is the Labusch parameter defined as $F_p=\alpha_L l$. Therefore, the attempt frequency may be

expressed as $\nu_o = AF_p/r_p\eta$, with a constant, A depending on the shape of the pin potential, and $\eta=B^2/\rho_{FF}$. The thermally activated flux flow expression becomes

$$\rho_{TAFF} \approx A\ f(b)\rho_n U/k_B T\ \exp(-U/k_B T), \qquad (7)$$

where f(b) is a function of magnetic field and can be adopted from theory (Bardeen and Stephen (1965) obtained f(b)=B), or from a fit to experimental data. The shape of the pin potential affects the factor A. For a sinusoidal potential $A=2\pi$ (Kes and van den Berg, 1990, p. 83).

Various forms for the temperature dependence of the activation energy have been suggested by many authors. Based on the dependence of the irreversibility line on temperature and magnetic field, Yeshurun and Malozemoff (1988) have suggested that $U=U_o(1-t)^{3/2}$, where t is the reduced temperature $t=T/T_c$, for magnetic fields of the order of $0.2H_{c2}$. Tinkham (1988) has argued that this form of U could be due to vortex lattice shear. Thuneberg (1989) has derived a form for the temperature dependent activation energy from anisotropic scattering pinning theory and obtains temperature dependencies that go as (1-t) or $(1-t)^2$. Geshekenbein *et al.* (1989) has derived a linear temperature dependence of the form (1-t) close to T_c, which is due to plastic deformations of the flux line lattice caused by thermally activated motion of dislocations over the Peierls barriers associated with the

periodic structure of the flux line lattice.

The magnetic field resisitivity extends as low as $T_c/2$ in a field of 1.6 T. Therefore, approximations for the temperature dependence of the activation energy must also extend to low temperatures. The temperature dependent activation energy we use here is given by Malozemoff *et al.* (1989) as

$$U=U_o(1-t^2)^{3/2}, \tag{8}$$

which is an extension to lower temperatures of the form first suggested by Yeshurun and Malozemoff (1988). Yeshurun and Malozemoff (1988) take the pinning energy of a flux line to scale as its condensation energy in an applied magnetic field. They start with the scaling form suggested by Anderson and Kim (1964), who consider the condensation energy in a volume ξ^3 given by $[H_c^2/8\pi]\xi^3$. When $H>H_{c1}$, the fluxons overlap as soon as $B>H_{c1}$, because their separation is less than the penetration depth, λ (Tinkham, 1988). The motion of the fluxons is now energetically correlated. Yeshurun and Malozemoff (1988) have argued that the smallest movable volume of flux is the cross-sectional area of the Abrikosov unit cell ϕ_o/B (ϕ_o is the flux quantum) multiplied by the coherence length, ξ. Therefore the activation energy can be written as

$$U=\beta H_c^2 \xi \phi_o/B\,, \tag{9}$$

where numerical factors have been absorbed in the factor β.

It has been determined empirically (Tinkham, 1975, p. 4) that the temperature dependence of the critical field is approximated by

$$H_c(T)=H_c(0)(1-t^2). \qquad (10)$$

This is also the temperature dependence assumed for $H_{c2}(T)$ as calculated by Kim *et al*. (1991). This can be taken to be the temperature dependence of H_{c2} since $H_{c2}=\sqrt{2}\kappa H_c$, where κ, the Ginzburg-Landau order parameter, varies only slowly with temperature (Tinkham, 1975, p. 129). H_{c2} can be written as $H_{c2}=\phi_o/(2\pi\,\xi^2(T))$ (Tinkham, 1975, p. 129). In this approximation the coherence length has a temperature dependence of the form

$$\xi(T)=\xi_o(1-t^2)^{-1/2}. \qquad (11)$$

Substitution of equations 10 and 11 into 9 produces the temperature dependence of equation 8 obtained by Malozemoff *et al*. (1989).

B. INTERGRAIN SUPERCONDUCTIVITY

The small coherence lengths and 2D layered structure, as well as leading to weak coupling between planes in a crystal, lead to weak links between grains in polycrystalline materials. Due to the short coherence lengths a suppression of the superconducting order parameter, Ψ, occurs at the grain boundaries in polycrystalline materials (Deutscher, 1988).

This leads to a suppression of the pair breaking J_c at the grain boundaries and allows for the relatively easy access of flux lines. A system in which many such grain boundaries are present can be modeled as a 3D array of Josephson weak links in a percolative matrix (Tinkham and Lobb, 1989, p. 91). Magnetic lines of flux enter relatively easily between the grains, the critical field for their entrance being of the order of a few gauss.

Tinkham and Lobb (1989, p. 91) view the superconducting transition that occurs in the polycrystalline materials as a dual transition. First, there is the intragranular transition, the superconducting transition that is within the grains and that occurs at a temperature T^0_c equivalent to that of a single crystal of the material. At a lower temperature, T_{cJ}, a second superconducting transition occurs. This is the intergrain transition. At this temperature long range superconducting order forms and phase coherence between the grains is established. This phase locking transition has been described by Pellam *et al.* (1972) and Deutscher *et al.* (1974). In the intragranular transition the modulus of the superconducting order parameter, $|\Psi|$, builds up a non-zero value within the grains. Due to the Josephson intergranular coupling, at a lower temperature T_c, the phases, θ_i, of the superconducting order parameter in the

grains $|\Psi_i|e^{i\theta_i}$, will lock and the system will become a superconductor.

Tinkham and Lobb (1989, p. 91) have considered a system of Josephson weak links, each characterized by the same critical current, I_c, and grain size, a. For such a system they have shown that a penetration depth and upper critical field for the junctions between the grains can be defined. In particular, the critical current density of the junction, J_{cJ}, is defined by the macroscopic intergranular critical current I_c as

$$J_{cJ}=I_c/a^2, \tag{12}$$

where a^2 is taken as the area of the junction. Tinkham and Lobb point out, however, that in real samples I_c, a, and the volume of the grains, V_g will have a range of values.

Imry (1980, p. 148) has discussed the complications that may exist in real experimental systems due to the presence of a range of I_c, a and V_g values that result in disorder. He points out that Josephson coupling is sensitive to the properties of weak intergrain contact. Any small nonuniformity may produce considerable variations in I_c as well as affect the phase locking transition.

The presence of nonuniformities with only short range correlations can lead to percolation effects in 3D systems (Imry, 1980, p. 148). This occurs when parts of the system

become ordered and span the whole system before other parts. The weak link system in granular high temperature superconductors has been modeled as such a percolation system (Pureur *et al.*, 1991). In this case the system is viewed as a lattice of Josephson junctions each of which possesses its own I_c within a range of possible values (i.e. from 0 to the maximum of the intragranular I_{cg}). A transport current choosing the path of least resistance, will minimize the number of junctions at which I_c is exceeded. Increasing the transport current increases the number of dissipative junctions as their respective I_c's are exceeded. Therefore, as Pureur *et al.* (1991) and Goldschmidt (1989) have shown, the superconducting transition temperature for coupling between the grains is suppressed.

The application of a magnetic field to a single Josephson junction results in a reduction of I_c. This can be seen from a consideration of I_c in a Josephson junction in a magnetic field given by Tinkham (1975, p.199) as

$$I_c = a^2 I_o \left| \frac{\sin(\phi/\phi_o)}{\pi \phi/\phi_o} \right| \qquad (13)$$

where ϕ is the flux enclosed in the junction and I_o is the maximum current through the junction. Tinkham and Lobb (1989, p. 91) state that allowing for randomness in the effective areas of the various junctions in a system of weak links, the macroscopic critical current becomes a nonoscillatory function

of the flux threading the system $\sim 1/\phi \sim 1/H$.

The formation of Josephson vortices in a magnetic field may also act to limit the critical currents within weak links. Josephson vortices are defined as having only one length scale, the penetration depth, λ_J and no normal core with the results that the modulus of the superconducting order parameter, $|\Psi|$, vanishes inside the entire junction (Fehrenbacher *et al.* 1992). A Josephson vortex has as its basic property the rapid change of the phase of the order parameter by 2π. Likharev (1979) points out that similar field dependencies for the penetration of flux into the weak link granular system and flux penetration as in the Bean model leads to pinning effects that are analogous to those of random inhomogeneities in a continuous superconducting medium. Although, Fehrenbacher *et al.* (1992) state that the pinning of Josephson vortices can be assumed to be much weaker than the pinning of Abrikosov vortices.

An intrinsic component in the intergranular transition of the anisotropic high temperature superconductors with and without a magnetic field can also be considered. Along with Josephson junctions formed due to the short coherence length, Ekin (1987) provides a further insight into the effects that intrinsic parameters have on coupling between grains. To form a good link between superconducting grains CuO_2 planes in

adjacent samples must be aligned. If perfect alignment does not occur a c axis component is introduced for the motion of a transport current from one grain to the next. Due to Josephson coupling between planes, the coupling between grains is weakened. Furthermore, with the application of a magnetic field parallel to the c axis of the grain the superconducting layers are even further decoupled resulting in a suppressed superconducting transition within the grains for currents along the c axis as Briceno *et al.* (1991) have demonstrated. This leads to a suppression of the superconducting coupling between grains.

To summarize, both *extrinsic* and *intrinsic* effects may combine in real experimental systems in polycrystalline high temperature superconductors to produce a dual superconducting transition. The behaviour of this dual superconducting transition is complicated by disorder or nonuniformity within the weak link structure resulting in percolation effects. The application of a magnetic field to the weak link structure results in effects on the critical currents in the weak links that are also strongly influenced by the presence of disorder or nonuniformity in the weak link characteristics.

C. POTENTIOMETRIC RING

Textured thick films are films where one of the crystallographic axes of the grains that make up the film is preferentially oriented with respect to the film surface. They provide a unique opportunity to study current configurations that have some of the anisotropic characteristics lost in polycrystalline samples. In this thesis we report on a potentiometric ring experiment on a textured Bi:2212 thick film.

In the potentiometric ring experiment, as first demonstrated by Gridin and Datars (1991), a minimum in the transverse voltage is measured just below the mean field transition temperature in zero magnetic field. This minimum was attributed to the difference in the current densities between the two superconducting paths in the ring. Gridin and Datars (1991), however, used a polycrystalline, granular sample, with nearly isotropic resistivity in both halves of the ring. Their description of the transverse voltage behaviour was based on the linear response formula:

$$V_T = \rho(T)[l_{AB}(J_u - J_l) + \Delta l_{AB} J_u], \qquad (14)$$

where V_T is the voltage between contacts 5 and 6 in figure 2, $\rho(T)$ is the temperature dependent resistivity, J_u is the current density in the upper branch and J_l is the current density in the lower branch. Referring to figure 2, L_{AB}

Figure 2

Thick film ring showing numbered 1-2 current contacts, 3-4 longitudinal voltage contacts and 5-6 transverse voltage contacts.

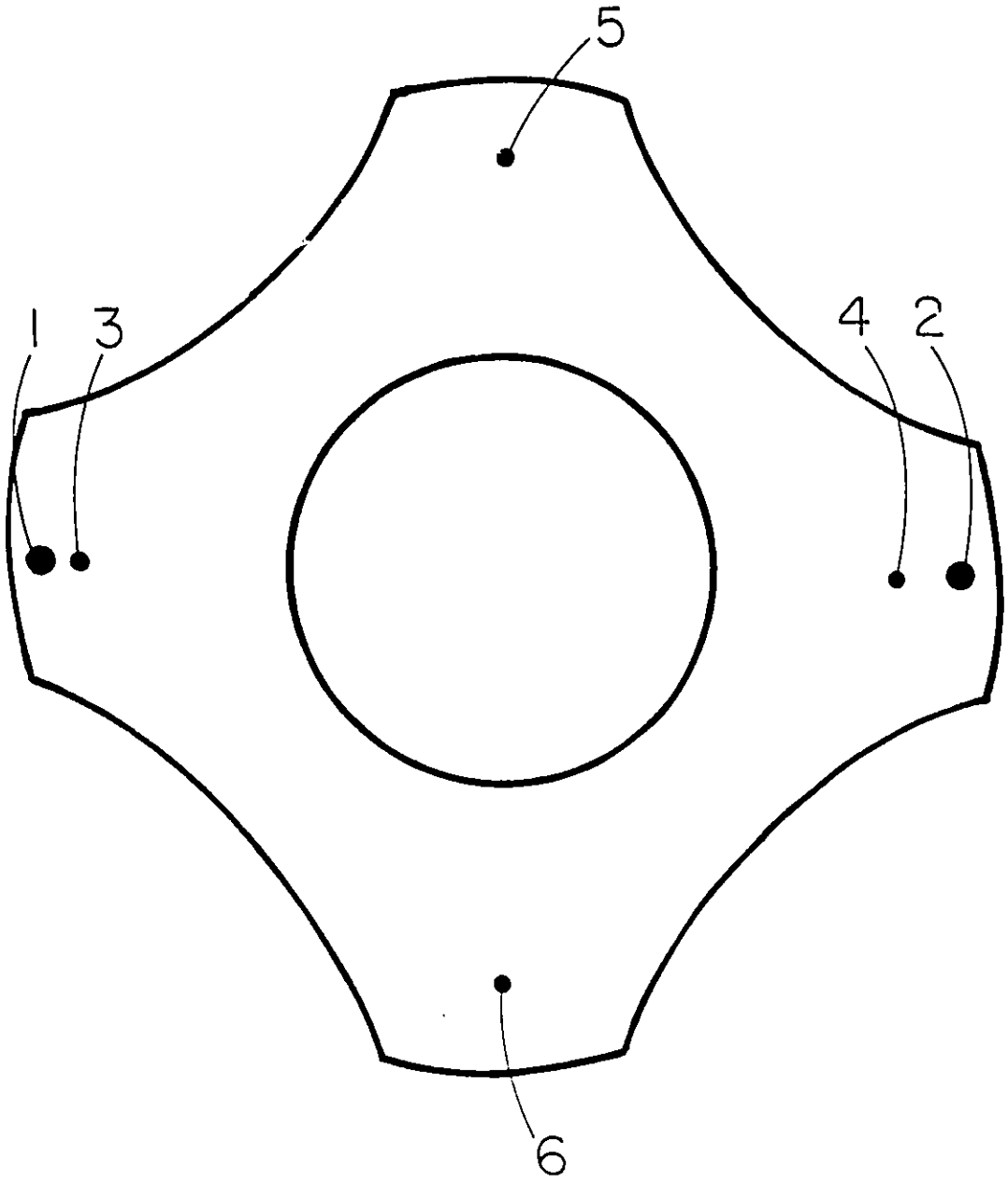

Figure 2

is the distance between the 3-6 contact pair. ΔL_{AB} is the difference between the distances between the 3-5 and the 3-6 contact pairs.

The potentiometric ring equation can be further generalized if the resistivities of the two branches are assumed not to be the same, i.e. each one has its own temperature dependence, particularly in the critical region close to T_c. From Kirchhoff's rules an expression for the current in the lower branch, the current flowing from contact 1 to 2 via contact 6, can be written as

$$I_L(T) = \frac{R_U(T) \times I}{R_L(T)+R_U(T)} , \qquad (15)$$

where $R_U(T)$ and $R_L(T)$ are the temperature dependent resistances of the upper and lower branches, respectively, and I is the applied transport current. In particular, if the lower branch is superconducting while the upper branch is going through its transition and therefore experiencing dissipation, all the current will flow through the lower branch. When there is dissipation in both branches the applied current will be divided as described by equation 15.

To relate the transverse voltage, $V_T(T)$, as measured between contacts 5 and 6 in figure 2, to the resistances in the upper and lower branch $V_T(T)$ can be written as

$$V_T(T) = \Re(T)\,(R_{IL}(T)+R_{IU}(T))\,I , \qquad (16)$$

where $R_{IU}(T)$ is the resistance between contact pairs 3 and 5, $R_{IL}(T)$ is the resistance between contact pairs 3 and 6, and $\Re(T)$ is defined as

$$\Re(T) = \frac{R_U(T)}{R_L(T)+R_U(T)} - \frac{R_{IU}(T)}{R_{IL}(T)+R_{IU}(T)} . \qquad (17)$$

The measurement of $V_T(T)$ gives an indication of how the difference in the ratios of the various resistances as defined by equation 17 varies with temperature.

CHAPTER III

SAMPLE PREPARATION

Single crystals of the Bi-Sr-Ca-Cu-O system were prepared with a sealed cavity technique developed by Guo *et al.* (1990). A mixture of Bi_2O_3, $CaCO_3$, $SrCO_3$ and CuO powders in the cation ratio of 1:1:1:2 were mixed and ground together in acetone in an agate mortar. The powder was calcined in air at 850°C for 16 hours in a silver boat placed in the center of a Lindberg oven. The material was then reground and pressed into pellets. These pellets were sintered in air at 860°C for 20 hours. $SrCaCu_4O_6$ pellets were also prepared to be used as a sealant and flux. $SrCO_3$, $CaCO_3$ and CuO were mixed in the cation ratio of 1:1:4 and ground together. The powder was calcined in air at 900°C for 12 hours in an alumina crucible. It was reground, pelletized and annealed at 950°C for 24 hours.

The Bi-Sr-Ca-Cu-O pellets were placed in an alumina crucible and broken pellets of $SrCaCu_4O_6$ were placed on top. The loaded crucible was rapidly heated to 1020°C, soaked at this temperature for 12 hours, cooled to 928°C at a rate of 60°C/hour, at 928 °C held for 5 hours, cooled at a rate of 0.6°C/hour to 800°C and finally cooled at a rate of 6°C/hour to room temperature. Crystals were mechanically removed from the

crucible. The largest and highest quality samples were chosen from the extracted crystals.

$Bi_2Sr_2CaCu_2O_y$ crystals have shiny mica like layers that are easily separated. Although fragile and easily deformed they are relatively stable in air and maintain their properties over a large period of time.

Samples of the Sn and Sb doped Bi-Pb-Sr-Ca-Cu-O were prepared by Robert Nkum. 99.999% pure powders of Bi_2O_3, PbO, Sb_2O_3 or SnO_2, $SrCO_3$, $CaCO_3$, and CuO were mixed in the cation ratio [Bi],[Pb],[Sb] or [Sn], [Ca],[Cu]=1.7:0.3:0.1:2:2:3.6 in acetone in an agate mortar. The nominal stoichiometry with $Cu_{3.6}$ instead of the ideal Cu_3 composition was used to stabilize the 110 K phase as demonstrated by Huang *et al.* (1990). The mixtures were calcined at a temperature of 820°C for 5 hours and furnace cooled. The material was then reground and pelletized at a pressure of 4 tons/cm^2. The pellets were then sintered at a temperature of 850°C for 72 hours, cooled at a rate of 6°C/hour to 750°C, at 12°C/hour to 600°C, at 30°C/hour to 400°C, and finally furnace cooled to room temperature.

The preparation of the $Bi_2Sr_2CaCu_2O_y$ diffused thick film was similar to that followed by Tachikawa *et al.* (1990). A $Sr_2CaCu_2O_5$ pellet was prepared by first calcining the correct stoichiometry of mixed and ground $SrCO_3$, $CaCO_3$ and CuO at 925°C for 5 h. This powder was reground and heat treated at

1025°C for 16 h. It was pressed into a circular pellet with a diameter of 12 mm and a thickness that varied from 1.63 mm at its thickest to 1.59 mm at its thinnest. This pellet formed the substrate for the diffusion grown thick film.

A dark green coloured mixture of $Bi_2CaCu_2O_5$ was produced by mixing and grinding Bi_2O_3, $CaCO_3$ and CuO in the correct stoichiometric ratios. The mixture was heated at 700°C for 6 h, reground and heat treated at 720°C for 12 h. Absolute alcohol was used to make a slurry of the $Bi_2CaCu_2O_5$. This slurry was coated on the $Sr_2CaCu_2O_5$ substrate.

The application of the slurry coating to the substrate was accomplished by the use of a screw piston arrangement which also controlled the thickness of the applied coating. The screw-piston arrangement consisted of a piece of cylindrical brass, machined to hold the pellet precisely and fitted with a threaded brass piston. The bottom of the piston was threaded into the brass cylinder and the top of the piston supported the pellet. Adjustment of the screw thread of the piston resulted in an adjustment of the top of the pellet with respect to the top of the cylinder. The position of the pellet was adjusted below the top of the brass cylinder to the desired thickness. A coat of the $Bi_2CaCu_2O_5$ and alcohol slurry was applied to the pellet. The coating was made level with the top of the brass cylinder by removing the excess with a

flat blade. This resulted in a $Bi_2CaCu_2O_5$ coating with a thickness of 120 μm on one side of the pellet to 76 μm on the other. Ummat *et al.* (1991) showed that measurements of the layer thickness using this technique agreed with measurements performed with a scanning electron microscope after the diffusion process was completed.

The $Bi_2CaCu_2O_5$ coating on the $Sr_2CaCu_2O_5$ substrate was treated first at 750°C for 12 h. The diffusion treatment was carried out at 850°C for 72 h followed by cooling at 12°C/h to 400°C. The sample was then furnace cooled to room temperature.

CHAPTER IV

EXPERIMENTAL TECHNIQUE

Measurements of the current voltage characteristics were made by using a standard four probe technique. Contacts were placed in a line on one surface of the sample. In the case that silver paste contacts were used the sample with contacts was annealed in an oven at 400 °C for less than one hour. In one case, gold contacts were evaporated on a Bi:2212 crystal. This was performed with the assistance of Rob Hughes. The sample was then mounted on a MgO_2 or sapphire substrate and placed on an electrically insulated brass heat sink on the end of a probe. Copper wires were attached to the contacts with silver paste. The sample was then sealed inside a stainless steel canister. The probe with a sample was placed inside a cryostat. The canister was evacuated of its original atmosphere and a helium atmosphere was introduced into the canister for heat exchange.

The sample was cooled through its superconducting transition with liquid nitrogen in which the cannister was immersed inside the cryostat. In order to cool to lower temperatures the the vapour pressure of the liquid nitrogen was lowered by pumping with a large mechanical pump for periods of up to 1 hour. Both calibrated carbon glass and

platinum thermometers indicated that the sample cooled to temperatures as low as 43 K. The sample was then allowed to warm very slowly through its superconducting transition while the current voltage characteristics were measured. Measurements of the effect of the magnetic field on thermometry in a liquid nitrogen bath indicated a negligible influence of the magnetic field on the carbon glass thermometer and about a 0.3 K suppression of the temperature reading for the platinum thermometer in fields greater than 0.05 T.

The system for measuring voltage for an applied current at a specific temperature is shown in figure 3. A Keithley 182 Sensitive Digital Voltmeter with a base noise level of 20 nV was used to measure the voltage drop across the sample. The output from this voltmeter was directly interfaced through an IEEE488 card to the computer. The current through the sample was computer controlled through a Keithley 224 programmable current source. A Keithley 199 System DMM/Scanner was used to scan and measure the voltage drop across two thermometers and a standard resistance through which the current for the thermometers flowed. Current for the thermometers was provided by a battery operated current source held at a fixed 0.2 mA. The current direction through the thermometers was changed by using an HP 59306A Relay Actuator.

The voltage drop across the sample was measured as a

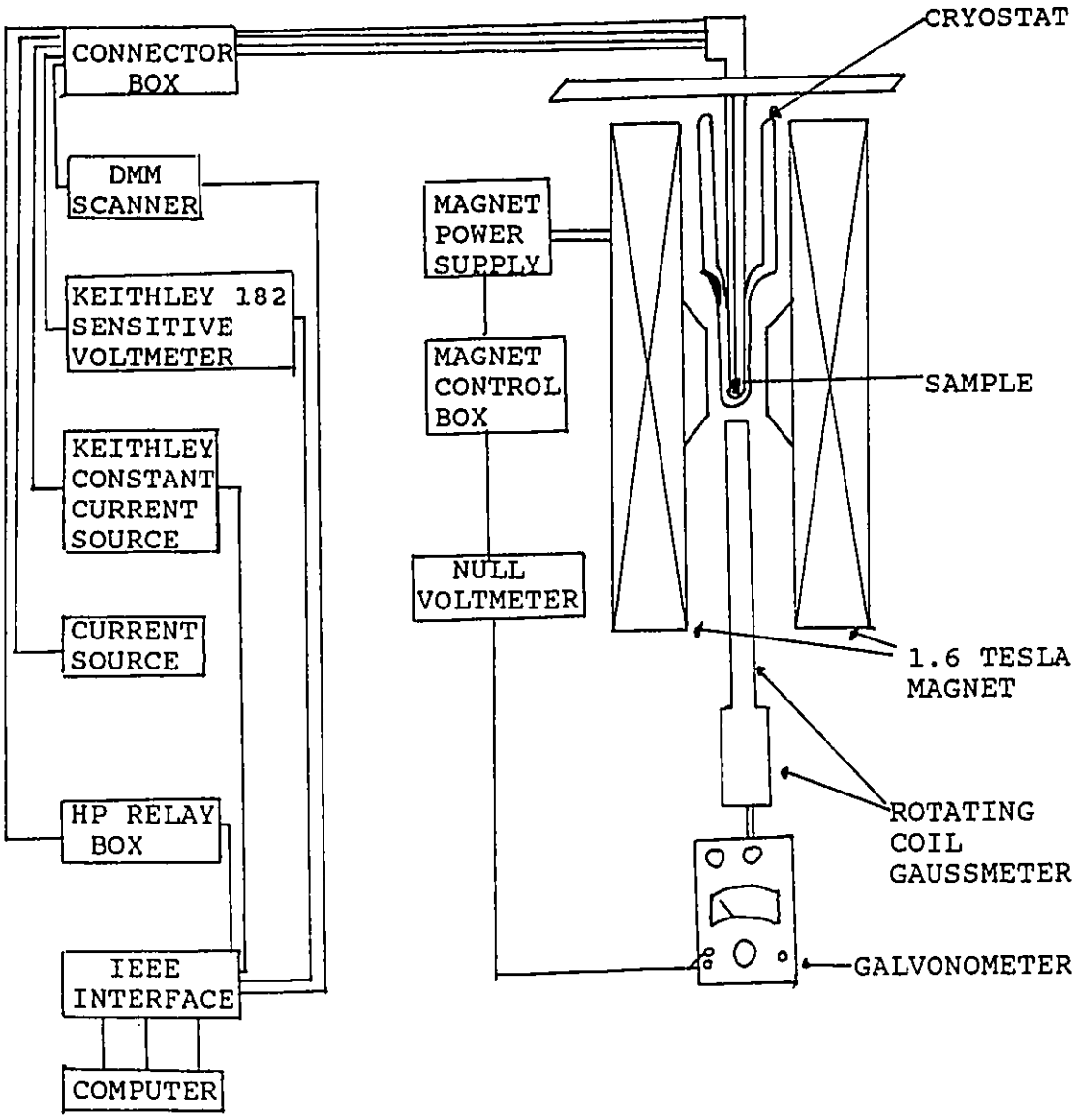

Figure 3

Experimental set up for measurement of voltage as a function of applied current and temperature in a fixed magnetic field.

function of current over a 32 second interval with the current direction changed after each sweep. One second intervals between current changes were allowed for currents within the sample to stabilize. 11 positive currents and their negative counterparts were applied and their corresponding voltages were measured. The average voltage of each positive and negative current pair was recorded. The temperature was taken as the average temperature of the temperatures measured before and after each I-V curve. For each I-V curve, temperature was measured to within 0.06 K.

Magnetic fields up to 1.7 T were applied using an electromagnet. The field was transverse and applied between two iron cores. The electromagnet could be rotated a full 360° in the transverse plane. A rotating coil gaussmeter was used to measure the magnitude of the field. A feed back system from the gaussmeter to a null voltmeter and the power supply was used to maintain a constant magnetic field for the required period of time.

For measurements of the I-V curves in a magnetic field, the sample was always cooled through its superconducting transition in the field before measurements were taken as the sample warmed through its superconducting transition. For all samples, the magnetic field was applied perpendicular to the macroscopic transport current.

CHAPTER V

TWO-DIMENSIONAL VORTICES

A. METHOD

Two samples were chosen for transport measurements from the set of prepared crystals. The first sample, here after designated as sample #1, was a single crystal with dimensions 2.15 x 0.94 x 0.12 mm^3 with the smallest dimension along the c axis. The second sample, sample #2, had dimensions of 2.71 x 0.82 x 0.23 mm^3 with the smallest dimension along the c axis. Laue diffraction was used to verify that they were single crystals. For each sample contacts were placed in a line along the length of the sample. Evaporated gold contacts with a contact resistance of $\approx 3\Omega$ per contact were used for sample #1. The voltage contacts were 0.81 mm apart. For sample #2 annealed silver paste contacts were used with a contact resistance of approximately 1Ω per contact. The voltage contacts were 1.38 mm apart.

Eleven current densities in the range of 0.04 A/cm^2 to 1.4 A/cm^2 for sample #1 and in the range of 0.05 A/cm^2 to 2.7 A/cm^2 for sample #2 were applied. Corresponding voltages for positive and negative current directions for a given temperature were measured. Magnetic fields up to 1.6 T were applied perpendicular to the ab plane (the CuO_2 layers) of

sample #1. For sample #2, magnetic fields up to 1.6 T were applied and the angular dependence with the magnetic field from 5° to 90° with respect to the ab plane was taken for the fixed field of 1.6 T.

B. RESULTS

The voltage changed linearly for the range of applied current densities. This is shown in figure 4 for sample #1 in a field of 0.8 T for temperatures between 49.4 K and 59.0 K. The resistivity was determined from the slope of the linear I-V curve. The resistivity is plotted as a function of temperature for zero field and for 1.55 T oriented perpendicular to the CuO_2 layers for sample #1 in figure 5. The broadening of the resistive transition in Bi:2212 with the application of a magnetic field is clearly demonstrated. The temperature of the onset of zero resistivity has been extended to lower temperatures by 40 K in a 1.55 T field.

The value of the transition temperature T_c was taken at the peak of the $d\rho/dT$ curve for H=0 (For sample #1, T_c=86.8 K and for sample #2, T_c=84.0 K). Estimates of the width of the superconducting transition were obtained from the width of the $d\rho/dT$ peak at half maximum (For sample #1, ΔT_c=3.8 K and for sample #2, ΔT_c=2.7 K). Plots of $d\rho/dT$ versus temperature for sample #1 for zero field and for 1.55 T oriented perpendicular

Figure 4

Voltage as a function of applied current density for sample #1 in a 0.8 T field perpendicular to the CuO_2 planes at the temperatures 49.4(o), 52.0(■), 53.8(+), 54.7(△), 56.1(●), 57.0(x), 57.9(□), and 59.0(★) K. Solid lines are linear best fits to the data.

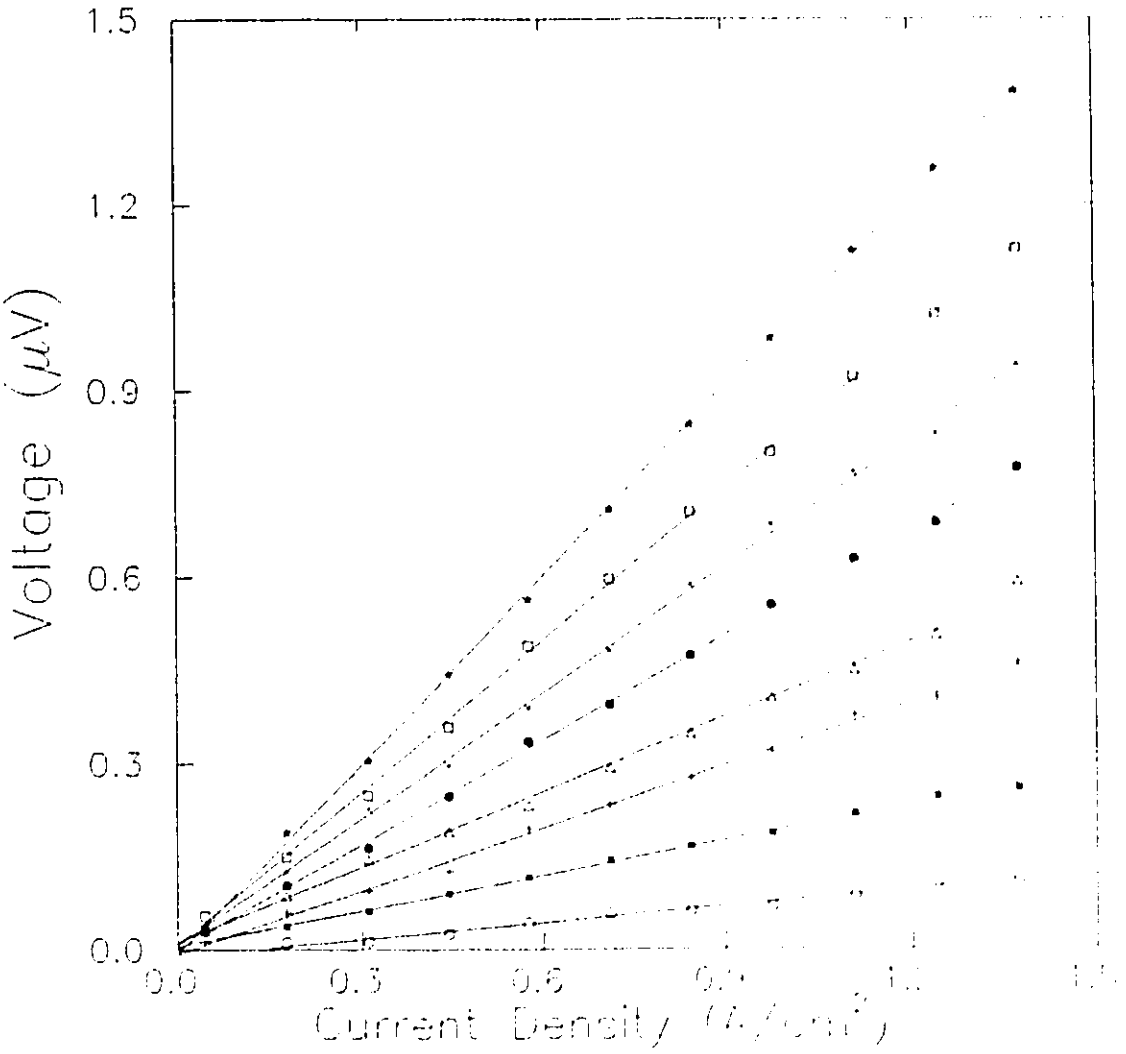

Figure 4

Figure 5

ρ as a function of temperature for sample #1 in zero field (_____) and in a 1.55 T (o) field perpendicular to the CuO_2 planes.

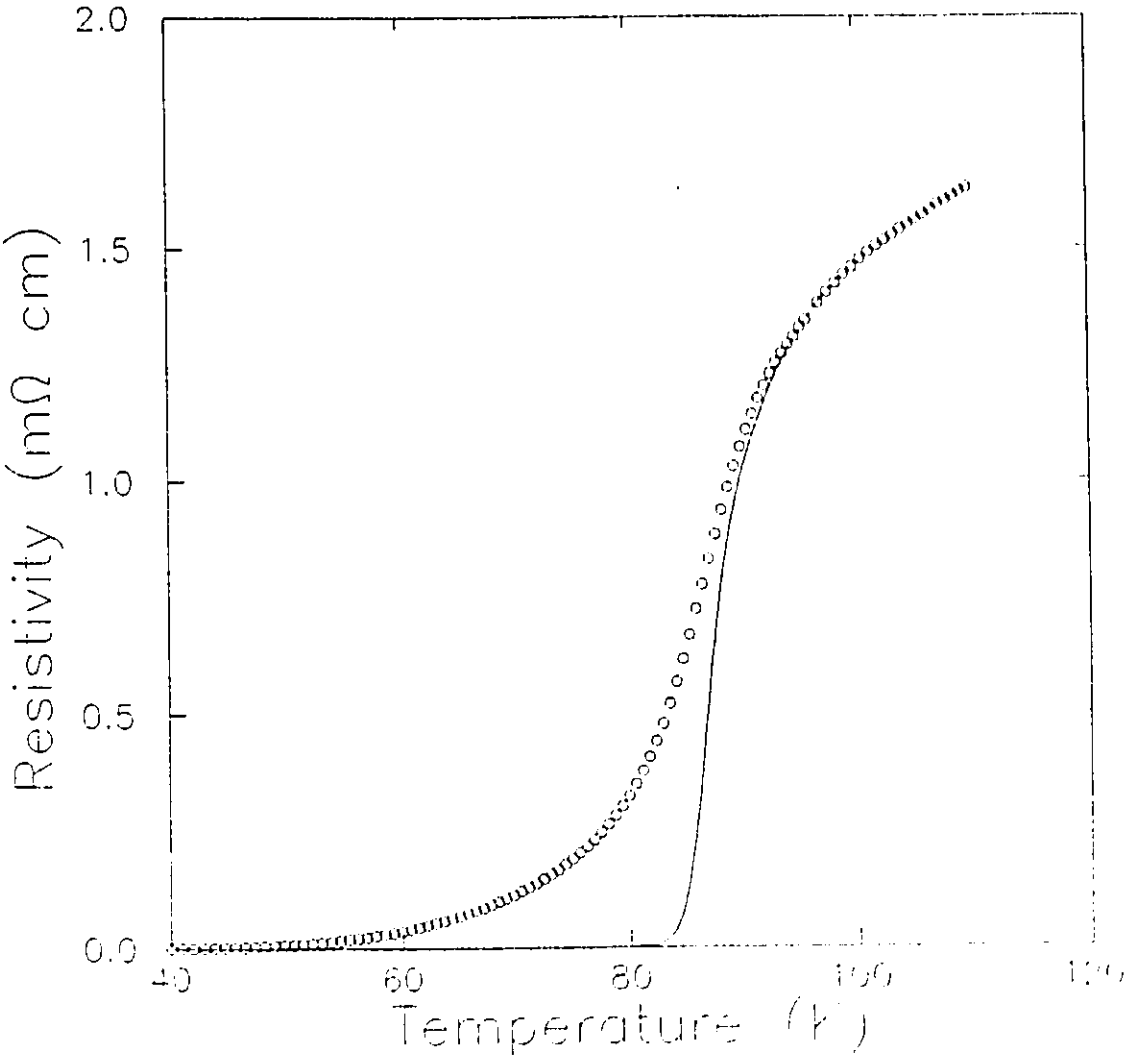

Figure 5

to the CuO_2 planes are shown in figure 6. A broadening of the resistive transition in a magnetic field can be seen in the $d\rho/dT$ plot. The height of the peak for 1.55 T is reduced to half that of the zero field peak. The shift of the peak in the $d\rho/dT$ curve with field is negligible.

For a fixed field, the temperature dependence of the resistivity was fit with the expression

$$\rho = \rho_o[U_o(1-t^2)^{1/2}/T]\exp[-U_o(1-t^2)^{3/2}/T], \qquad (18)$$

where t is the reduced temperature, $t=T/T_c$. This equation is the expression for the small current density regime as expressed by equation 7 with the Boltzmann factor absorbed by the activation energy, U. The activation energy is given by equation 8. ρ_o is temperature independent and is given in terms of the Bardeen Stephen (1965) flux flow resistivity by

$$\rho_o = 2\pi\rho_{FF}(1-t^2) = 2\pi\ B\ \rho_n/H_{c2}(0), \qquad (19)$$

where ρ_n is the normal state resistivity. Equation 18 has two independent fitting parameters, U_o and $C=\rho_o U_o$. A best fit was performed for the temperature region up to temperatures satisfying the condition $\rho=\rho_{FF}$ where ρ is given by equation 18 or temperatures that are a solution of

$$2\pi\ U_o(1-t^2)^{3/2}/T = \exp[(U_o(1-t^2)^{3/2}/T]. \qquad (20)$$

$Ln\rho$ is plotted versus 1/T for different fields for sample #1 in figure 7, and for different orientations in a magnetic field of 1.6 T for sample #2 in figure 8.

Figure 6

$d\rho/dT$ as a function of temperature for sample #1 in zero field (_____) and in a 1.55 T (o) field perpendicular to the CuO_2 planes.

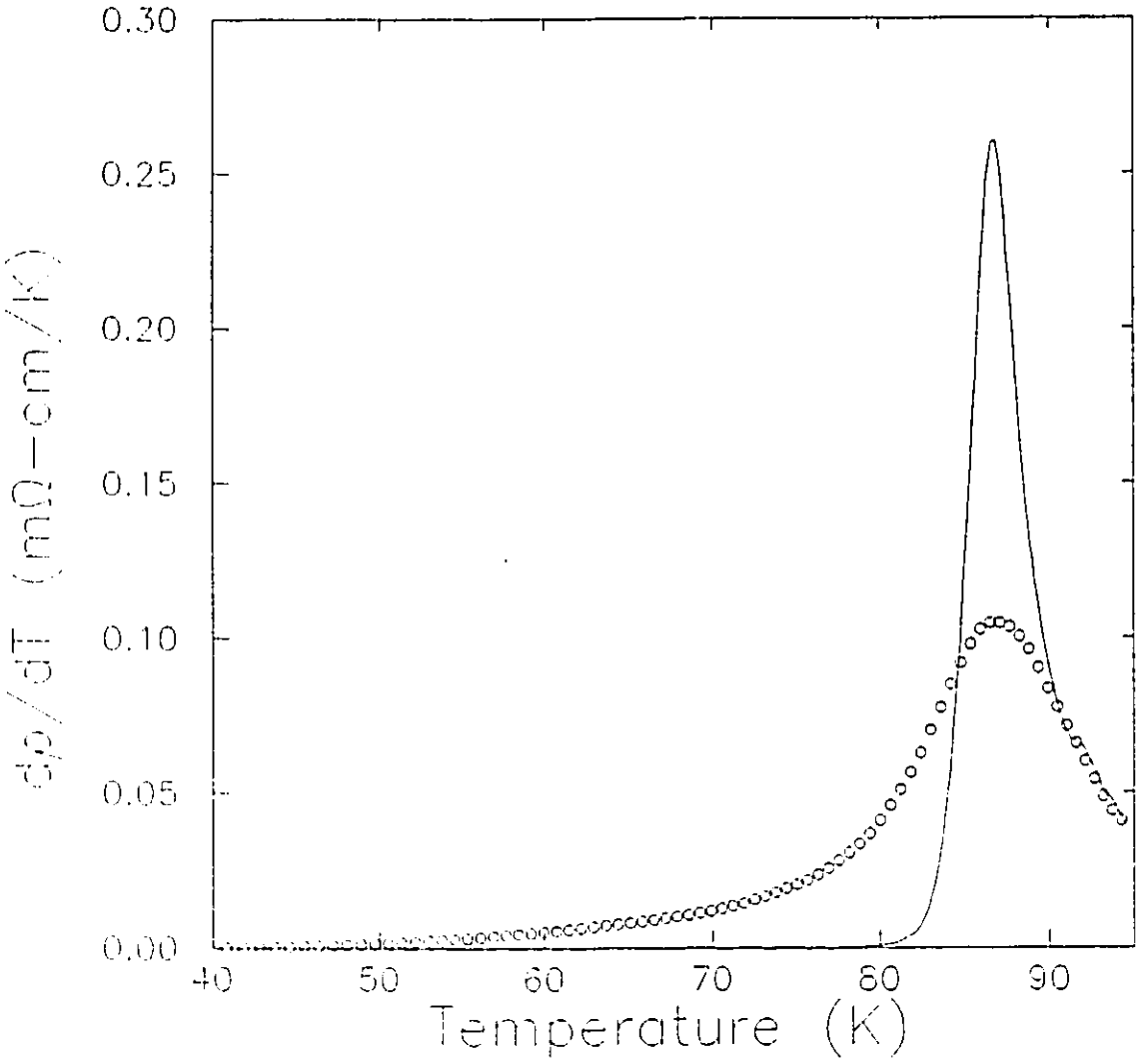
0.30
0.25
0.20
0.15
0.10
0.05
0.00
dρ/dT (mΩ−cm/K)
40
50
60
70
80
90
Temperature (K)

Figure 6

Figure 7

$\ln\rho$ versus 1/T for sample #1 for different magnetic fields perpendicular to the CuO_2 planes [H=0.2(o), 0.65(+) and 1.55(Δ) T]. The critical temperature, T_c, is indicated by the arrow. Solid curves are best fit to the low temperature portion.

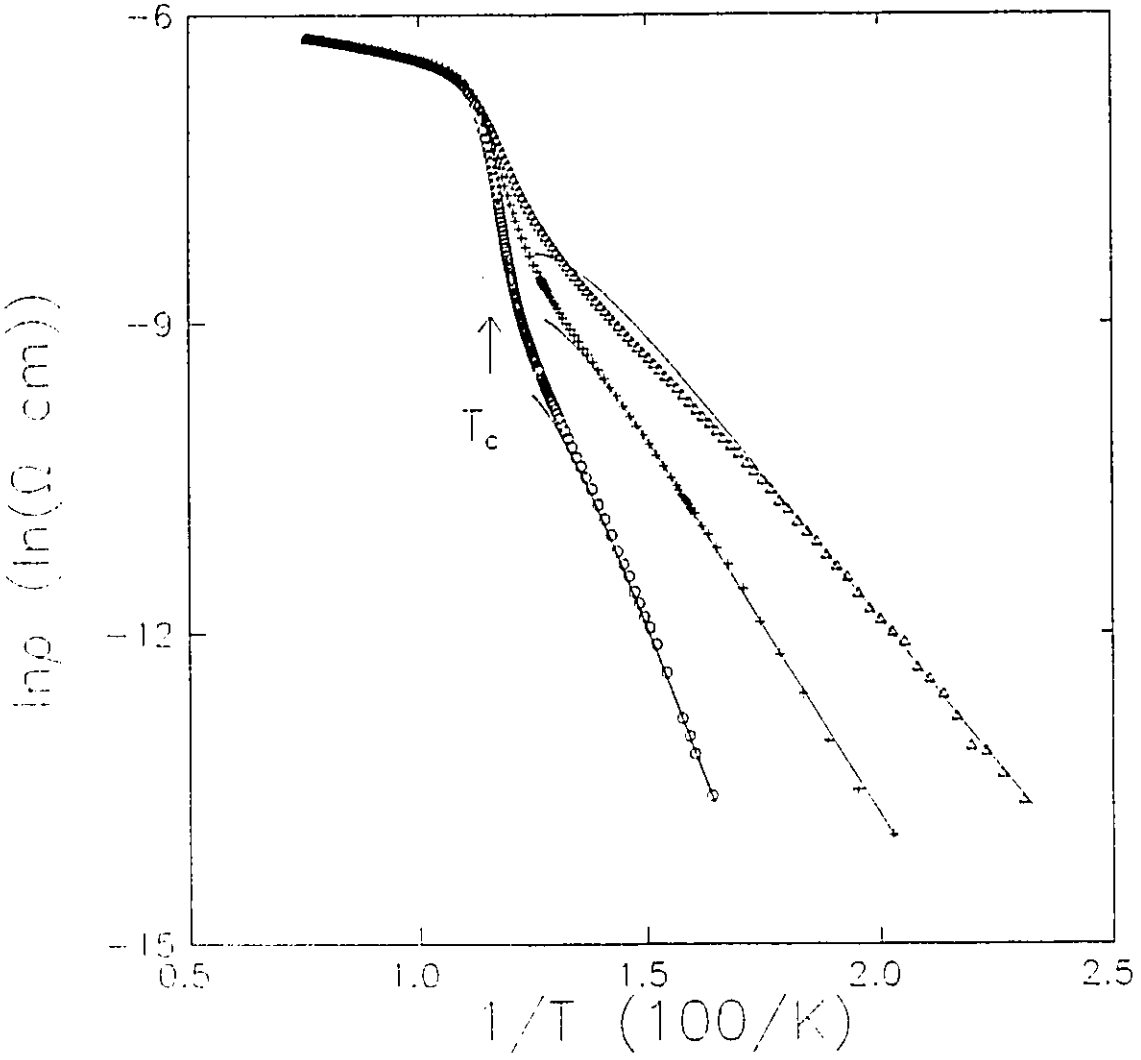

Figure 7

Figure 8

$\ln\rho$ versus 1/T for sample #2 at 1.6 T for different angles θ with respect to the CuO_2 planes [θ=9°(o), 20°(+) and 90°(Δ)]. The critical temperature, T_c, is indicated by the arrow. Solid curves are best fit to the low temperature portion.

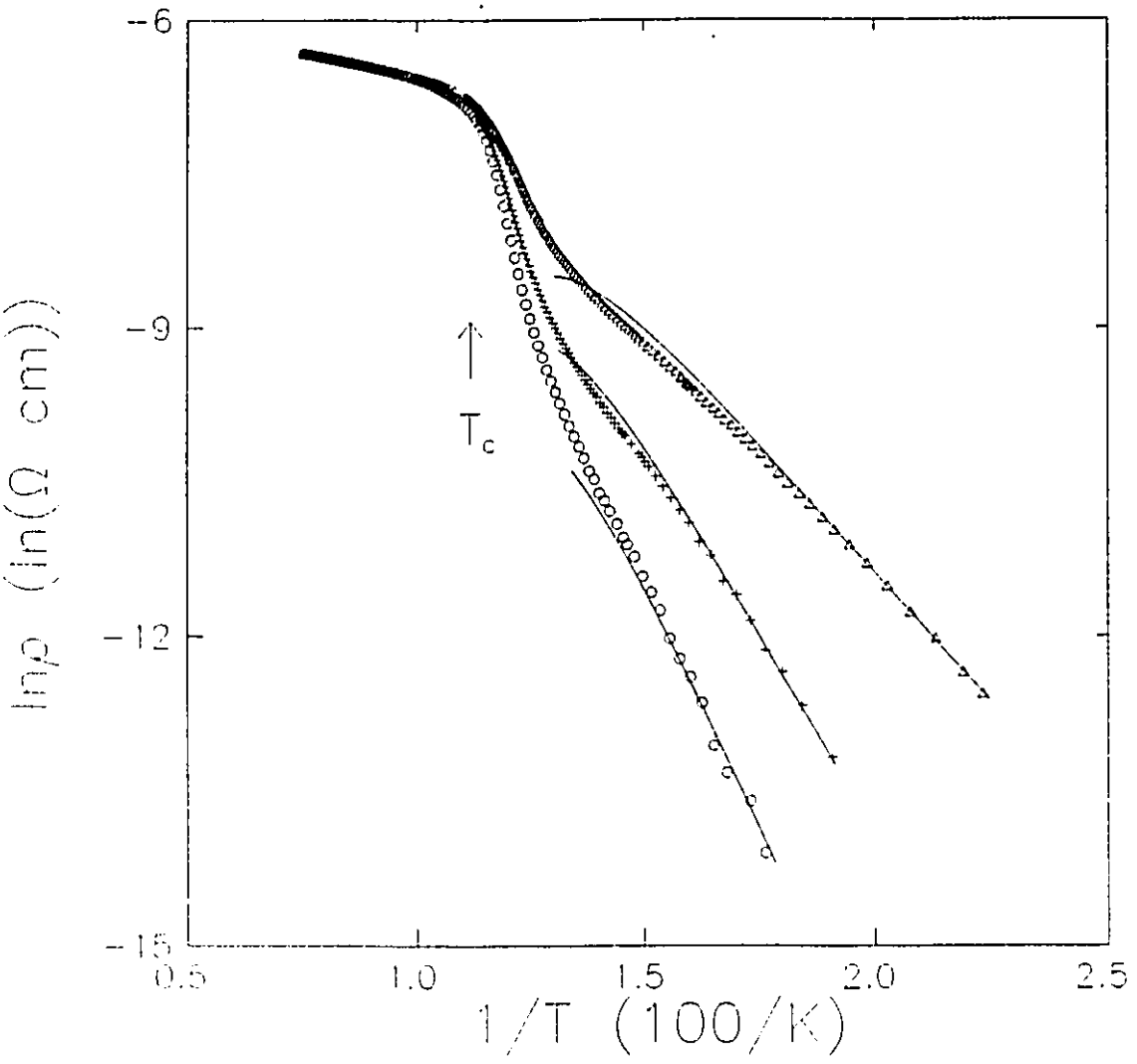

Figure 8

The solid curves are best fits to the low temperature portion of the data. T_c is indicated by the arrow on the plot. As T_c is approached the fitting curves show deviations from the data, indicating other dissipation mechanisms including strong fluctuation effects. There is a similarity in the temperature dependent resistivity in figures 6 and 7, indicating that changing H and changing θ have similar effects on ρ.

The activation energy U_o for sample #1 is plotted as a function of field (θ=90, where θ is the angle between the applied field and the CuO_2 layers), in figure 9. The activation energy is best fit with a power law, shown by the solid curve, with the form $U_o = 530\ H^{-0.36\pm0.03}$ (K).

Values of ρ_o extracted from the best fit data are plotted as a function of magnetic field for sample #1 in figure 10. The solid line is a best fit line through the origin and is given by the expression $\rho_o = (0.10\pm0.01)$ H (mΩ cm/T). The value of ρ_n in the superconducting state in equation 19 is not known accurately. As well there is considerable uncertainty as to the exact shape of the pinning potentials derived for equation 19 (Kes and van den Berg, 1990, p. 83). Arbitrarily applying the normal state resistivity, ρ_n, at T_c, as extrapolated from higher temperatures ($\rho_n(T_c)$ = 1.51 mΩ cm), $H_{c2}(0)$ as determined by equation 19 is $H_{c2}(0)=95\pm11$ T which is in order of magnitude

Figure 9

The activation energy U_o is plotted as a function of H for the field perpendicular to the CuO_2 planes for sample #1. The solid curve is a power law best fit to the data.

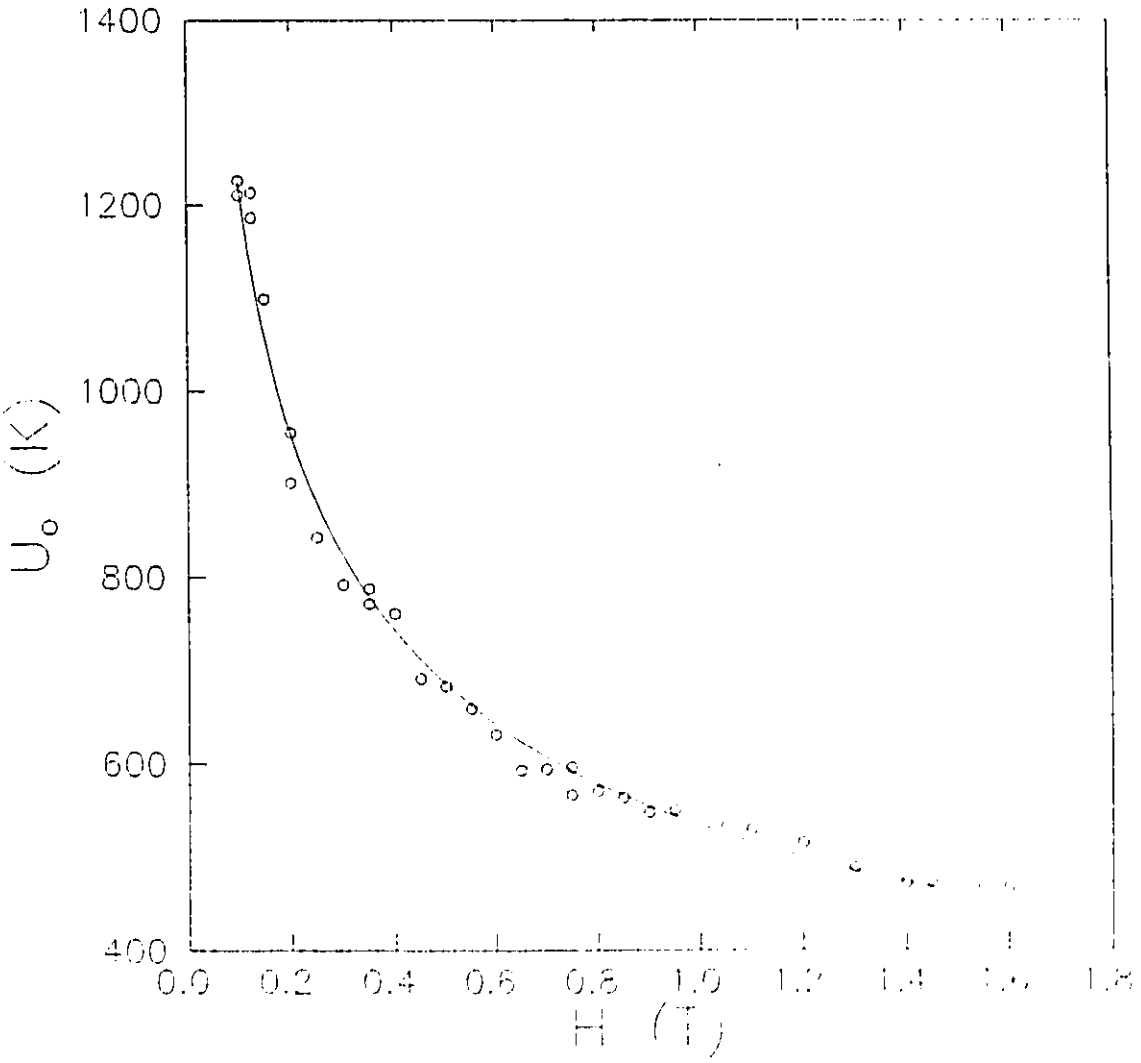

Figure 9

Figure 10

The prefactor ρ_o is plotted as a function of H for the field perpendicular to the CuO_2 planes for sample #1. The solid line is a best fit through the origin.

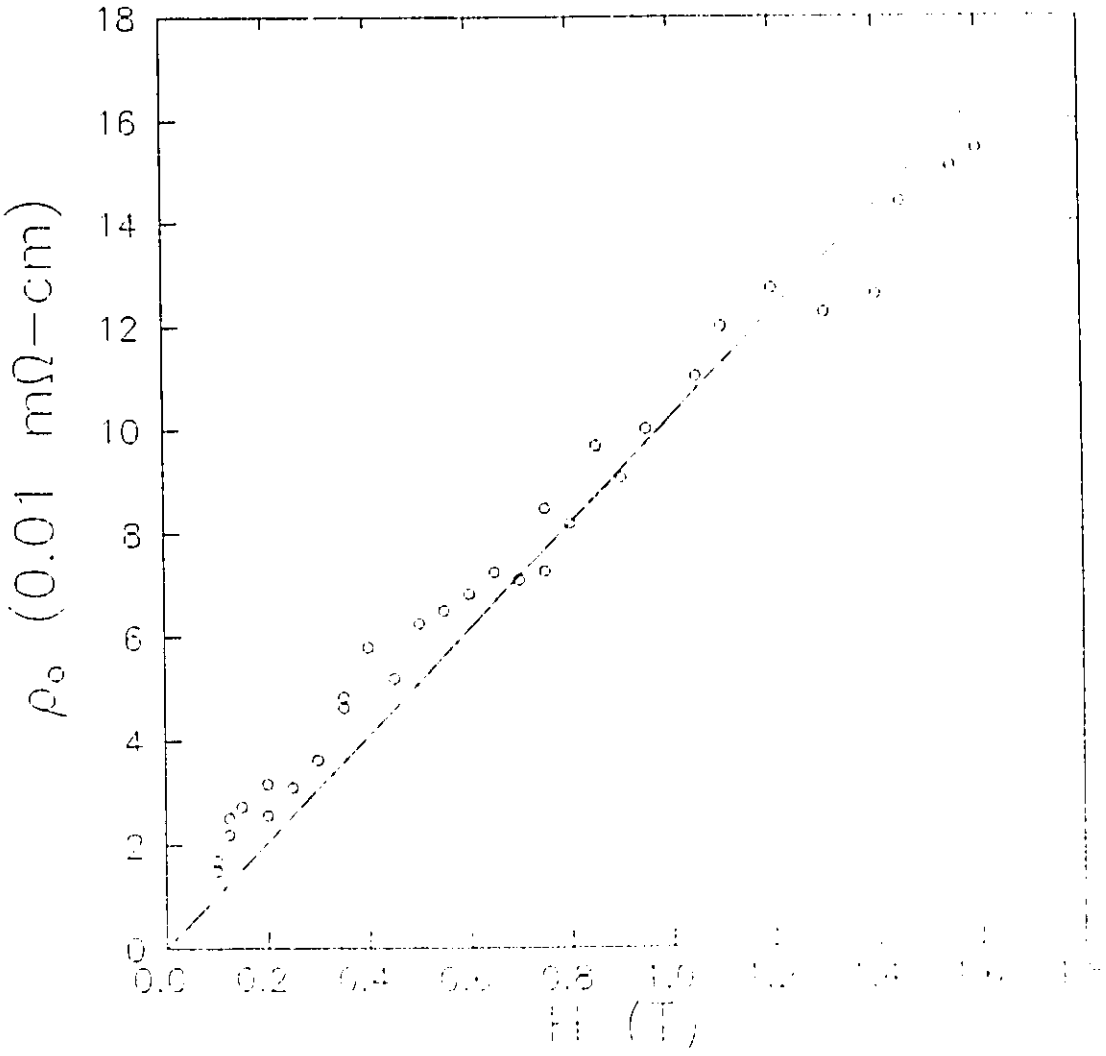

Figure 10

agreement with the value $H_{c2}(0)$=40 T of Bi:2212 perpendicular to the CuO_2 planes as measured by Kim *et al*. (1991). If, on the other hand, the value of 40 T for $H_{c2}(0)$ is applied to equation 19 the value of ρ_n is more than double that obtained from an extrapolation of ρ_n from high temperatures to T_c.

Activation energies as a function of the sine of the angle are plotted in figure 11 for sample #2 in a constant field of 1.6 T. In order to demonstrate the behaviour of the field projected on to the CuO_2 planes the field dependent activation energies are plotted together with the angular dependent activation energies as a function of field normalized by 1.6 T for a constant angle of 90°. The two sets of activation energies demonstrate the same projected magnetic field dependence. The solid curve is a power law best fit to both sets of data. Alternatively for each set of data the best fit expression for the activation energy obtained for the angular dependence at 1.6 T is given by $U_0 = (432\pm4)x(\sin\theta)^{-0.31\pm0.02}$ (K) and for the normalized field dependence by $U_0 = (437\pm2)x(H/1.6)^{-0.32\pm0.02}$ (K).

Values of ρ_0 extracted from the best fit data are plotted as a function of the sine of the angle in a constant field of 1.6 T and as a function of field, normalized by 1.6, for a constant angle of 90° for sample #2 in figure 12. Here, the projected magnetic field

Figure 11

The activation energy U_o is plotted as a function of the normalized field H/1.6 for the field perpendicular and in a field of 1.6 T as a function of $\sin\theta$ (+) for angles θ with respect to the CuO_2 planes for sample #2. The solid curve is a power law best fit to both sets of data.

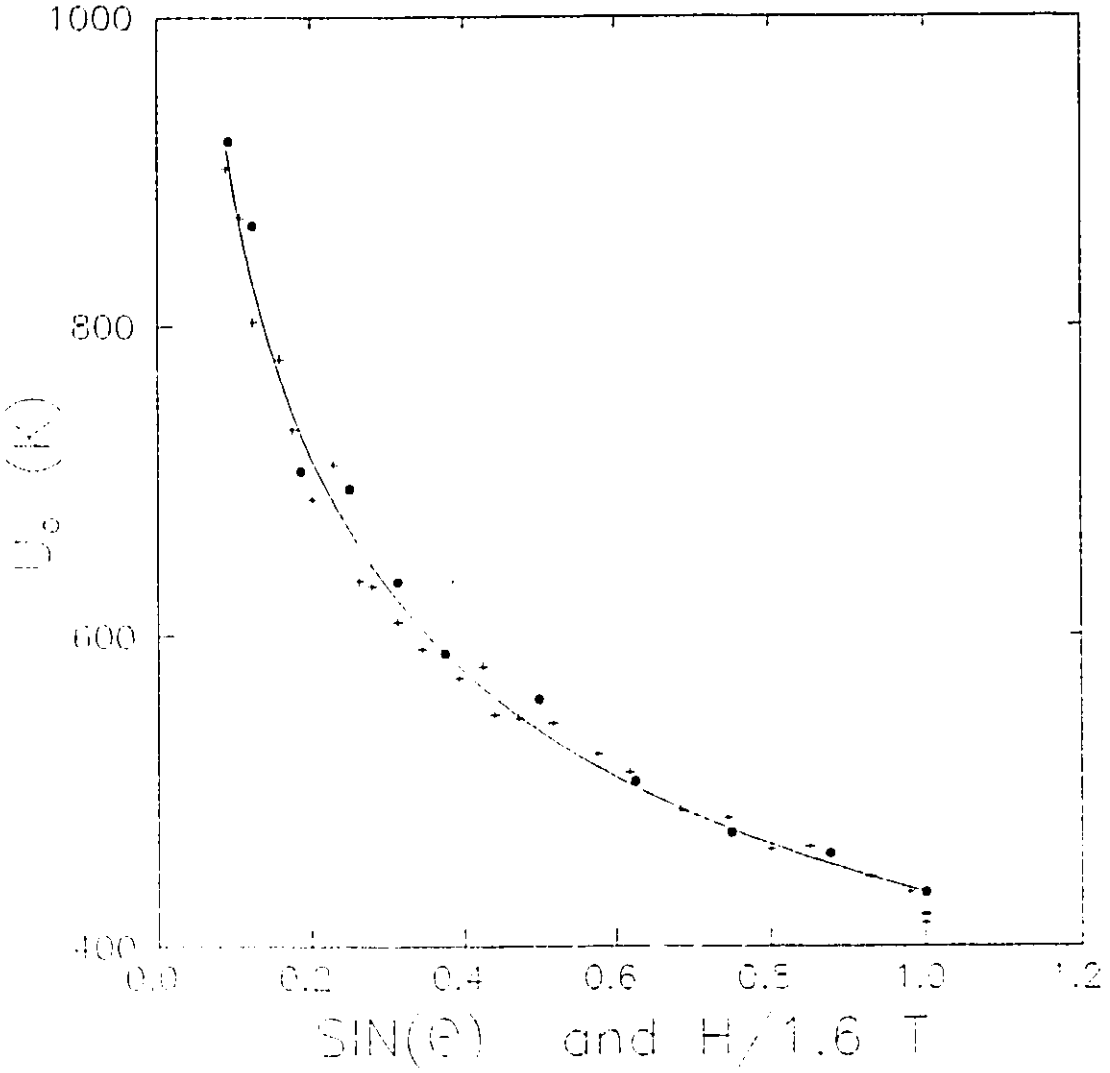

Figure 11

Figure 12

The prefactor ρ_o is plotted as a function of H/1.6 (●) for the field perpendicular and as a function of $\sin\theta$ (+) for angles θ with respect to the CuO_2 planes for sample #2. The solid line is a best fit through the origin to both sets of data.

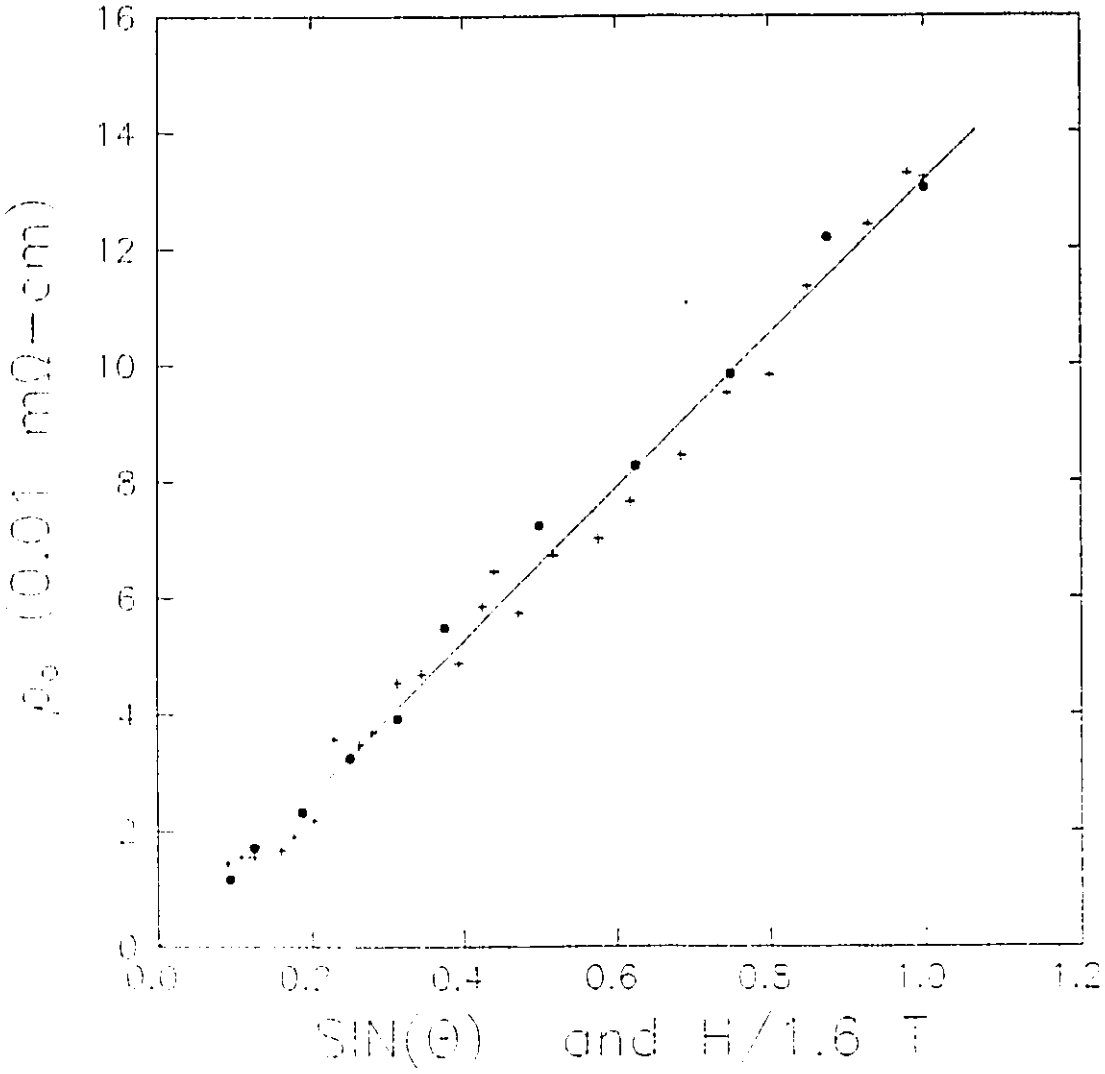

Figure 12

behaviour is once more seen to be the same as a function of $\sin\theta$ in a 1.6 T field and H/1.6 dependence of the prefactor. The solid line is a best fit line through the origin for both sets of data. Alternatively, a best fit line through the origin for the $\sin\theta$ dependence in a 1.6 T field is given by the expression $\rho_o=(0.131\pm0.004)\ \sin\theta$ (mΩ cm/T). For the H/1.6 dependence $\rho_o=(0.134\pm0.003)$ (H/1.6) (mΩ cm/T). Applying a linear best fit for both sets of data and taking ρ_n, at T_c as extrapolated from higher temperatures ($\rho_n(T_c)$ = 1.41 mΩ cm) equation 19 produces $H_{c2}(0)=108\pm3$ T. This value is in agreement with the value of the upper critical field obtained in the same manner for sample #1.

The results of these measurements are summarized as: The resistivity is described by the expression $\rho = \rho_o U(T)/T\exp(-U/T)$. The activation energy U(T) has the form

$$U(T) = A(B\sin\theta)^{-\alpha}(1-(T/T_c)^2)^{3/2}, \qquad (21)$$

where $\alpha \approx 1/3$ and A is a sample-dependent constant. Furthermore, the extracted parameter ρ_o has the Bardeen Stephen form of the flux flow resistivity multiplied by 2π, given by $\rho_o=2\pi\rho_{FF}(1-(T/T_c)^2)$ as derived by Kes and van den Berg (1990, p. 83). This fit is applied up to a temperature criterion determined by equating the flux flow resistivity, ρ_{FF}, with the expression for the total resistivity as shown in equation 20.

These results demonstrate that the measured resistivity can be accounted for with the assumption that only the field component $H_\perp = H\sin\theta$ influences the low temperature dissipation processes for the temperature and field range investigated in our experiments. Therefore, our result provides clear evidence that dissipation in the system is due to the motion of 2D vortices, as proposed by Kes *et al.* (1990).

C. DISCUSSION

In conventional superconductors, at small current density $J<J_c$ the vortices are pinned by inhomogeneities in the material. In the absence of thermal fluctuations, only when J exceeds a critical current J_c do the vortices move and dissipate energy. As predicted by Anderson (1962), thermally activated depinning of the vortices may occur at finite temperatures T. For the high T_c superconductors, Dew-Hughes (1988) and Kes *et al.* (1989) have argued that thermally assisted flux flow (TAFF) with a linear (Ohmic) I-V curve is observable at a small current density J. For the current densities used in our experiments, all the I-V curves are linear, which indicates that our measurements are in the TAFF regime.

Various forms of the temperature dependence of the

activation energy have been suggested by many authors (Geshkenbein *et al.* 1989, Tinkham 1988, Kes and van den Berg, 1990, p. 83, and Malozemoff *et al.* 1989). The temperature dependence of the activation energy is presented in the form $U=U_0 g(t)$ where $g(t)$ is given by $(1-t)^q$ or $(1-t^2)^q$, with q= 1 or 3/2. If ρ_{FF} is held fixed with respect to temperature, the mapping of the $\sin\theta$ dependent U_o on to the H dependent U_o, as well as the $\alpha\approx 1/3$ power law of U_o with respect to H and $\sin\theta$, is maintained. However, the temperature dependence of $H_{c2}(T)$ requires that ρ_{FF} has a $(1-t^2)^{-1}$ temperature dependence. In this case it is only with q=3/2 that the linear dependence of ρ_{ff} with applied magnetic field, as predicted by the Bardeen Stephen model of flux flow, is obtained.

Values obtained for $H_{c2}(0)$ from the two samples are in agreement with each other and in order of magnitude agreement with published values (Kim *et al.* 1991). ρ_n is not known accurately in the superconducting state and the shape of the pinning potential has been assumed to be sinusoidal (Kes and van den Berg, 1990, p. 83). Furthermore, different prefactors can enter the flux flow resistivity expression (Gor'kov and Kopnin, 1976). Therefore, the order of magnitude agreement between the result for $H_{c2}(0)$ obtained here and that suggested by Kim *et al.* (1991) is reasonable.

The mapping of the $\sin\theta$ dependence of U_o on the

normalized H clearly indicates the presence of activation barriers to the motion of 2D vortices. Furthermore, the mapping of the $\sin\theta$ dependence of ρ_0 on to H indicates that the measured dissipation is due to the motion of these 2D vortices as they are projected onto the CuO_2 layers.

D. CONCLUSION

We have studied the resistivity of Bi:2212 single crystals. The measured resistivity can be described by thermally assisted flow of two dimensional vortices. The activation energy depends only on the projected field $H_\perp = H\sin\theta$, $U \propto (H\sin\theta)^{-\alpha}$ where $\alpha \approx 1/3$. The prefactor is consistent with the Bardeen Stephen result for the flux flow resistivity due to motion of vortices in an applied magnetic field. An analysis of the prefactor utilizing an arbitrarily chosen value for the normal state resistivity, ρ_n, gives a reasonable order of magnitude estimate of the upper critical field for Bi:2212 when compared with other measurements of $H_{c2}(0)$ (for example Kim *et al.* 1991). These results show that the system is in the two-dimensional regime, and the dissipation can be accounted for by the motion of the two-dimensional vortices, whose density is given by $H_\perp$, in the CuO_2 planes.

CHAPTER VI

INTERGRAIN AND INTRAGRAIN SUPERCONDUCTIVITY

A. INTRODUCTION

Tinkham and Lobb (1989, P.91) have proposed a dual superconducting transition model for a network of weak links that connect superconducting grains. First, the superconducting transition within grains occurs, followed, at a lower temperature by the establishment of long range superconducting order, or phase coherence, between grains. These are referred to as the *intragranular* and *intergranular* superconducting transitions, respectively.

Observations of a current dependence in the zero field resistive tail, the low temperature extension of the resistive superconducting transition in high temperature superconductors, have been explained in terms of a weak link intergranular transition model (Pureur *et al.* 1991 and Svoboda *et al.* 1990). The current dependence of the resistivity in the resistive tail regime is associated with the critical current, I_c, of the weak links that are part of the transport current path between the two potential contacts. If the applied transport current is increased in this regime, where the transport current path includes superconducting weak links, the critical current of some of the weak links are

exceeded and switch to a dissipative state. This increases the measured resistivity. The temperature where the resistivity goes to zero, T_c^0, for a particular transport current is the temperature at which long range superconducting order between the two potential contacts is established. This temperature is suppressed by increasing the transport current density.

Pureur *et al.* (1991) determined the temperature derivative of the resistivity, $d\rho/dT$ in $MBa_2Cu_3O_7$ (M=Y, Eu and Gd) in zero field and observed a current dependent two-step transition associated with the *intragranular* transition followed by the superconducting transition in the weak linked granular network, the *intergranular* transition. Magnetic fields were not applied.

Svoboda *et al.* (1990) demonstrated that fields below 0.1 mT are sufficient for a partial decoupling of superconducting grains in samples of $Bi_{1.4}Pb_{0.6}Sr_2Ca_2Cu_{3.6}O_x$. Also, the application of a small magnetic field (B=0.015 T) produced a similar change in the R(T) curve as that produced by an increase in the transport current. Also, Li *et al.* (1989) have reported that the observed current dependence of the resistivity in a 110 K phase Bi-Sr-Ca-Cu-O sample, with a zero field resistive tail that extended to 94 K, was suppressed by an applied magnetic field of 1 T.

A detailed investigation of the intergranular transition in a magnetic field in the polycrystalline bismuth based superconductors has not been performed previously. Broadening of the resistive transition in a magnetic field has been attributed to Josephson weak links (Ekin *et al.* 1987), however, the degree of broadening in a magnetic field of bismuth based high temperature superconductors with different weak link characteristics has not been compared. This situation is complicated in the bismuth based superconductors by considerable intragranular broadening observed with the application of a magnetic field (Palstra *et al.* 1988 and this thesis). While a determination of the temperature derivative of the resistivity, $d\rho/dT$, has been used to analyze the current dependence of the resistive transition in $YBa_2Cu_3O_y$ and related materials (Pureur *et al.* 1991 and Goldschmidt, 1989), this method of analysis has not been employed for the magnetic field dependence of the resistive transition in the bismuth based high temperature superconductors. Furthermore, measurements of the current dependent resistivity in a magnetic field nave been considered briefly (Li *et al.* 1989 and Svoboda *et al.* 1990). A detailed study of how the current dependence of the resistivity with field at constant temperature and how this relates to an intergranular transition has not been performed. In this chapter we will

consider the resistivity, and $d\rho/dT$ as a function of magnetic field and also consider the current dependent resistivity at 77 K as a function of magnetic field. We define a model of the intergranular transition that includes a distribution of weak link strengths for a polycrystalline high temperature superconductor. A consideration of such a distribution has important consequences in the interpretation of resistive broadening and the current dependence of the resistivity with and without an applied magnetic field.

A variety of weak links are possible in the bismuth based high temperature superconductors. They may result from semiconducting layers at the surface of grains due to extended exposure to air or exposure to water (Svoboda *et al.* 1990) or they may be due to Pb rich surface layers in Pb-doped compounds (Ramesh *et al.* 1988). Large angle grain boundaries can act as weak links due to the severe anisotropy of the conductivity of the bismuth based superconductors (Jin *et al.* 1988). The coexistence of multiple phases is another source of weak links. In particular, Nkum and Datars (1992), have demonstrated that in Sn doped BiPbSrCaCuO samples with a large resistive tail the Bi:2212 phase is observed in the magnetization. Investigations of the microstructure of undoped Bi-Sr-Ca-Cu-O ceramics by Ramesh *et al.* (1988) have demonstrated that the low T_c Bi:2212 phase has a tendency to

form in a layer on the surface of the grains composed of the high T_c Bi:2223 phase. A variation in the size of the grains and variation in contact area between grains also introduces variations in the weak link critical current, I_c, between grains (Tinkham and Lobb, 1989, p. 91).

We define a model of the intergranular superconducting transition that incorporates a range of weak link strengths. A weak link is characterized by its critical temperature, T_c, the temperature at which phase coherence between the two superconducting grains occurs and by its critical current, I_c, the maximum current that can flow through the weak link without dissipation. Just below the intragranular transition the first superconducting link between two superconducting grains forms. If it is in the transport current path it will decrease the resistivity. This marks the onset of the measured intergranular superconducting transition. At lower temperatures more weak links in the transport current path will become superconducting and the measured resistivity will be reduced. The onset of zero resistivity, T_c^0, for a particular applied current density occurs when the last weak links become superconducting in the transport current path.

The presence of weak links with a range of T_c's and I_c's implies a current dependence in the measured resistivity throughout the intergranular transition. When the applied

transport current is increased and I_c is exceeded for a particular weak link in the percolative system, the current is redistributed among the other weak links. The critical currents, I_c, of these other weak links may or may not be exceeded due to this redistribution. If some of the critical currents of the superconducting weak links are exceeded they become dissipative, increasing the measured resistivity. An increase in current density, therefore, can also suppress T_c^0. Samples with weak links that have lower T_c's and I_c's can be characterized by a larger zero field resistive tail. Likewise, a range of weak link strengths may affect the resistivity measured in an applied magnetic field. The presence of a magnetic field implies Josephson vortices which have associated with them a pinning energy and therefore a critical current (Likharev, 1979). Correspondingly, a current dependent resistivity should also be measurable in an applied magnetic field due to the continued presence of critical currents at weak links.

In this chapter we report investigations of the resistive transition in two Sn-doped and two Sb-doped $Bi_{1.7}Pb_{0.1}Sr_2Ca_2O_y$ samples in magnetic fields up to 1.6 T. For three of these samples the current dependent resistivity in magnetic fields up to 1.7 T at 77 K are reported. The samples were Pb-doped to stabilize the 110 K phase. The 110 K phase

of BiPbSrCaCuO can be grown with a very sharp transition with very little evidence of a resistive tail (Gridin *et al.* 1990). The samples were doped with Sn and Sb to attain a variation in their weak link polycrystalline characteristics in the 110 K phase (This thesis and R. K. Nkum). The range of critical weak link strengths in each of the samples was characterized by the size of the resistive tail and the value of T_c^0 in zero field. A determination of the temperature derivative of the resistivity, $d\rho/dT$, and a comparison with single crystal data were used to verify the presence of a dual superconducting transition in a magnetic field. A Bi:2212 crystal with a T_c of 87 K was chosen for this comparison since Bi:2223 crystals of the 110 K phase have not yet been grown. A description of the magnetic field dependence of the *intergranular* superconducting transition is made. The current dependent resistivity at 77 K demonstrates a magnetic field dependence that is described in terms of an intergranular transition with a distribution of weak links and is consistent with the results of the $d\rho/dT$ analysis.

B. METHOD

Measurements were performed on four polycrystalline samples of the BiPbSrCaCuO family of 110 K superconductors of the form $Bi_{1.7}Pb_{0.3}A_{0.1}Sr_2Ca_2Cu_3O_x$ (A = Sb or Sn). A summary of the dimensions and experimental parameters of the samples is shown in table 1. Silver paste electrical contacts with a resistance of approximately 1Ω per contact and area of 0.05 cm^2 per contact were placed at the ends of the longest dimension of the samples. For the first 3 samples eleven currents in the positive and negative direction were applied between the minimum and maximum current values shown in table 1 and the corresponding voltages measured. In sample #4 only one current in the positive and negative direction was applied.

Voltage as a function of current was measured at higher current densities for various applied fields with samples #1, #2 and #3 in a liquid nitrogen bath at 77 K. Larger current densities were possible since heat generated by the contact resistance was absorbed by the liquid nitrogen. The current densities were between 0.034 A/cm^2 and 0.45 A/cm^2 for sample #1, between 0.18 A/cm^2 and 2.93 A/cm^2 for sample #2 and between 0.094 A/cm^2 and 1.47 A/cm^2 for sample #3.

Table 1

Summary of dimensions and experimental parameters for the four $Bi_{1.7}Pb_{0.3}A_{0.1}Sr_2Ca_2Cu_3O_x$ (A = Sb or Sn) samples.

Table 1

SAMPLE	DOPANT A	DIMENSIONS (cm)			VOLTAGE CONTACT DISTANCE (cm)	MINIMUM CURRENT (A/cm^2)	MAXIMUM CURRENT (A/cm^2)
		LENGTH	WIDTH	THICKNESS			
#1	Sb	0.98	0.182	0.178	0.307	0.002	0.157
#2	Sn	0.99	0.19	0.09	0.475	0.006	0.591
#3	Sn	1.30	0.185	0.14	0.745	0.006	0.298
#4	Sb	0.9	0.22	0.10	0.39	0.03	-

C. RESULTS

The resistive transition of sample #1 and sample #2 for zero field are compared in figure 13. The onset of the superconducting transition and the steepest portions of the transition for the two samples are almost the same. However, the resistive tail of sample #2 goes to zero resistivity at 90.0±0.2 K for a current density of 0.59 A/cm^2. In contrast, sample #1 has a zero resistivity temperature, T_c^0, at 102.8±0.1 K for a current density of 0.14 A/cm^2. In a magnetic field of 1.2 T sample #2 has greater resistive broadening than sample #1 as shown in figure 14.

The resistive transition of samples #3 and #4 in zero field and in a magnetic field of 1.2 T of samples #3 and #4 are shown in figure 15. Sample #3 has a small resistive tail, but has a critical temperature that is 3 K higher than sample #4 in zero field. Both samples have a T_c^0 of 101 K for applied current densities of 0.035 A/cm^2 and 0.03 A/cm^2 for sample #3 and sample #4, respectively. The slightly higher transition temperature of sample #3 may be the cause of the slightly less broadening observed for this sample when compared to sample #4 in a field of 1.2 T. Both samples #3 and #4 exhibit a larger resistive tail in zero field and greater resistive broadening in a field of 1.2 T than sample #1.

More information about the shape of the resistive

Figure 13

ρ as a function of temperature in zero field for sample #1 (___) and for sample #2 (Δ).

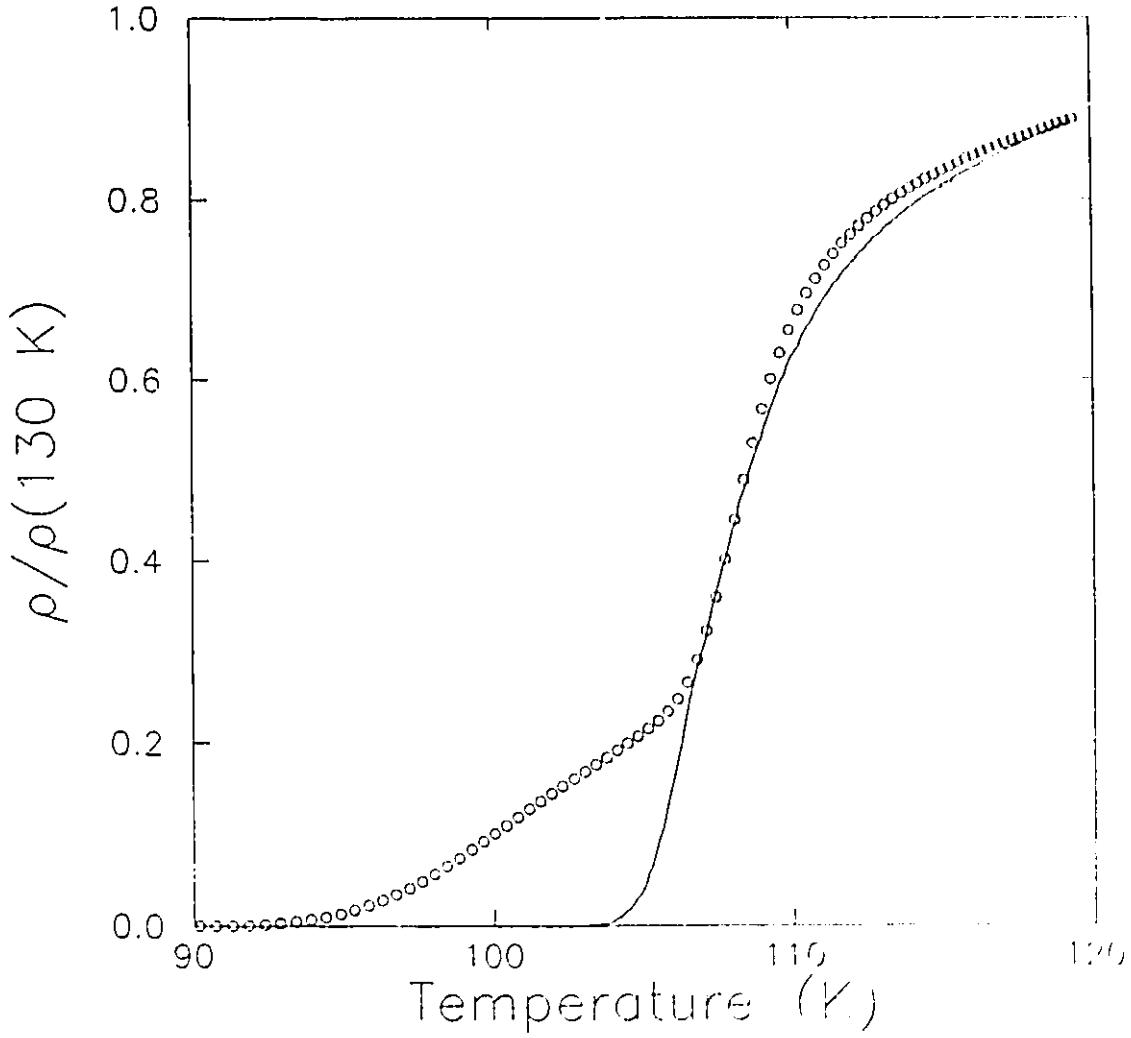

Figure 13

Figure 14

ρ as a function of temperature in a magnetic field of 1.2 T for sample #1 (- - -) and for sample #2.

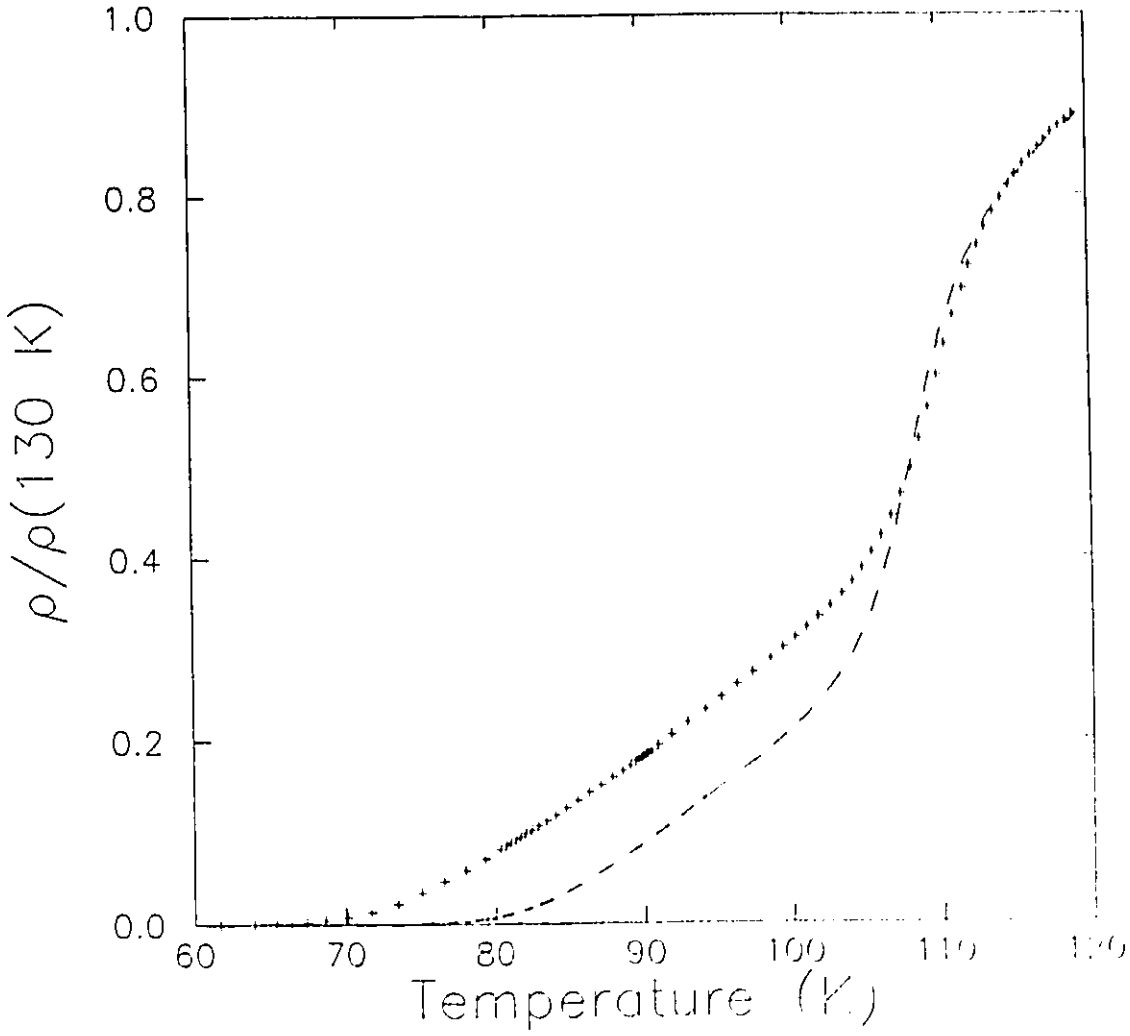

Figure 14

Figure 15

ρ as a function of temperature for the sample #3 for zero field(●) and for 1.2 T (o), and for the sample #4 in zero field (□) and for 1.2 T (■).

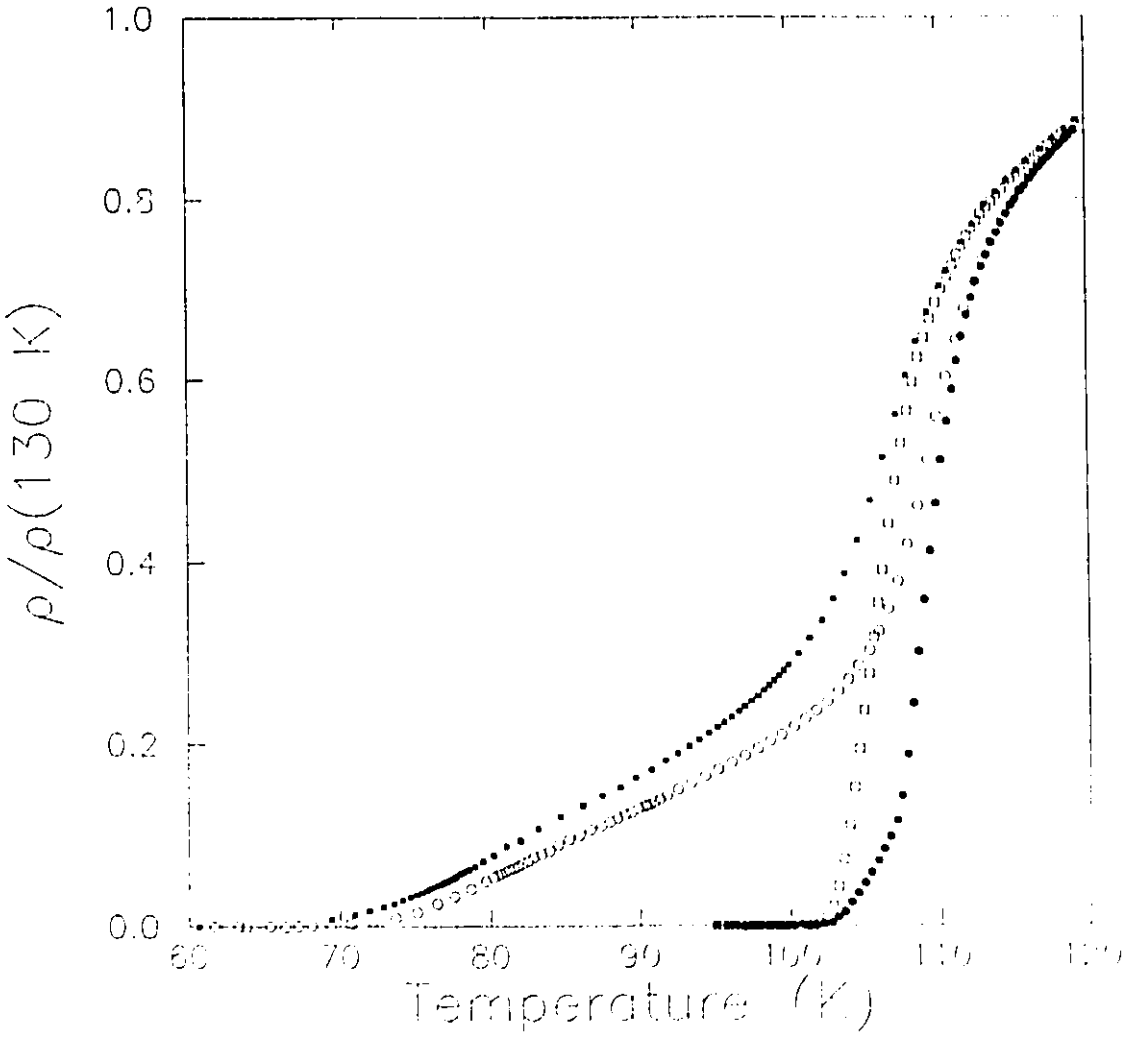

Figure 15

transition can be obtained from a plot of $d\rho/dT$ as a function of temperature. $d\rho/dT(T)$ was obtained by evaluating the linear least squares slope of a set of adjacent points of the resistivity curve. Standard deviation was obtained by determining the variation of the slope for sets containing from 7 to 20 points.

$d\rho/dT(T)$ for a Bi:2212 crystal is shown in figure 6 for both zero field and 1.55 T. The temperature of the zero field peak is 86.8 K. The magnitude of the peak is reduced and its width at half maximum is broadened and the $d\rho/dT$ curve extends smoothly down to 40 K in a 1.55 T field. The temperature at the peak, T_p, is independent of field to within the limits of uncertainty.

$d\rho/dT(T)$ for sample #1 in zero field, 0.4 T and 1.6 T is shown in figure 16 for a current density of 0.14 A/cm^2. The peak of the derivative of the zero field curve is at a temperature of 107.1±0.2 K and has a width at half maximum of 5.8±0.1 K. There is a decrease in the magnitude of the peak and an increase in the width of the peak at half maximum with increasing field, similar to what is observed for the crystal $d\rho/dT$ curve. The $d\rho/dT$ curve in a magnetic field has a broad hump feature below the temperature of the peak in the $d\rho/dT$ curve. This broad hump decreases in magnitude and extends to lower temperatures with increasing applied field. There is an

Figure 16

$d\rho/dT$ as a function of temperature for the sample #1 for zero field(___), 0.2 T(□), and 1.6 T(●).

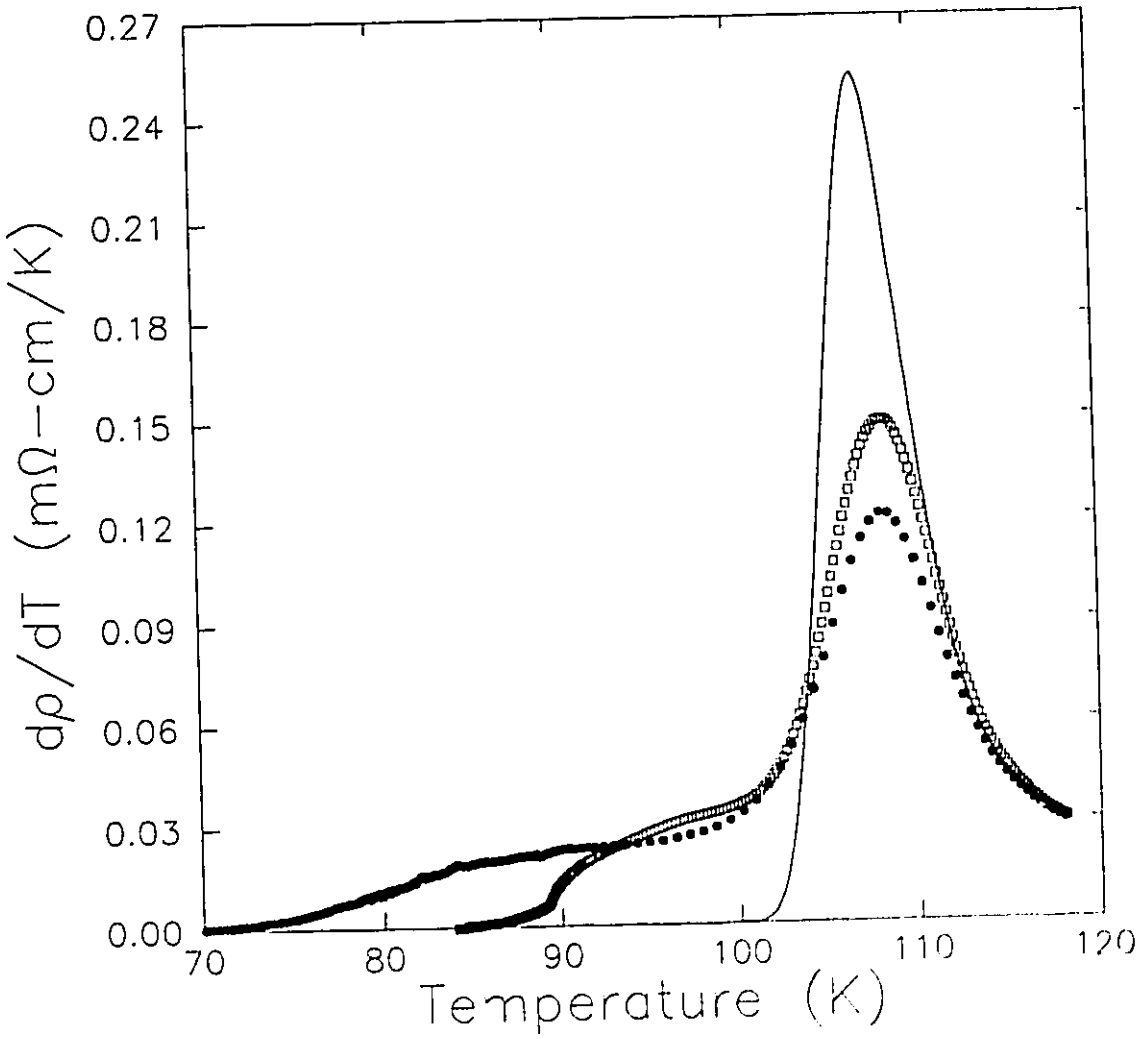
0.27
0.24
0.21
0.18
0.15
0.12
0.09
0.06
0.03
0.00
dρ/dT (mΩ−cm/K)
70
80
90
100
110
120
Temperature (K)

Figure 16

increase of 1.2 K of the temperature at the peak with the application of a magnetic field of 0.4 T. The temperature at the peak is independent of field between 0.4 T and 1.6 T.

$d\rho/dT$ as a function of temperature is shown in figure 17 for sample #2 for fields of 0.1 T, 0.2 T, 0.3 T and 0.6 T. In a field of 0.1 T there is a broad maximum below the main peak in the $d\rho/dT$ curve. This is similar to the secondary peak observed by Goldschmidt (1989) in the $d\rho/dT(T)$ curve of a ceramic $YBa_2Cu_3O_x$ sample at large current densities and zero field. The broad maximum decreases in magnitude and shifts to lower temperatures with increasing applied magnetic field. Only a broad hump remains in a field of 0.6 T. The temperature at the peak, T_p, in zero field is at 108.1±0.1 K and the width of the peak at half maximum is 5.0±0.1 K. T_p increases continuously from its value in zero field by 1.6±0.2 K in 0.6 T after which it remains constant, within the limits of uncertainty, in fields up to 1.6 T.

$d\rho/dT(T)$ for a current density of 0.298 A/cm^2 is shown for zero field, 0.2 T, 0.6 T and 1.0 T for sample #3 in figure 18. $d\rho/dT$ has a peak in zero field at 108.8±0.1 K with a width at half maximum of 5.1±0.1 K. Sample #4 has similar features with a peak in zero field at 105.8±0.1 K and width at half maximum of 7.3±0.1 K.

Plots of resistivity as a function of current density,

Figure 17

$d\rho/dT$ as a function of temperature for sample #2 for 0.1 T(___), 0.2 T(...), 0.3 T(- - -) and 0.6 T(xxx).

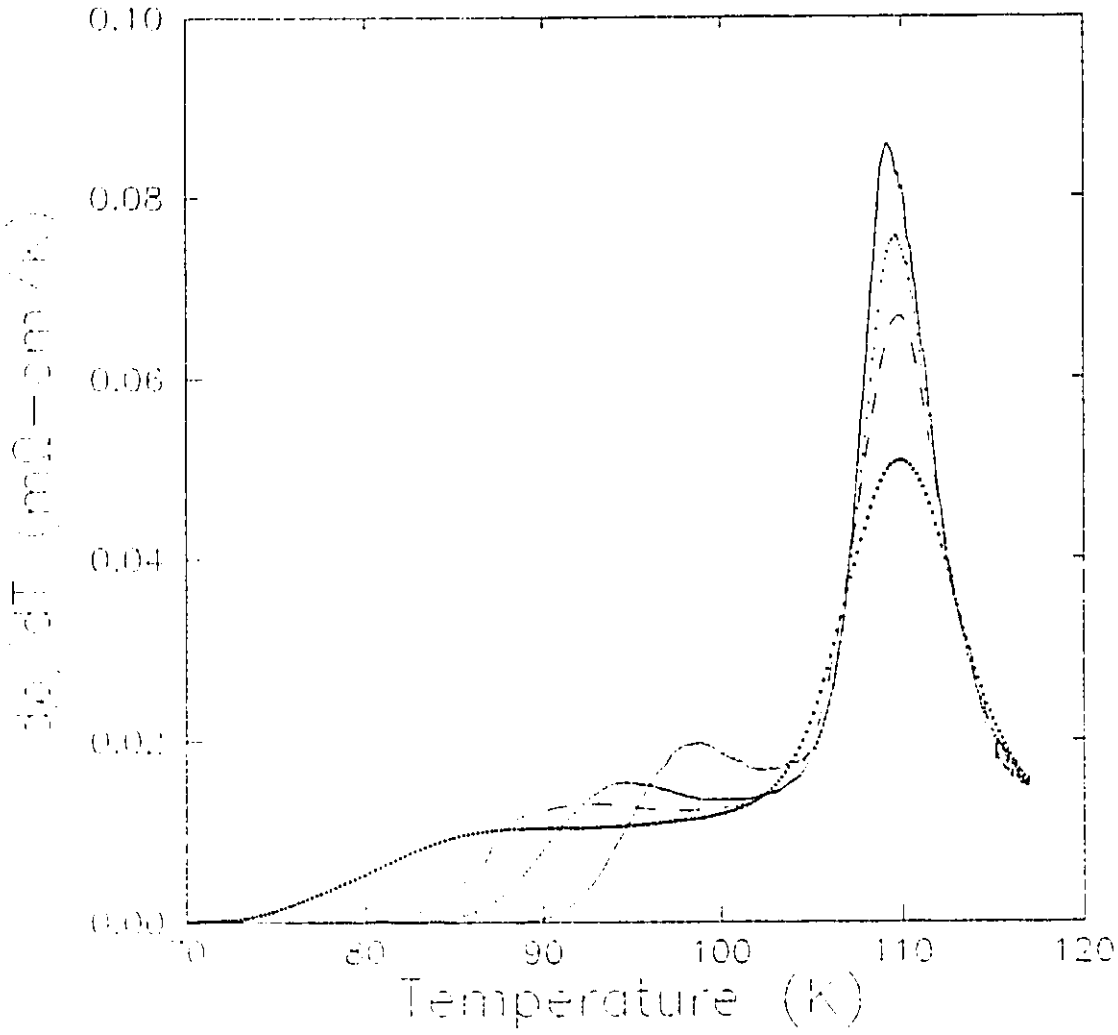

Figure 17

Figure 18

$d\rho/dT$ as a function of temperature for sample #3 for zero field(___), 0.2 T(■), 0.6 T(x) and 1.0 T(o).

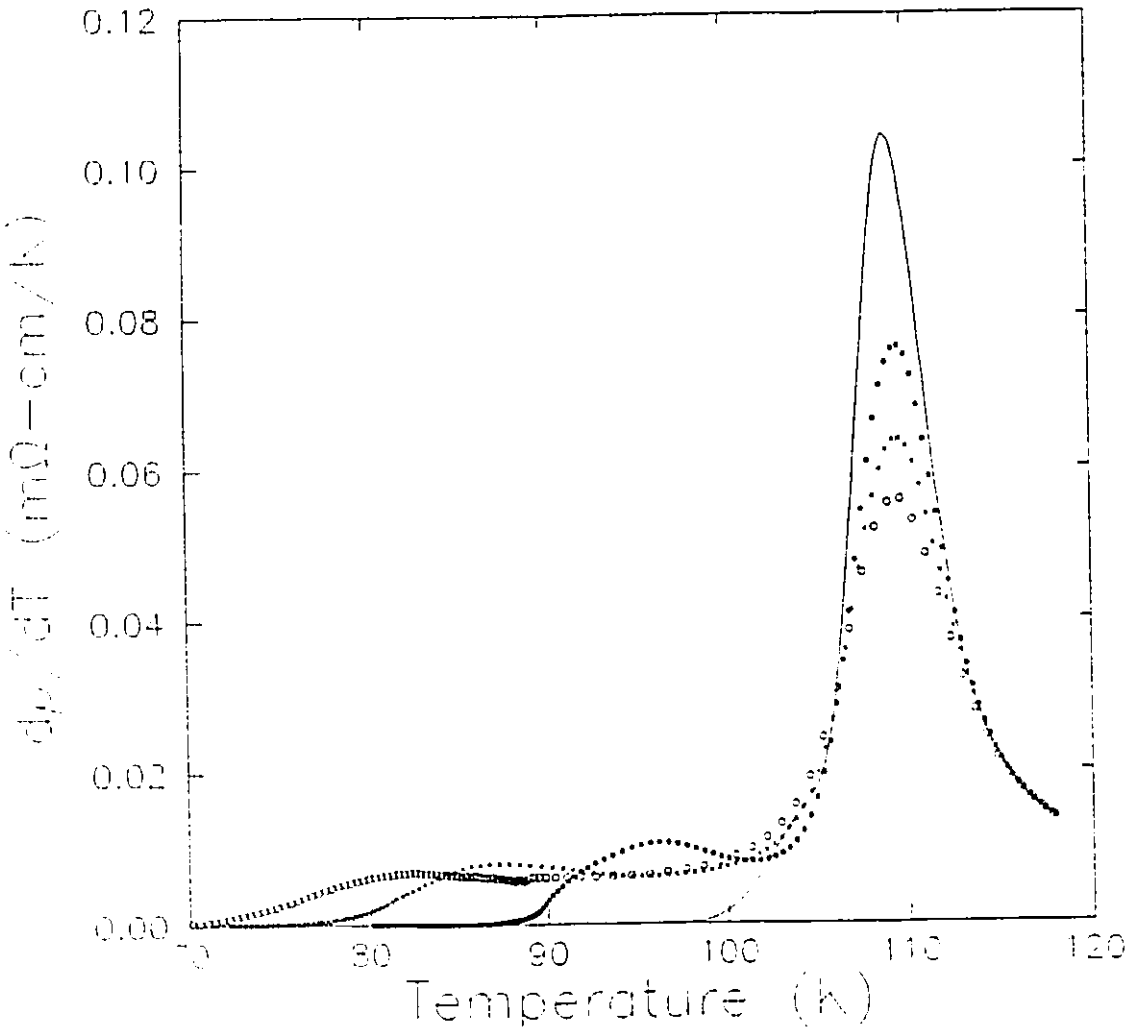
0.12
0.10
0.08
0.06
0.04
0.02
0.00
dρ/dT (mΩ-cm/K)
80
90
100
110
120
Temperature (K)

Figure 18

$\rho(J)_T$ taken at constant temperature for temperatures between 101.2 K and 103.5 K in zero field are shown for sample #3 in figure 19. The current dependence of the resistivity is a consequence of the nonlinear current-voltage characteristic and exists in the resistive tail region of the transition at temperatures below 107 K. T_c^0 was also lower with increasing current density. For example, T_c^0 is 101.1±0.2 K for the smallest current density and 98.3±0.2 K for the largest. Similar current dependent resistivities were also observed for sample #1 and #2. These observations are in agreement with current dependent resistivity measurements performed on high temperature superconducting ceramics by other groups (Svoboda *et al.* 1990, Goldschmidt, 1989, and Pureur *et al.* 1991).

The rate of change of the resistivity with respect to a particular applied current density is given by $d\rho/dJ$ at that current density. For smaller values of $d\rho/dJ$, $d\rho/dJ$ is almost constant over the applied range of current density. $d\rho/dJ$ at a current density of 0.17 A/cm^2 is plotted as a function of temperature for the zero field resistive tail region of the transition in figure 20. In this plot $d\rho/dJ$ with value zero describes ohmic behaviour with no current dependence of the resistivity. Therefore, the plot is a measure of the deviation from ohmic behaviour of the resistivity at a particular current density. The curves demonstrate an

Figure 19

ρ as a function of current density for sample #3 in zero field at the temperatures; 101.2 K (●), 101.9 K (o), 102.4 K (■), 102.8 K (+), 103.2 K (*), and 103.5 K (□). Solid lines are quadratic best fits to the data to guide the eye.

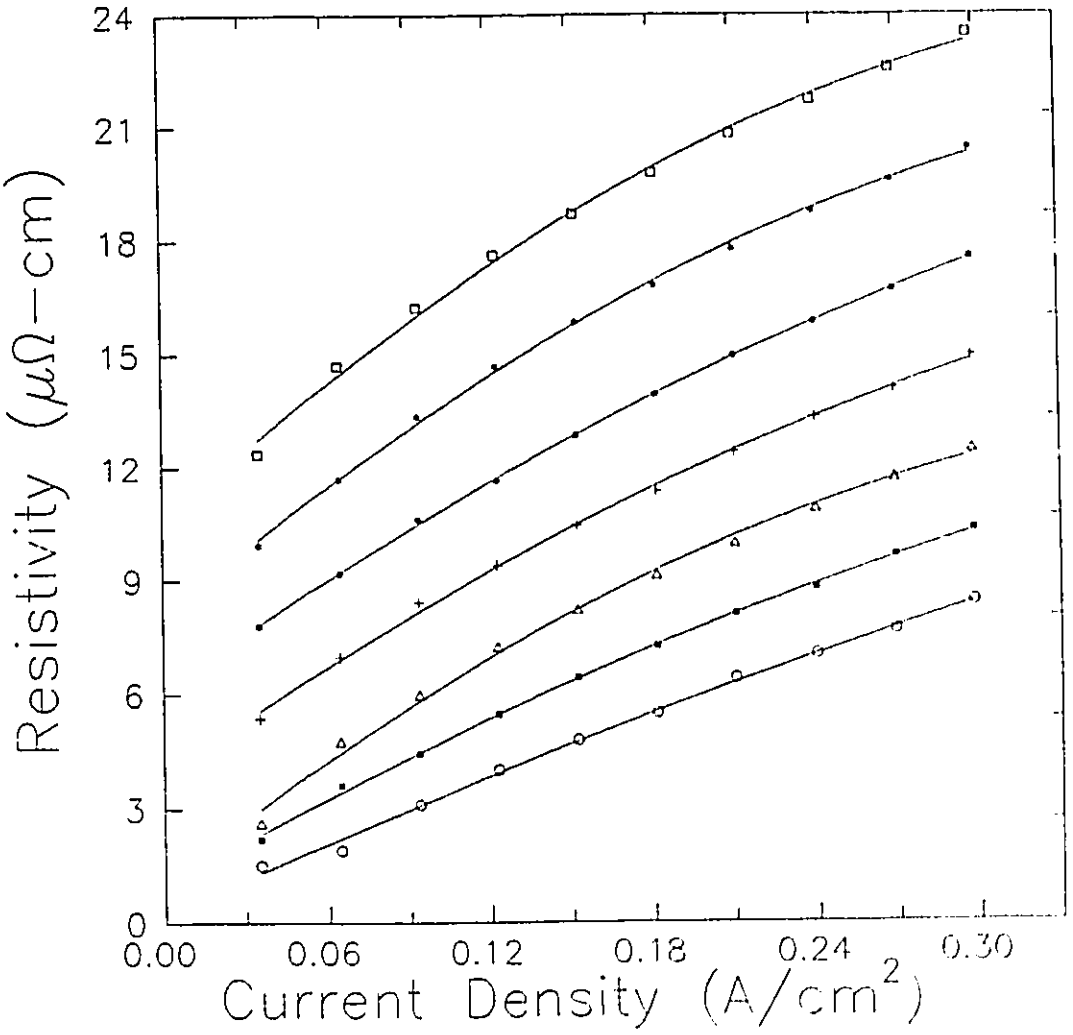
Resistivity ($\mu\Omega$-cm)
24
21
18
15
12
9
6
3
0
0.00
0.06
0.12
0.18
0.24
0.30
Current Density (A/cm^2)

Figure 19

Figure 20

$d\rho/dJ$ at 0.17 a/cm^2 as a function of temperature for sample #3 in zero field.

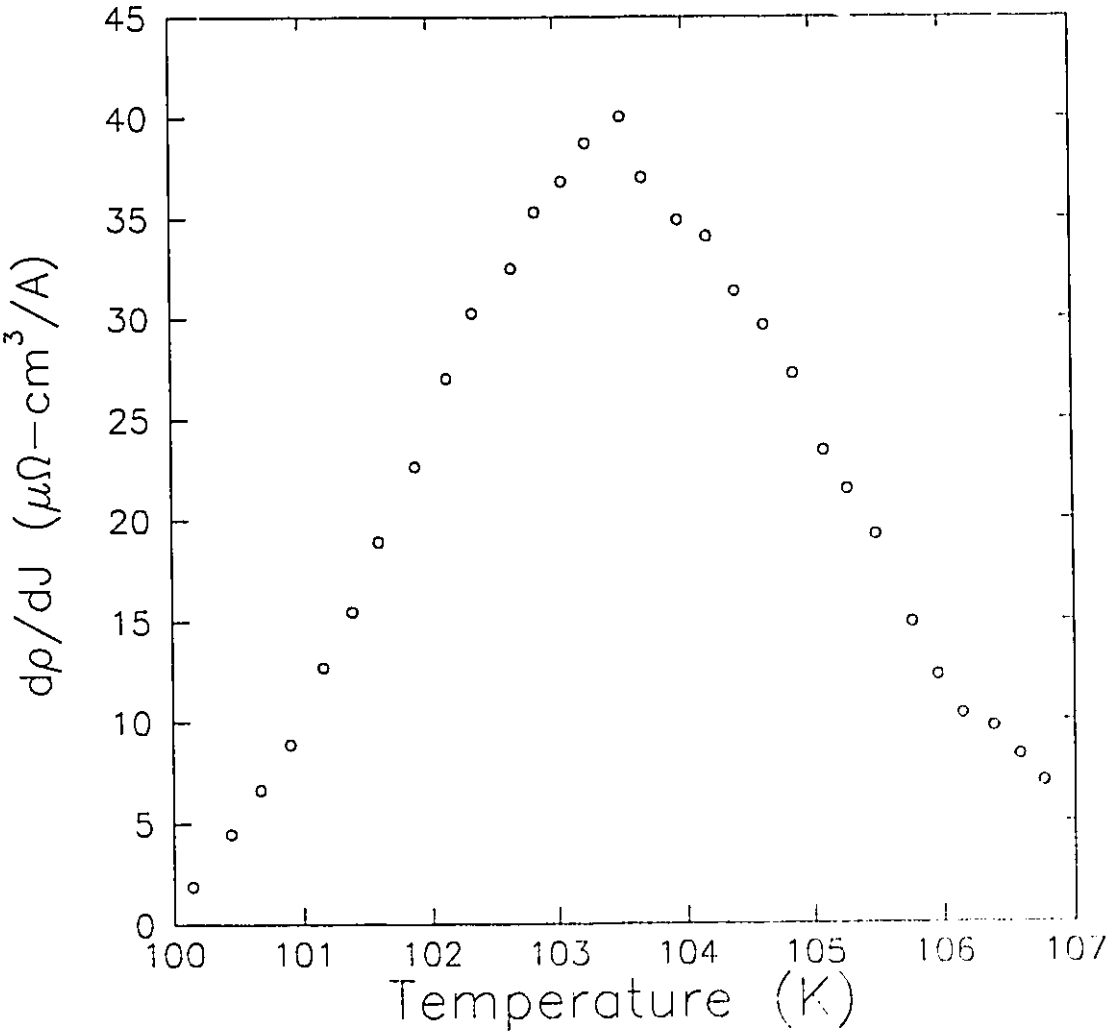
45
40
35
30
25
20
15
10
5
0
100
101
102
103
104
105
106
107
dρ/dJ (μΩ−cm³/A)
Temperature (K)

Figure 20

increase of the $d\rho/dJ$ value from 0 $\mu\Omega$-cm^3/A in the superconducting state to a maximum of 40±3 $\mu\Omega$-cm^3/A at a temperature of 103.5±0.2 K. This range of $\rho(J)$ curves was shown in figure 19 with the curve with a maximum $d\rho/dJ$ value corresponding to the $\rho(J)$ curve at the top of the plot. This curve is also the most nonlinear as can be seen by inspection. With a continuing increase in temperature $d\rho/dJ$ decreases until the steep portion of the resistive transition is reached at 107 K.

Resistivity as a function of current density for sample #2 at 77 K for fields between 0.35 T and 0.6 T is shown in figure 21. The rate of change of the resistivity as a function of current density increases with increasing field. Sample #1 and #3 have a similar current dependent resistivity.

$d\rho/dJ$ at a current density of 2.17 A/cm^2 is plotted as a function of applied magnetic field for sample #2 in figure 22. The error bars were determined from two sets of V(I) curves. The maximum $d\rho/dJ$ value as a function of field for this sample and current density occurs at 0.75±0.05 T. $d\rho/dJ$ as a function of field at a current density of 1.0 A/cm^2 has a maximum at the same position, however, the magnitude of the peak is larger by a factor of 1.6.

A similar behaviour of $d\rho/dJ$ as a function of field is observed for sample #3. However, the maximum value for $d\rho/dJ$

Figure 21

ρ as a function of current density for sample #2 for the applied fields; 0.35 T K (o), 0.40 T (■), 0.45 T (x), 0.5 T (●), 0.55 T (+), 0.6 T (▵).

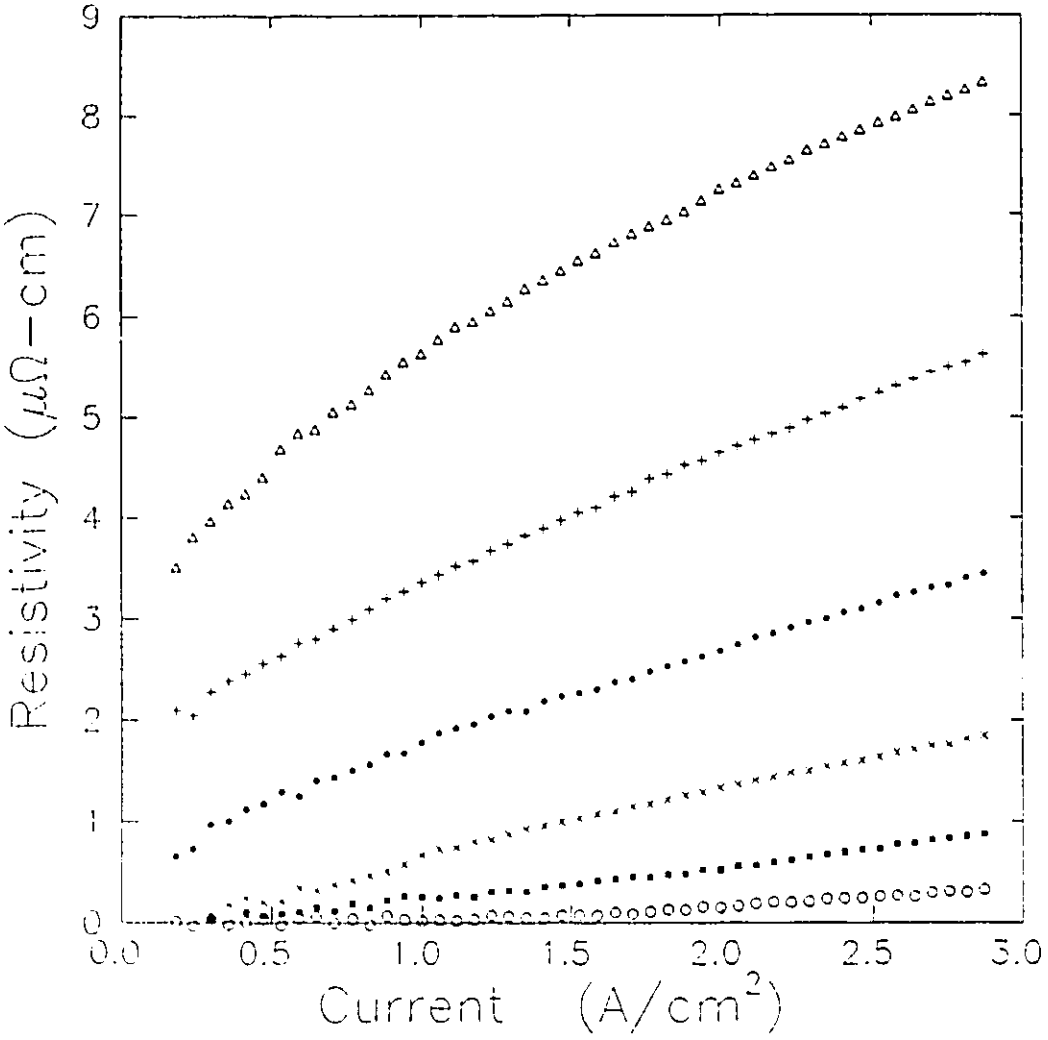
Resistivity ($\mu\Omega$-cm)
Current (A/cm^2)
0
1
2
3
4
5
6
7
8
9
0.0
0.5
1.0
1.5
2.0
2.5
3.0

Figure 21

Figure 22

$d\rho/dJ$ at 2.17 A/cm^2 as a function of applied magnetic field for sample #2 at 77 K. The solid line is a guide to the eye.

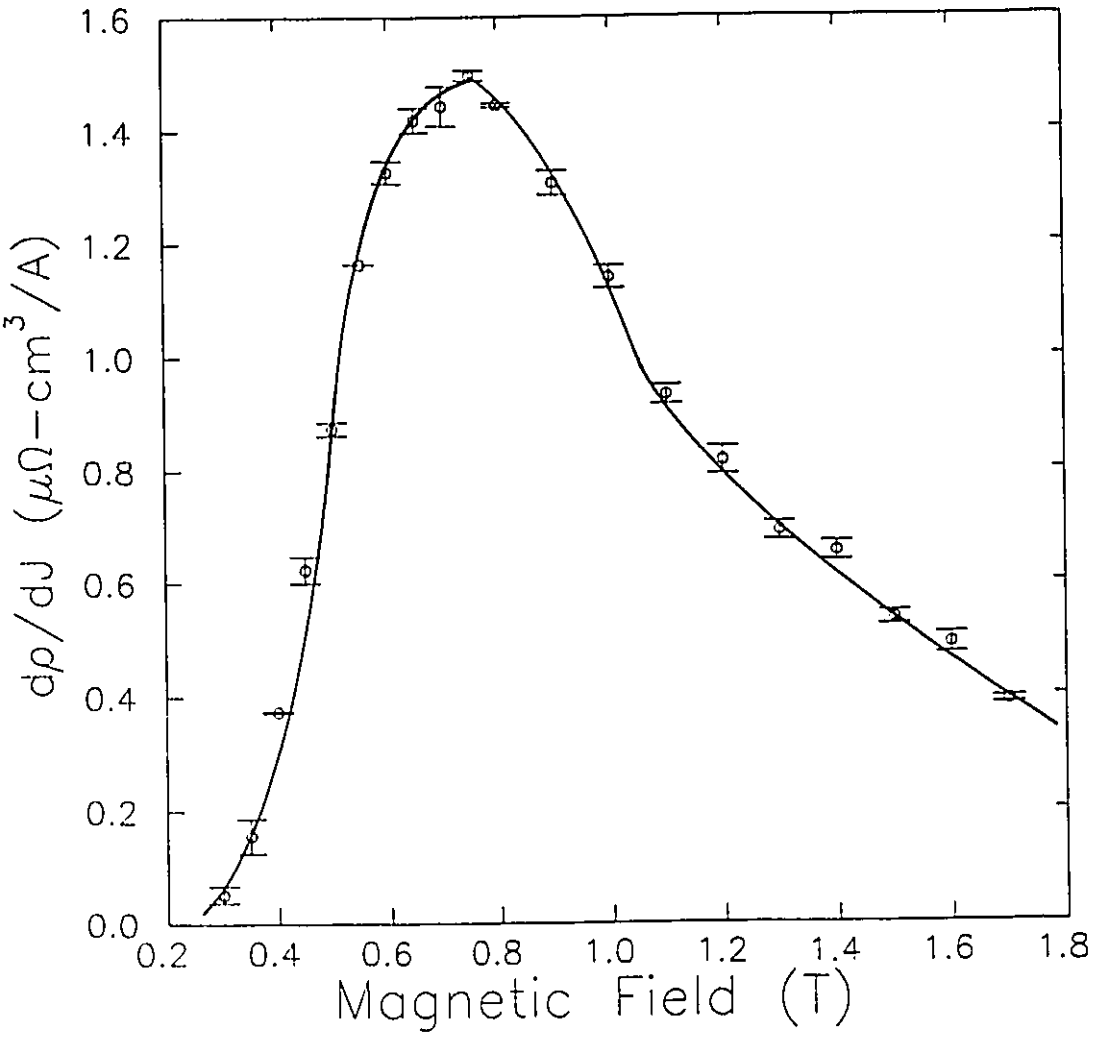
1.6
1.4
1.2
1.0
0.8
0.6
0.4
0.2
0.0
dρ/dJ (μΩ−cm³/A)
0.2
0.4
0.6
0.8
1.0
1.2
1.4
1.6
1.8
Magnetic Field (T)

Figure 22

at the current density of 1.0 A/cm^2 occurred at 1.0±0.1 T with a value of 2.7±0.2 $\mu\Omega$-cm^3/A. For sample #1, dρ/dJ at 0.31 A/cm^2 increased with increasing applied field from a value of 0 $\mu\Omega$-cm^3/A at 0.6 T up to 9 $\mu\Omega$-cm^3/A at 1.7 T.

D. DISCUSSION

The variation of the magnitude of the resistive tails and values of T_c^0 in zero field implies a range of weak link characteristics for the samples investigated. In terms of our model for a distribution of weak links, those samples with a larger zero field resistive tail and lower T_c^0 for a given current density have a distribution of weak links that includes weak links in the transport current path with lower T_c's and I_c's. Applying this criteria to the samples measured we can order them in terms of the strength of coupling between grains. The sample with weak links in the transport current path with the lowest T_c's and I_c's is sample #2. Sample #1 has weak links in the transport current path that on average have the largest T_c's and I_c's of the samples investigated. Samples #3 and #4 fall between the range defined by samples #1 and #2 as can be seen from a comparison of the relative magnitude of their resistive tails and T_c^0.

The current dependence of the resistivity in the zero field resistive tail can be interpreted in terms of the number

of weak links that switch from superconducting to dissipative at a particular current density and temperature. Experimentally, we have related this to $d\rho/dJ$ at that current density and temperature. The presence of a range of weak link strengths and the percolative nature of the transport current path imply that not all weak links will switch at the same temperature. This implies that the current dependence of the resistivity should vary over the entire range of the resistive tail. The variation of the current dependence of the resistivity as observed in figure 20 can be explained in terms of a variation of the number of weak links that can be switched from superconducting to dissipative at a specific current density and temperature. Warming from the superconducting state this number increases with temperature reaching a maximum. As the temperature approaches the steepest portion of the resistive transition at 107 K the number of weak links that can be switched from superconducting to dissipative decreases since most of the superconducting grains have been decoupled from each other.

To summarize: The weak link intergranular transition is associated with the current dependent resistive tail in zero field resulting from a distribution of weak link strengths present in the transport current path. Next, we want to consider the effect a magnetic field has on the intergranular superconducting transition.

Samples with weak links with lower T_c's and I_c's in the transport current path also demonstrate greater broadening in a magnetic field. This suggests that the application of a magnetic field suppresses the weak link intergranular transition more in these samples. This can be seen from a comparison of the relative broadening of samples #1 to #4 in a 1.2 T field in figures 14 and 15.

In samples characterized by lower I_c and T_c weak links, the application of a small magnetic field resolved a broad maximum in $d\rho/dT$ which disappeared into a broad hump with increasing applied magentic field as observed in figures 17 an 18. We propose that the broad maximum or hump present in the $d\rho/dT$ curves of the polycrystalline samples, but not in the $d\rho/dT$ curves of the single crystal data, is due to a superposition of the weak link *intergranular* transition on top of the *intragranular* transition. The shift of the broad hump to lower temperatures with increasing applied field is, therefore, interpreted as a suppression of the intergranular transition with the application of a magnetic field.

Given that the *intergranular* transition is superimposed on the *intragranular* transition it is expected that features in the $d\rho/dT$ curves are due to a combination of the two transitions. In particular, the initial increase of the temperature at the peak, T_p, with applied field can be

explained in this case. In zero field, the temperature at which some of the weak links become superconducting is very close to the intergranular superconducting transition temperature. Since the weak links in the *intergranular* transition have a T_c that is just below that occurring within grains, the net affect of these weak links is to suppress the entire superconducting transition, the sum of the *intergranular* and *intragranular* superconducting transitions. This results in a suppressed T_p in zero field. When a magnetic field is applied, the *intergranular* transition is suppressed, while the *intragranular* transition remains relatively unchanged as seen in the single crystal data. T_p now represents the intragranular transition to a greater extent since the two transitions are no longer as closely superimposed upon one another. This results in a shift up of T_p with applied field. Likewise, the broadening of the *intragranular* transition may be expected to distort the smaller but broader *intergranular* transition.

The current dependence of the resistivity in a magnetic field is in marked contrast to the linear V(I) curves observed in single crystal work in a magnetic field for about the same range of current density as seen in figure 4. In the crystal case the V(I) curves are strictly linear indicating purely ohmic behaviour, while the current dependence of the

resistivity in polycrystalline high temperature superconductors shows a magnetic field dependence as seen in figures 21 and 22.

The behaviour of $d\rho/dJ$ at a particular current density as a function of applied magnetic field is similar to the behaviour of the same quantity as a function of temperature. This can be seen from a comparison of figures 20 and 22. Likewise, we attribute this behaviour to a similar mechanism. However, rather than an increase in temperature that results in a decoupling of the superconducting grains, an increase in the applied magnetic field does so. The maximum value of $d\rho/dJ$ occurs at the magnetic field at which the maximum number of weak links can be switched from superconducting to dissipative for the applied current density. At the highest applied fields most of the weak links for the applied current density have been decoupled and, therefore, the current dependence of the resistivity is less. This effect is due only to the *intergranular* transition since the *intragranular* transition as measured in the single crystals in this current and field range exhibits only ohmic behaviour. That the application of a magnetic field decouples superconducting grains and leads to a suppression of the intergranular transition is in agreement with the results of the $d\rho/dT$ analysis that suggest that the magnetic field suppresses the weak link intergranular transition.

A comparison of the field at which the maximum value of $d\rho/dJ$ occurs for the different samples indicates that this field is lower for samples characterized by lower T_c and I_c weak links. This implies that smaller magnetic fields are required to decouple the superconducting grains at a specific temperature for these samples. This behaviour agrees with the observation of a stronger suppression of the intergranular transition to lower temperatures with applied magnetic field in the lower T_c and I_c samples.

E. CONCLUSION

Resistivity measurements of two Sn and two Sb doped BiPbSrCaCuO polycrystalline samples indicated a range of weak link characteristics in the superconducting properties of the samples. A model for the intergranular transition, the superconducting transition between grains, was described incorporating the presence of a range of weak link strengths for each sample. A distribution of critical currents and critical temperatures for individual weak links making up the weak link structure of each sample was used to explain variations in the onset of zero resistivity and size of the zero field resistive tail amongst the various samples. A determination of the derivative of the resistivity with respect to temperature, $d\rho/dT$, in applied magnetic field

revealed a dual superconducting transition when results were compared with results of $d\rho/dT$ in a magnetic field in a single Bi:2212 crystal. The dual superconducting transition was interpreted as a superposition of an *intergranular* transition on top of an *intragranular* superconducting transition. Both transitions were broadened with the application of a magnetic field. While the *intragranular* transition remained relatively fixed in temperature the *intergranular* transition showed a strong magnetic field dependence. The *intergranular* transition was strongly suppressed with increasing applied magnetic field. Samples characterized as having weaker coupling between superconducting grains, demonstrated a greater suppression of the intergranular transition in an applied magnetic field.

The presence of a current dependent resistivity in zero field that varies over the resistive tail region was taken as indicative of the presence of a weak link structure and the intergranular transition. This current dependence was maintained at 77 K with the application of a magnetic field. The application of a magnetic field had the same qualitative effect on the current dependence of the resistivity as an increase in temperature had on the zero field resistive tail current dependence. This is further support for an intergranular transition description that is valid for the applied field case.

CHAPTER VII

POTENTIOMETRIC RING

A. INTRODUCTION

The measurement of the voltage transverse to the applied current direction is a technique applied in a variety of situations for the investigation of the superconducting transition in high temperature superconductors. Measurements of the magneto-thermoelectric effects in high temperature superconducting $Tl_2Ba_2CaCu_2O_y$ crystals were performed by Koshelev *et al.* (1991). In these measurements a transport current and a temperature gradient were applied perpendicular to each other, both lying within the base plane of the crystal. The measured transverse voltage had a temperature dependence which depended on both the temperature gradient and the current. A crossover from negative to positive measured transverse voltage was observed as the sample went through its bulk superconducting transition. Measurements of the Hall voltage by Iye *et al.* (1989) on sputtered thin films also demonstrate a change in the sign of the transverse voltage as the sample goes through its bulk superconducting transition. Gridin and Datars (1991) measured the transverse voltage across separate branches in each of two ring shaped polycrystalline $Bi_{1.6}Pb_{0.4}Sr_2Ca_2Cu_3O_y$ samples. A small minimum in

the transverse voltage was observed in the region of the bulk superconducting transition. To further elucidate the nature of results obtained by measuring the transverse voltage in the region of the bulk superconducting transiton, measurements of the transverse voltage of a $Bi_2Sr_2CaCu_2O_y$ diffused thick film ring were performed.

B. METHOD

The thick film ring was patterned from a diffusion grown thick film sample which had been prepared as described in the sample preparation section. The ring consisted of branches 1.7 mm wide with a hole 4.6 mm in diameter in its centre. One branch had a thickness of 76 μm and the other 120 μm. Silver paste contacts were placed on the sample as shown in figure 2. Contact pair 1-2 were for the transport current. Contact pair 3-4 were used to measure the longitudinal voltage, V_L. The contact pair 5-6 were for the measurement of the transverse voltage, V_T. The thick film ring provided two superconducting paths with different textures as determined by x-ray diffraction and scanning electron microscopy. The application of a magnetic field parallel and perpendicular to the sample surface confirmed texturing in the sample. Measurements of the

transverse voltage V_T in a magnetic field confirmed that the branches were differentially textured.

Two transport currents were applied to the potentiometric ring sample. These were 1.0 and 5.0 mA which produced a current density of approximately 0.3 A/cm^2 and 1.5 A/cm^2, respectively. Unless otherwise indicated all results reported here are for the 1.0 mA applied transport current.

After measurements on the thick film ring were completed the sample was separated into its two branch components. Voltage as a function of current at fixed temperature was then measured on a portion of each of the two branches. Eleven equivalent current densities ranging from 0.04 A/cm^2 to 2 A/cm^2 were applied to each portion. The measurements confirmed the differential texturing and difference in resistance due to thickness between the two branches. As well, a difference in the critical temperatures within the two branches was observed. The branch with the lower T_c also had a broader superconducting transition.

Measurements of x-ray diffraction, scanning electron microscopy and resistivity on separate portions of the branches were consistent with measurements of the temperature dependent behaviour of the transverse voltage on the ring. A change in sign of the transverse voltage as the temperature was increased from below the bulk superconducting transition

could be understood in terms of relative changes in the temperature dependence of the resistances in portions of the two branches.

C. RESULTS

Both x-ray and scanning electron microscope measurements demonstrate the differences in textural structure between the two halves of the ring. X-ray data for the upper and lower halves of the ring are represented by figure 23(a) and figure 23(b), respectively. Figure 23(a) is the x-ray plot of a 120 μm thick film corresponding to the upper branch of the potentiometric ring. Figure 23(b) is the x-ray plot for a 76 μm thick film. The presence of a larger (200) peak relative to the other peaks in figure 23(b) is a clear indication of more crystallites with the a axis parallel to the normal of the plane for the lower 76 μm thick branch. The x-ray diffraction of the 120 μm thick film indicates less a-axis texturing and more crystallites with random orientation with respect to the normal. This result verifies work by Ummat *et al.* (1991) who demonstrated a correlation between texturing and the thickness of the applied diffusion film with the greatest texturing occuring for a diffusion film of thickness 76 μm.

Scanning electron micrographs at 1000x magnification of the upper and lower branches of the ring, respectively, are

Figure 23(a)

Relative intensity of x-ray diffraction for 120 μm thick film as a function of angle 2θ from 10° to 60°.

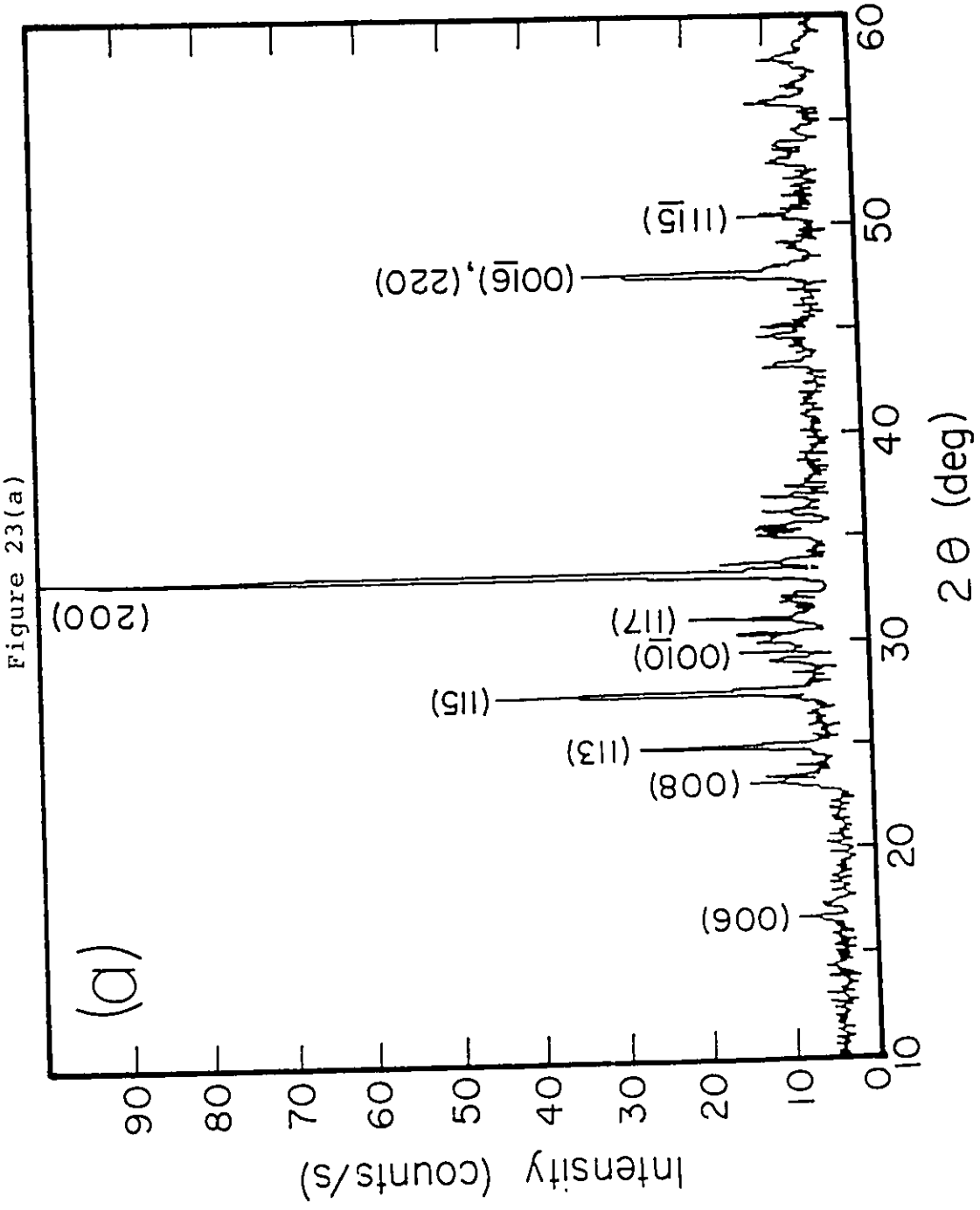
(a)
Intensity (counts/s)
2θ (deg)
(006)
(008)
(113)
(115)
(0010)
(117)
(200)
(00$\bar{1}$6), (220)
(111$\bar{5}$)

Figure 23(a)

Figure 23(b)

Relative intensity of x-ray diffraction for 76 μm thick film as a function of angle 2θ from 10° to 60°.

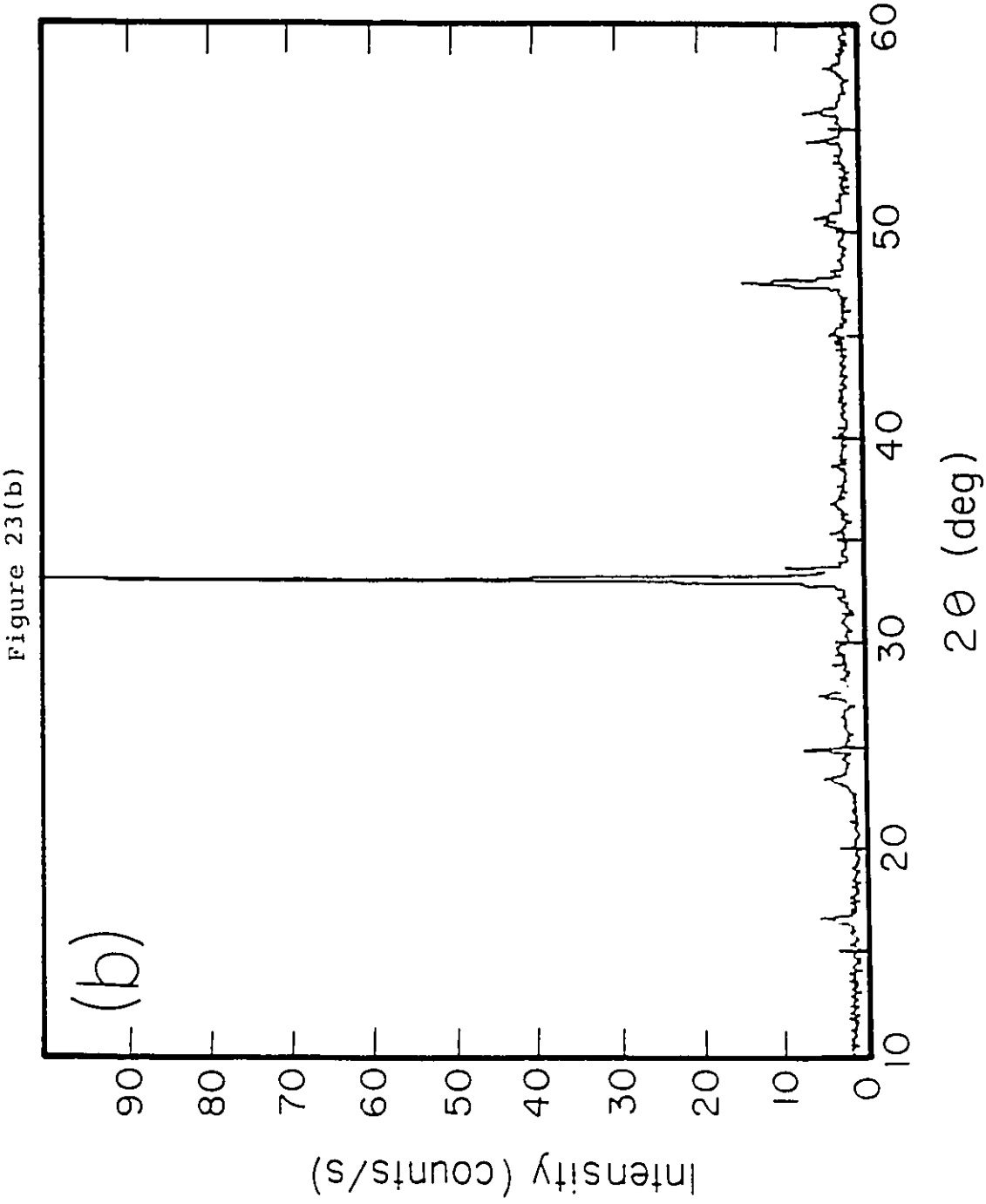
(b)
Intensity (counts/s)
2θ (deg)
0
10
20
30
40
50
60
70
80
90
10
20
30
40
50
60

Figure 23(b)

presented in figure 24(a) and figure 24(b). There is a larger number of crystalline platelets pointing out of the sample plane in figure 24(b) than in figure 24(a). Platelets that lie flat on the substrate surface can be seen in the lower left portion of figure 24(a). Micrographs at 530x magnification demonstrate a finer granular structure with more platelets appearing to lie flat on the sample surface on average for the upper branch. Since $Bi_2Sr_2CaCu_2O_y$ grows with its thinnest direction parallel to the c axis, we conclude that for the lower branch represented by figure 24(b) a larger fraction of platelets is oriented with the c axis perpendicular to the normal of the plane. The c axis of these platelets lie on or close to the normal of the plane. As well, the finer granular structure indicates the presence of many more grain boundaries for the upper branch of the ring.

To summarize the results of the x-ray and scanning electron micrographs; the upper branch of the ring has a finer granular structure with crystallites oriented more randomly. The greater a-axis texture of the lower branch implies an overall greater alignment of the grains. The lower branch has more large platelets and therefore fewer grain boundaries.

Figure 25 shows the zero-field results for the transverse voltage, V_T, and the longitudinal voltage, V_L, measured between the contact pairs 5-6 and 3-4, respectively.

Figure 24(a)

Scanning electron micrograph taken from the upper 120 μm thick branch.

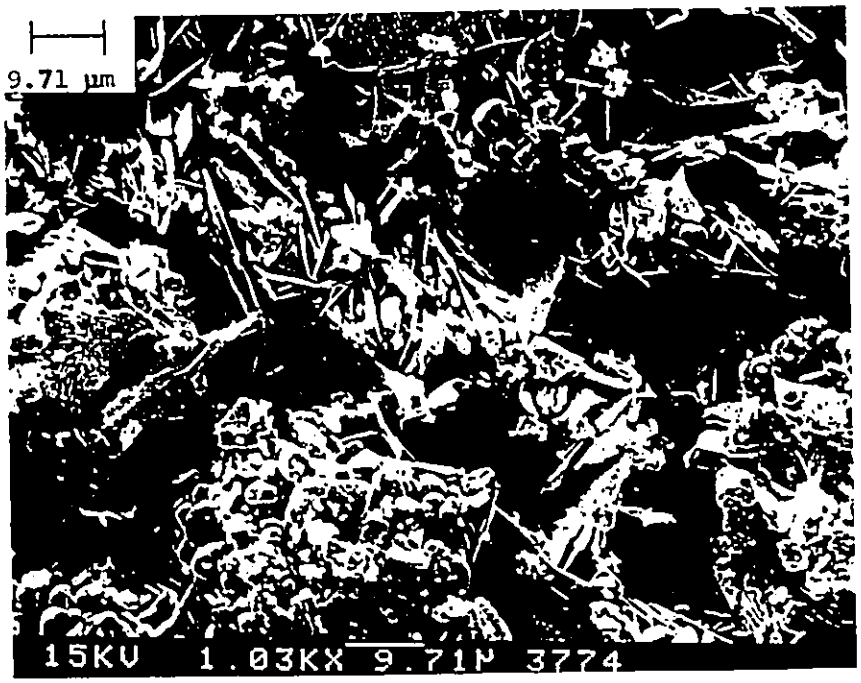

Figure 24(a)

Figure 24(b)

Scanning electron micrograph taken from the lower 76 µm thick branch.

Figure 24(b)

Figure 25

Comparison of the temperature dependence of the longitudinal and transverse voltages for 1.0 mA applied current. The curve represented by the open circles is the longitudinal voltage. The solid curve is the transverse voltage with units on the right hand side of the graph.

Figure 25

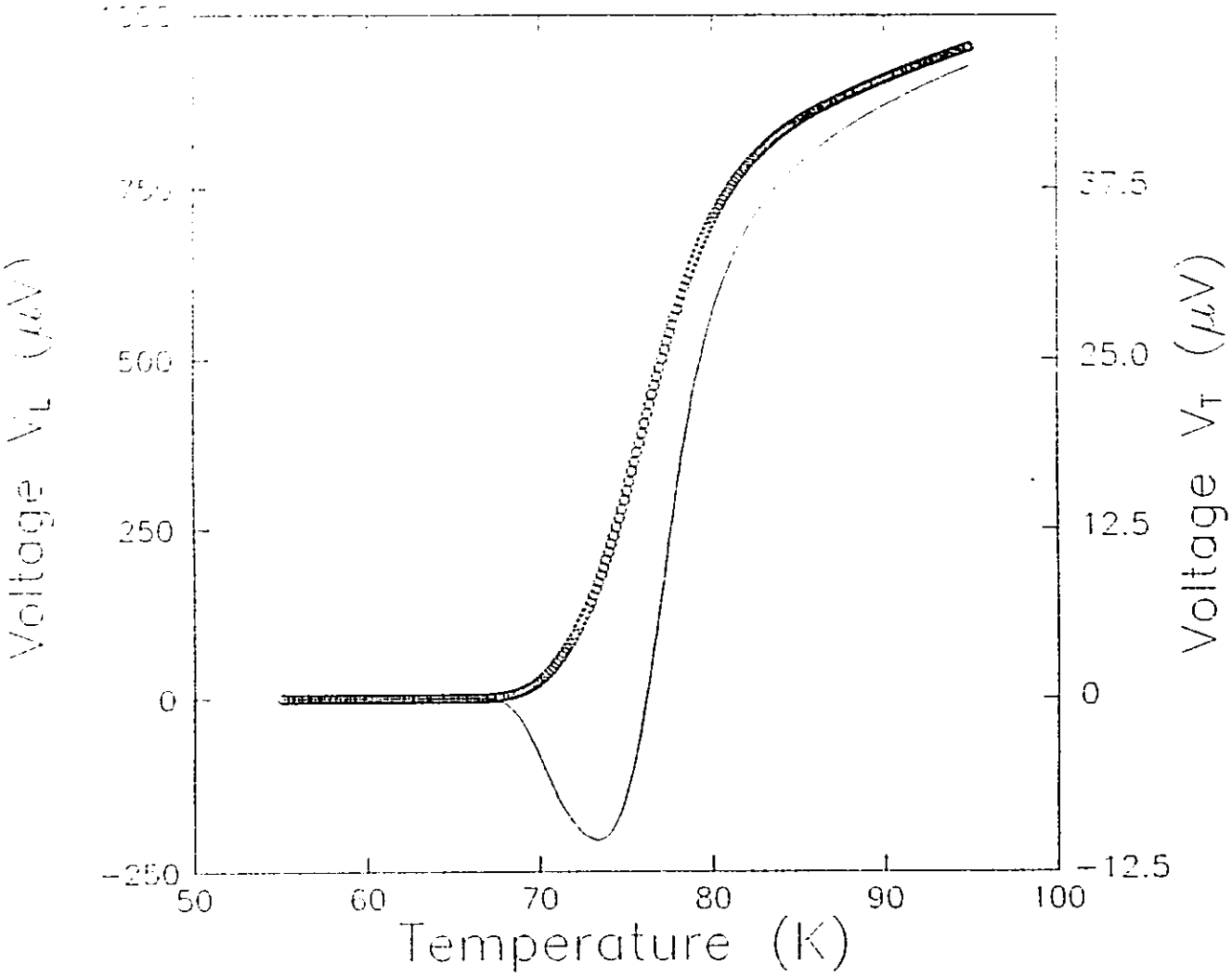
Voltage V_L (μV)
500
250
0
−250
50
60
70
80
90
100
Temperature (K)
25.0
12.5
0
−12.5
Voltage V_T (μV)

Both voltages were measured with a current of 1 mA. The solid line represents V_T with its corresponding scale on the right hand side of the graph. V_T is approximately 20 times smaller than V_L. The onset of V_T begins at 67.1±0.3 K. V_L begins 0.5 K higher than V_T (in magnetic fields this difference grows to 2 K). The minimum in the dip at 73.4±0.1 K is below a T_p of 75.4±0.1 K that was determined from the peak of the temperature derivative of the longitudinal voltage plotted versus temperature. V_T changes sign at 76.1 K. As expected, well above the transition, the temperature dependencies of V_T and V_L are similar. Here the linear response given by equation 14 is applicable and V_T measures the 5-6 contact mismatch.

The effect on the longitudinal resistance $R_L(T)$ of an external field of 0.5 T applied parallel ($H \| \mathbf{n}$) and perpendicular ($H \perp \mathbf{n}$) to the normal of the sample plane (in both cases $H \perp I$, where I is the current passing between the 1-2 pair) is shown in figure 26. The dissipation occurs at a lower temperature for $H \perp n$ than for $H \| \mathbf{n}$.

Figure 27 shows the reduction of the minimum in the temperature dependence of V_T for increasing magnetic field values in the $H \| \mathbf{n}$ geometry.

The transverse resistance R_T is shown in figure 28 for two different currents, 1.0 mA and 5.0 mA, with a 1.1 T field

Figure 26

Temperature dependence of $R_{\perp}$ for a 0.5 T magnetic field oriented parallel (□) and perpendicular (●) to the normal of the plane.

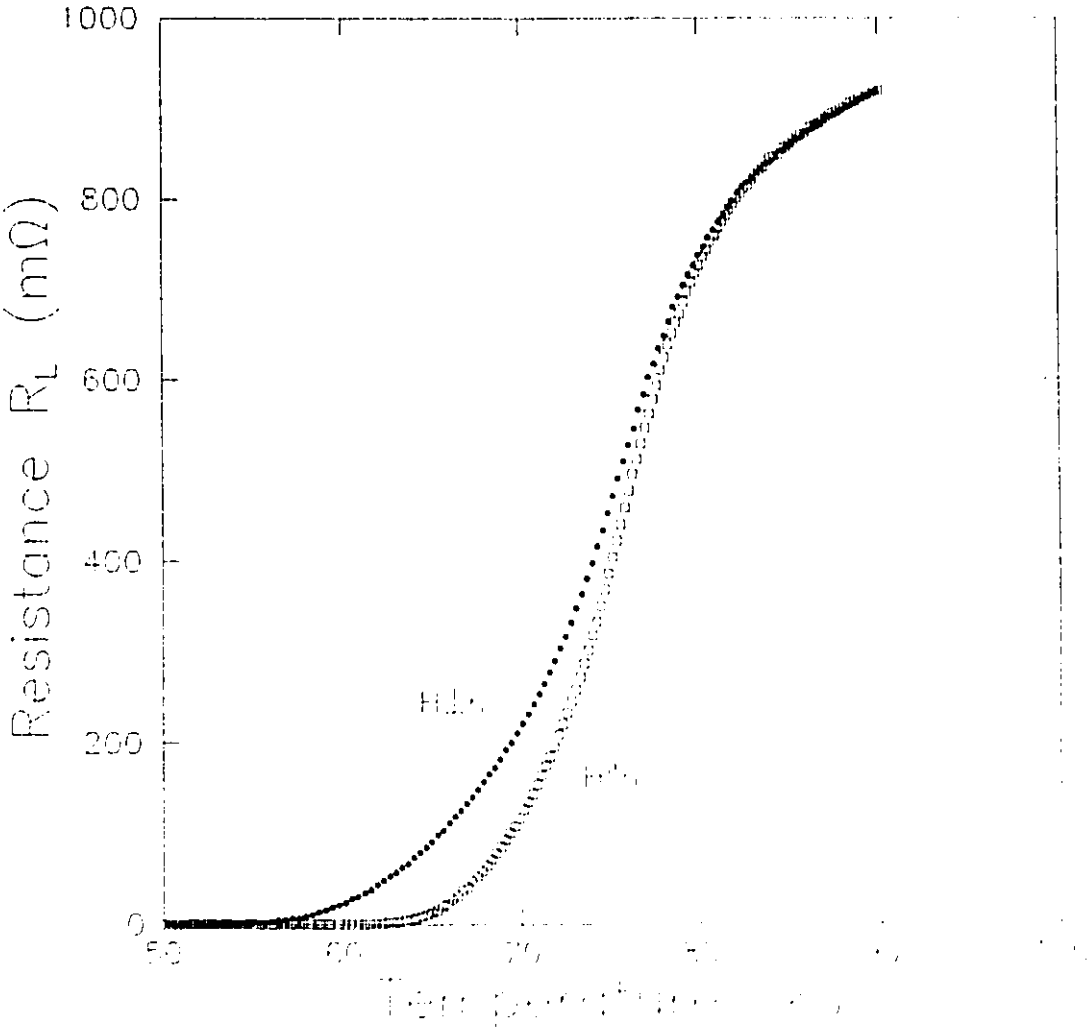

Figure 26

Figure 27

Temperature dependence of V_T in 0.3 T (+), 0.5 T (▲), 0.75 T (□), 1.1 T (■) and 1.6 T (o) applied magnetic fields.

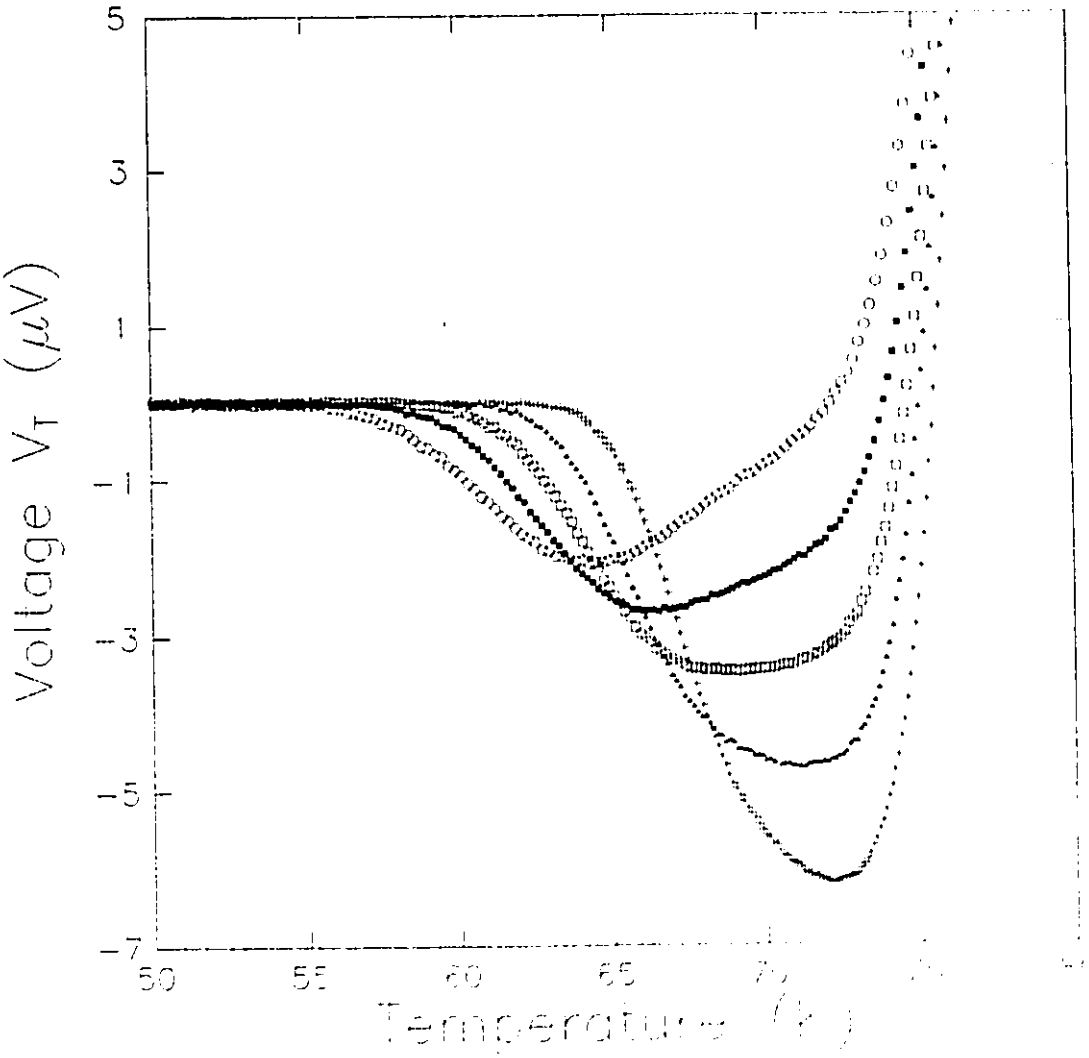

Figure 27

Figure 28

Transverse resistance, R_T, as a function of temperature in a 1.1 T field for two currents 1.0 mA (open circles) and 5.0 mA (solid line).

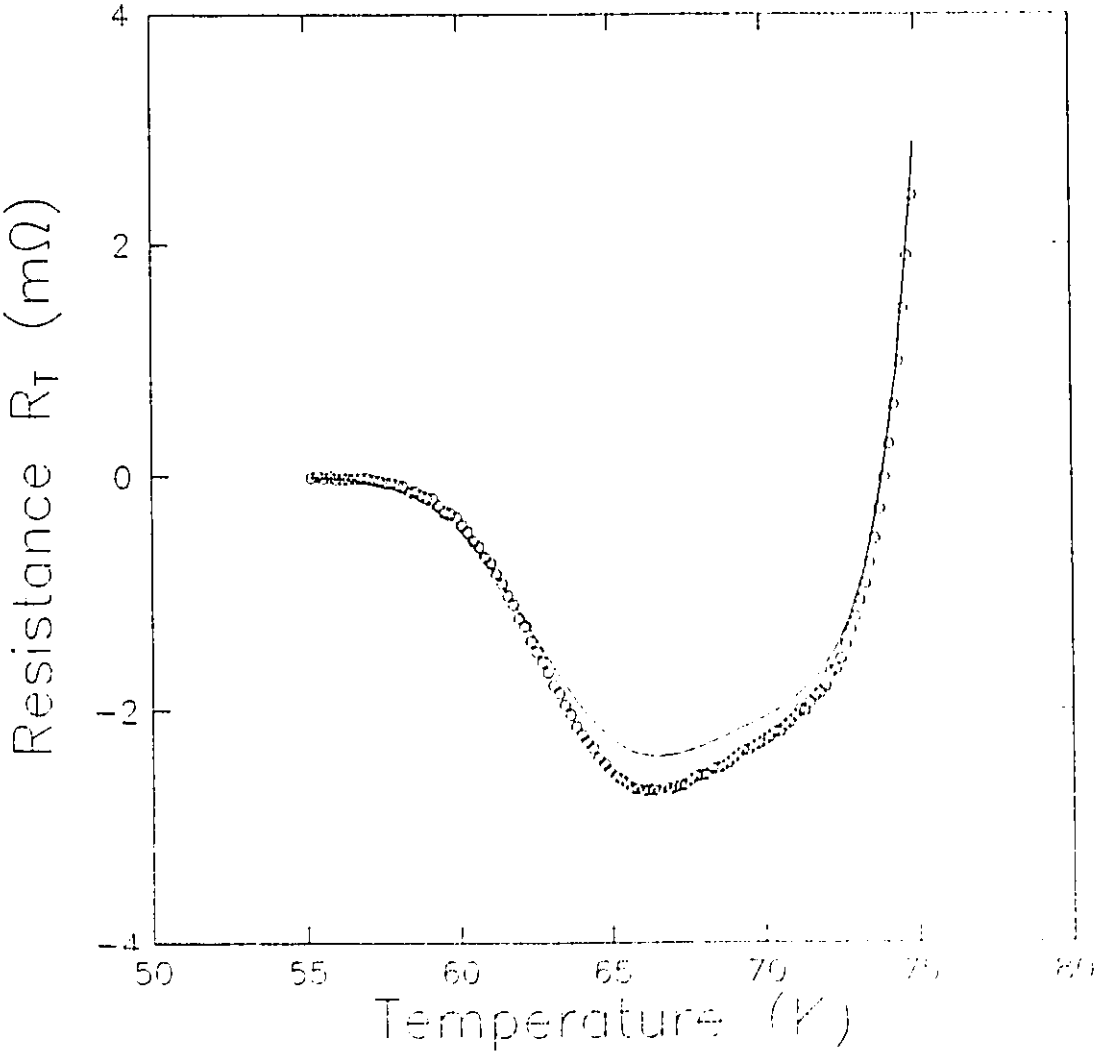

Figure 28

applied parallel to the normal of the plane. The resistance depends on current for temperatures between 60 and 75 K. The resistance depended on current for all fields investigated.

Figure 29 shows V_T with H⊥**n** and H∥**n** for a 0.5 T field. Here the minimum in V_T is considerably smaller for H⊥**n** than for H∥**n**.

The area between the zero voltage line and $V_T(T)$ is plotted in figure 30 versus the applied magnetic field for the two orientations H∥**n** and H⊥**n**. The area, obtained by a numerical trapezoidal technique, decays exponentially with field. The decay is much more rapid with the magnetic field oriented perpendicular to the normal.

The normalized resistivity in zero fields versus temperature is plotted for the samples in figure 31 for the 76 μm thick branch (dashed curve) and for the 120 μm thick branch (solid curve). For the 76 μm sample the temperature at the peak of the $d\rho/dT$ curve, T_p is 80.7±0.1 K and the width of the peak at half maximum is 6 K. The onset of resistivity is at 67.6±0.3 K. In a magnetic field of 1.0 T parallel to the normal of the sample plane, **n**, T_p is 81.1±0.1 K. For the 120 μm sample, the T_p in zero field is 77.7±0.2 K with a width of the peak at half maximum of 8 K. The onset of resistivity is at 66.5±0.3 K. In a magnetic field of 1.0 T parallel to the normal of the sample plane, **n**, T_p increased to 78.4±0.2 K.

Figure 29

Transverse voltage as a function of temperature for 0.5 T applied parallel (□) and perpendicular (●) to the normal of the sample plane.

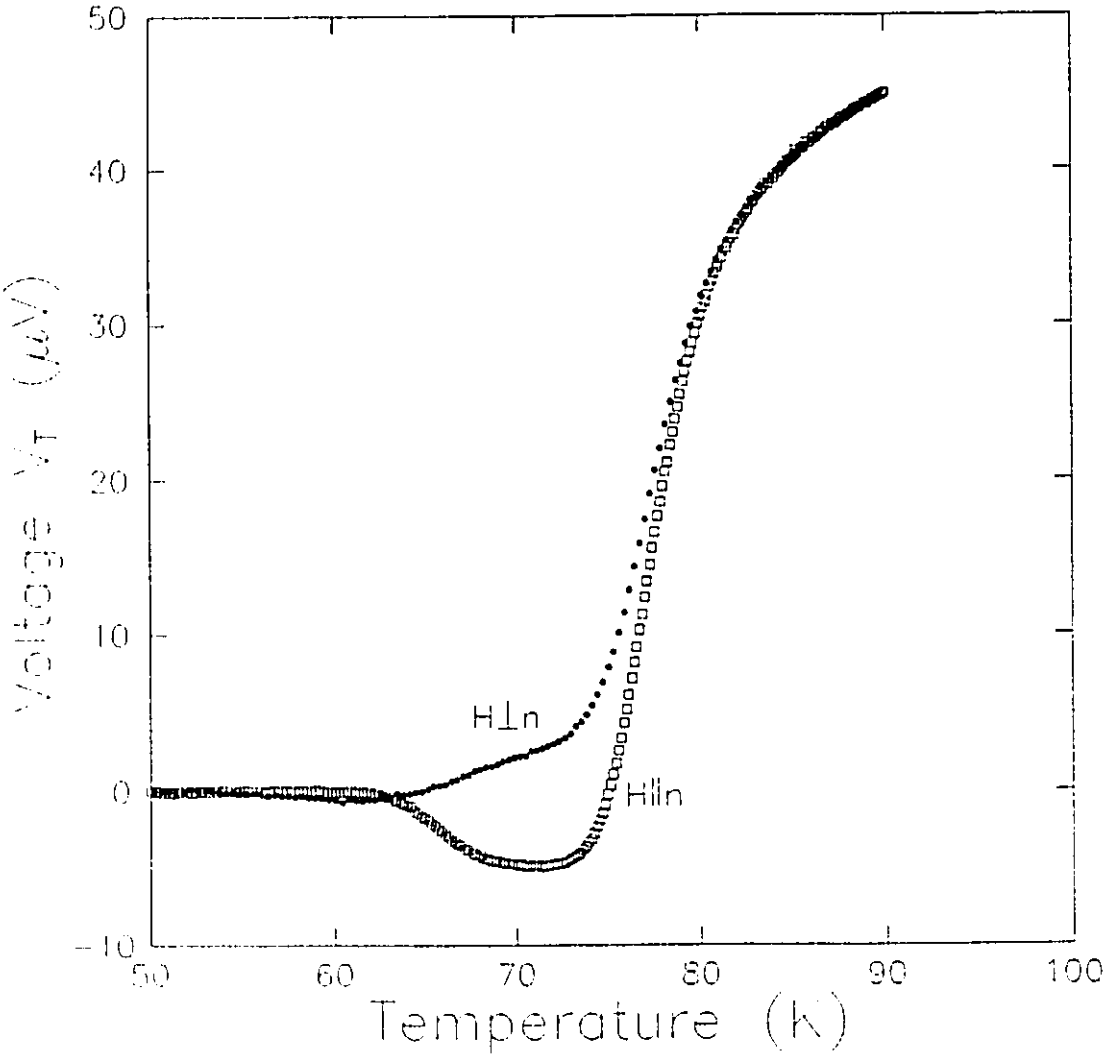
50
40
30
20
10
0
-10
50
60
70
80
90
100
Voltage (μV)
Temperature (K)
H⊥n
H∥n

Figure 29

Figure 30

Area under the V_T=0 line as a function of magnetic field applied parallel (o) and perpendicular (+) to the sample normal.

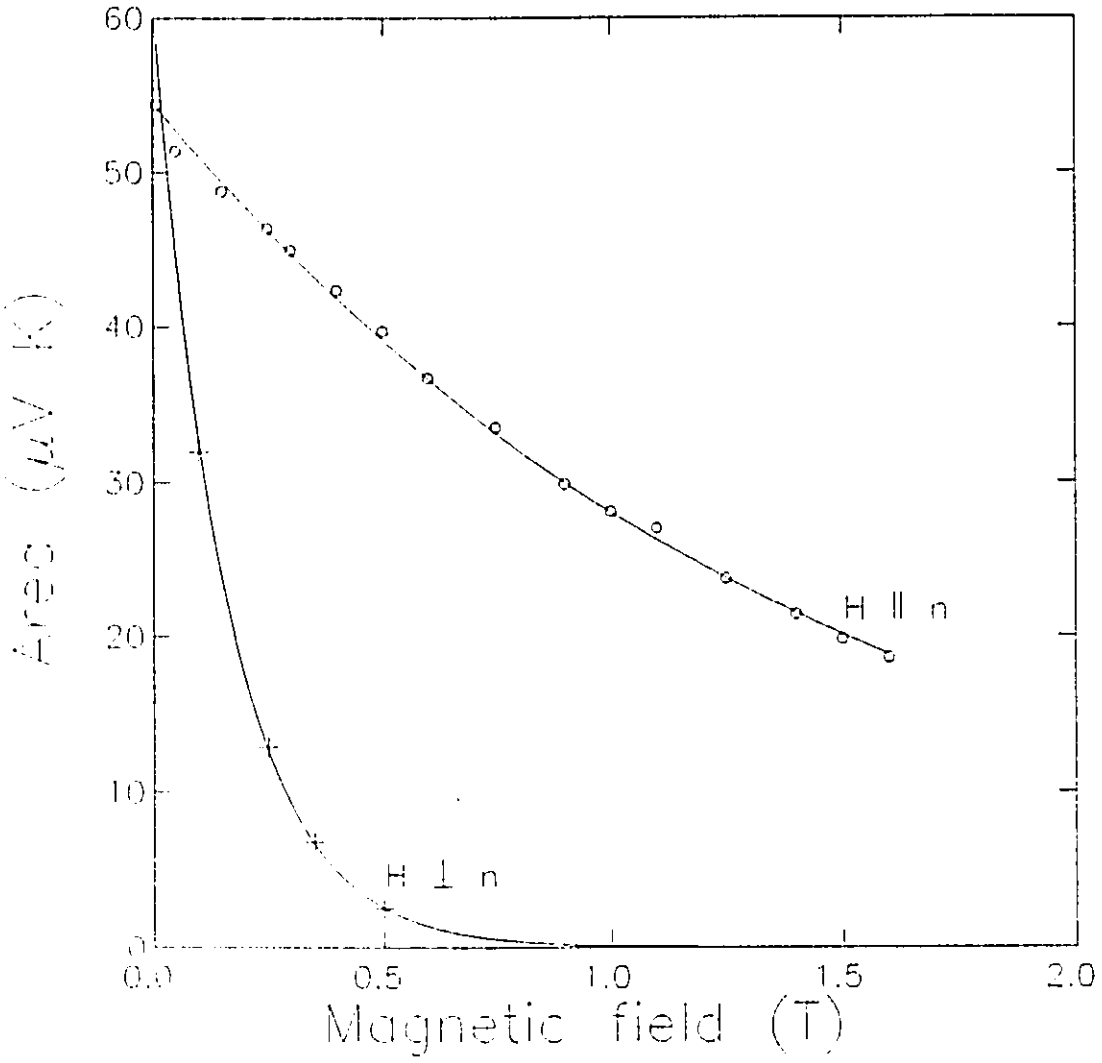

Figure 30

Figure 31

Resistivity normalized by resistivity at 105 K as a function of temperature for separated portions of the lower 76 μm thick branch (- - -) and the upper 120 μm thick branch (_____).

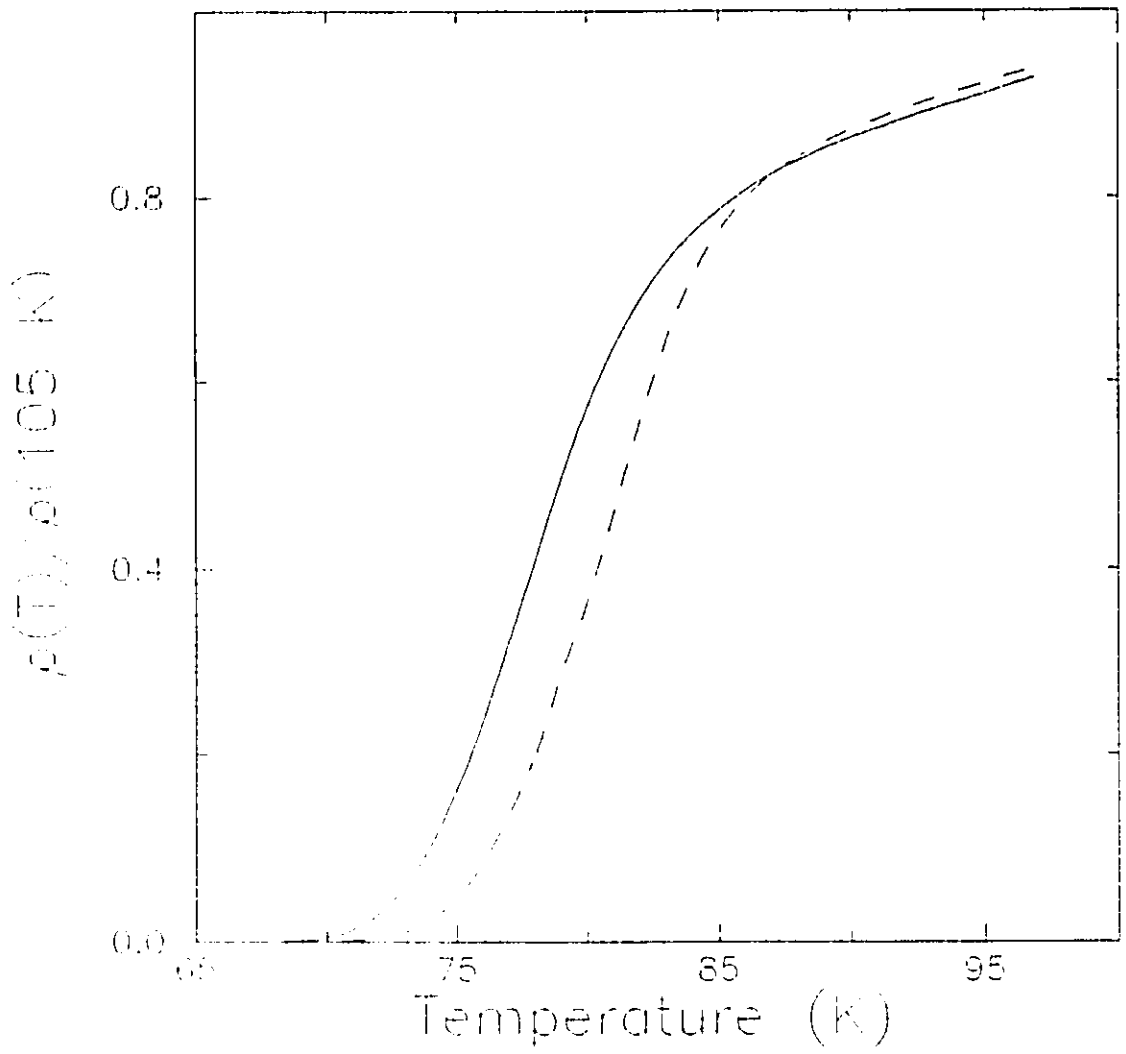

Figure 31

Figure 32

Voltage as a function of current density at the temperatures 44.6 (o), 45.1 (+), 45.7 (□), 46.8 (◇), 47.4 (*), 47.9 (●), 48.1 (□) and 48.5 (x) K in a field of 1 T. Solid lines are quadratic best fits to the data and are only to guide the eye.

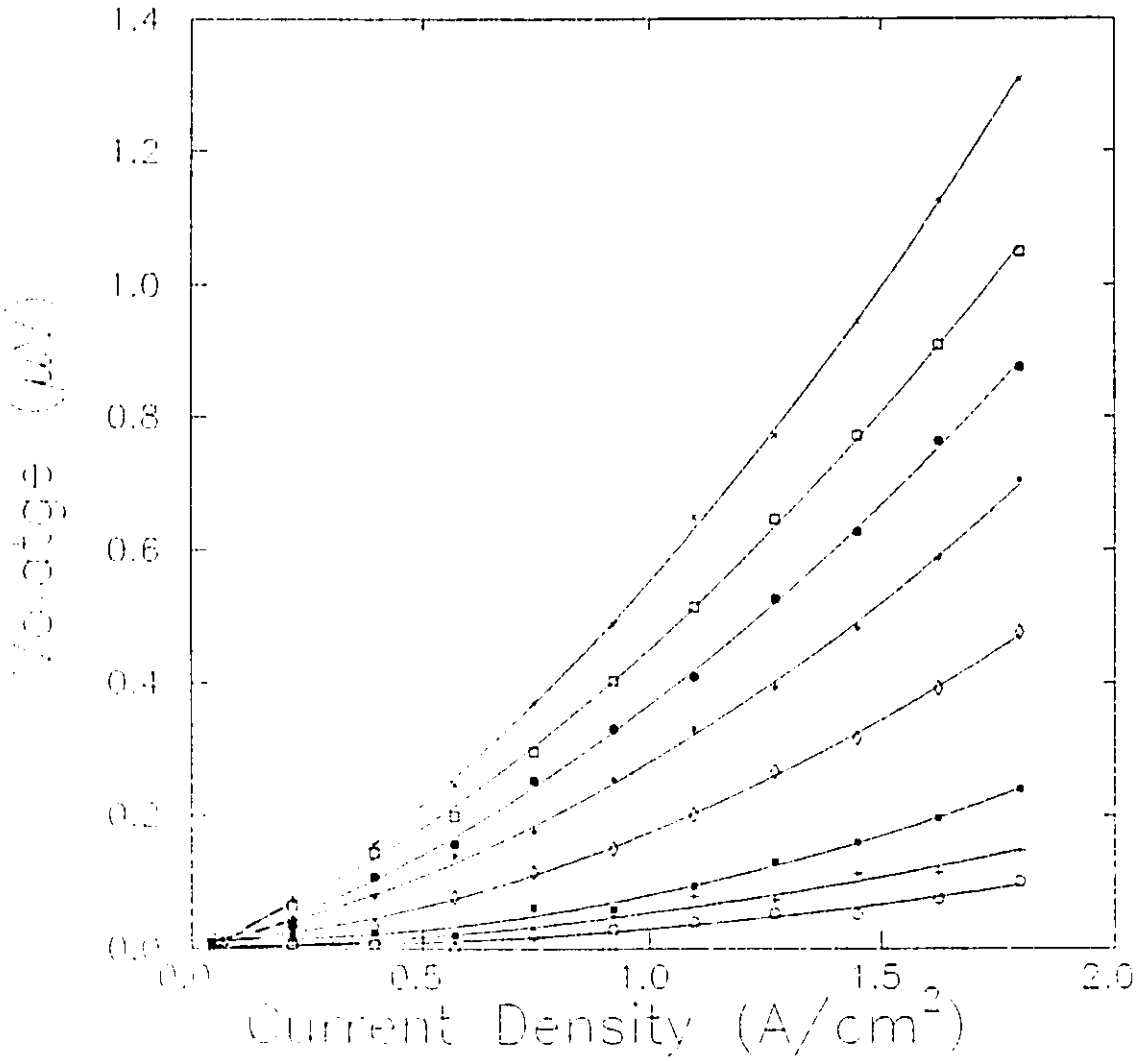

Figure 32

While the distance between the voltage contacts and the width of the two samples were about the same the resistance of the 120 μm branch was about 1/2 that of the 76 μm branch. Therefore, values of the resistance were in agreemet with the difference in thickness between the two branches.

Voltage as a function of current for the 76 μm sample is plotted in figure 32. The solid curves are quadratics best fit to the data and demonstrate the nonlinearity of the IV curves.

D. DISCUSSION

A negative voltage minimum was observed in the transverse voltage, V_T as shown in figure 25. The presence of this minimum can be understood in terms of the resistive superconducting transition for portions of each branch as shown in figure 31. Figure 31 demonstrates that the upper 120 μm thick branch has a lower critical temperature, indicated by the smaller value of T_p, than the lower 76 μm thick branch. As the sample is warmed up through its superconducting transition there is dissipation in the upper branch first, while the lower branch is still superconducting and carries all the current as described by equation 15. This explains the fact that the onset of V_T always occurs at a lower temperature than V_L. Measurements of V_T in the critical region are very

sensitive to any differences in dissipation between the two branches.

To explain the temperature dependence of V_T in the critical region where both branches of the ring are resistive we consider the difference in the relative ratios of resistances in portions of the upper and lower branches, $\Re(T)$ as defined in equation 17. The sign of $\Re$ corresponds to the sign of the transverse voltage. If R_L is zero and R_U is finite, it can be seen from equation 17 (since $R_L=R_{1L}+R_{2L}$) that $\Re$ will be zero and therefore, from equation 16, V_T is zero. As the temperature is increased dissipation occurs in both branches and a finite transverse current is produced. Since V_T changes sign at higher temperatures we initially take V_T to be negative and therefore, from equation 13 $\Re$ is also negative. The negative minimum in V_T corresponds to the maximum product of $\Re$ and the sum of R_{1L} and R_{1U} below T_c. Defining the resistances between the contact pair 4-5 in the upper branch as R_{2U} and between the contact pair 6-4 in the lower branch as R_{2L} equation 17 can be written as

$$\Re(T) = \frac{R_{1L}R_{2U}-R_{1U}R_{2L}}{(R_L+R_U)(R_{1L}+R_{1U})} \quad , \tag{22}$$

where $R_L=R_{1L}+R_{2L}$ and $R_U=R_{1U}+R_{2U}$. From equations 16 and 22 it can be seen that V_T is zero when the condition $R_{1L}R_{2U}=R_{1U}R_{2L}$ is satisfied. This occurs at the temperature when V_T crosses over

from a negative to positive value. That the voltage V_T changes sign is a result of the fact that for a certain temperature range below the superconducting transition of both branches, the lower branch carries a larger current. Above T_c, where the resistivities of the two branches are about the same, the thicker upper branch carries the larger current. In the normal state V_T resembles V_L due to current and transverse voltage contact mismatch.

It has been proposed that in granular superconductors the current flows through complex paths formed by a network of junctions connecting the grains (Maury *et al.* 1990). The critical current density of this array of weak links is dependent on the alignment of the grains (Kumakura *et al.* 1989 and Deutscher, 1988) and the presence of connecting material between the grains (Dimos *et al.* 1990). Texturing increases the grain alignment which increases the grain boundary critical current density J_J (Ekin, 1987).

As the x-ray (figure 23) and scanning electron microscopy (figure 24) demonstrate, the diffusion grown thick films are characterized by considerable granularity (see also Ummat et al. 1991). The nature of this granularity is different in the two branches. From the x-ray diffraction the lower branch is more textured. One can see from the scanning electron micrographs that the lower branch along with

greater grain alignment also has higher quality growth with its larger grains and fewer grain boundaries. This suggests, in light of Tinkham and Lobb's (1989) dual superconducting transition, that the upper branch may have an apparent lower T_c due to the morphology of its grain structure. The presence of more grain boundaries, unaligned grains and possibly larger regions of undiffused material (Tachikawa *et al.* 1990 and Ummat *et al.* 1991) may result in a lower intergranular superconducting transition. Regions of lower T_c and a lower intergranular superconducting transition may suppress the entire superconducting transition.

The effect of a magnetic field on the longitudinal voltage, V_L, transition is shown in figure 26. The application of a magnetic field parallel to the c axis results in the onset of dissipation at a lower temperature than that for the H⊥c case for single crystals (Palstra *et al.* 1988). The preferred a-axis orientation implies that the c axis lies preferentially in the plane of the thick film, i.e. c⊥n. Therefore, with H⊥n, H and c are in the same plane and there is an increased broadening of the resistive transition compared with H∥n. This observation supports our x-ray data presented in figure 23.

The effect of a magnetic field on the magnitude and temperature of the voltage minimum is demonstrated in figure

27 for H∥n. *Intragranular* and *intergranular* broadening of the resistive transition in a magnetic field result in the onset of V_T at lower temperatures due to the earlier onset of dissipation in both branches. The reduced current carrying capacity of the lower branch relative to the upper branch results in the reduced size of the minimum in V_T. For a magnetic field increasing at a fixed temperature, differences between the resistances in the two branches become smaller due to resistive broadening in a magnetic field. From equation 22 it can be seen that this results in a decrease of $\mathfrak{R}$ with a corresponding decrease in V_T.

The parallel path available to the applied transport current in a potentiometric ring and the different temperature dependence of the resistance in each of the paths must be considered in describing V_T. The current in each branch depends on the relative resistances of the branches. In the transition region, there can be a relatively large difference in the resistance and the current in the branches for a small difference in the properties of the branches. That is, a difference in T_c and J_c (particularly the intergranular J_c's) affects the current distribution and V_T. Thus, V_T is very sensitive to small differences. In terms of the transverse voltage, applied current and resistances the current through the upper branch for example can be expressed as

$$I_U = \frac{V_T - R_{1L} I}{(R_{1U} - R_{1L})}. \qquad (23)$$

It is difficult to express all dependencies in the above equation, since, as will be shown, the resistances and V_T also have a current dependence.

Pureur *et al.* (1991) have indicated that weak link Josephson junctions capable of supporting small supercurrents are no longer able to do so when the current is increased. When the critical current I_c of a junction is exceeded dissipation occurs and a junction voltage is produced. In the critical region the lower branch is carrying a greater current density since it experiences less dissipation. An increase in the applied transport current increases the dissipation in the lower branch since fewer junctions can carry the increased current density nondissipatively. Again the current carrying capacity of the lower branch has been reduced with a resultant decrease in the measured V_T. This is observed in the results on the current dependence of the minimum as depicted in figure 28.

The granular nature of the thick film investigated here resulting in a current dependent resistance as shown in figure 32, results in a current dependent V_T as well. This was seen for V_T in figure 28. When we consider only the current dependence of R_U a first order expression is

$$R_U = R_{UO} + (dR_U/dI_U)\ I_U, \qquad (24)$$

where R_{UO} is the current independent contribution to the resistance, I_U is the current through the upper branch and dR_U/dI_U is the rate of change of R_U with respect to current or slope at that temperature. Applying Kirchhoff's laws and the loop equations and applying the equivalent of equation 24 for the lower branch V_T can be written in terms I_U as

$$V_T = (dR_U/dI_U - dR_L/dI_L)\ I_U^2 + (R_{UO}+R_{LO}-R_{2U}-R_{2L}+2(dR_L/dI_L)I)\ I_U - (R_{LO}-R_{2L}+(dR_L/dI_L)I^2), \quad (25)$$

where R_{LO} is the ohmic contribution to the resistance in the lower branch and dR_L/dI_L is the derivative of the resistance in the lower branch with respect to the current through the lower branch. Equation 25 describes the effect that changing the current has on the measured value of V_T. As discussed in the previous chapter the value of $d\rho/dJ$, and, therefore dR/dI, has a current dependence. Therefore, from equation 25 it can be seen that V_T will also have a current dependence.

The difference in V_T as a function of temperature for the two 0.5 T field orientations as shown in figure 29 results from the more textured nature of the lower half compared to the upper half. With H$\|$n, the magnetic field is perpendicular to the c axis in the a-oriented grains. This results in less broadening of the resistive transition within the crystallites than with H$\|$c (Palstra *et al.*, 1988). For H$\|$n the magnetic field lies parallel to a larger portion of c-axis

components in the platelets. That the minimum of V_T occurs at a lower temperature for H⊥n than for H∥n reflects the greater broadening observed for the applied magnetic field in the H⊥n orientation.

The anisotropic effect of H∥n and H⊥n on $V_T(T)$ is demonstrated by the dependence of the area between V=0 and $V_T(T)$ on magnetic field in figure 30. The advantage of the lower branch to carry a larger current density than the upper branch is clearly reduced with the application of a magnetic field. Because of texturing, this reduction is much greater for H⊥n. The presence of texturing indicates the presence of intrinsic components in the resistive broadening. The decay of the area between $V_T(T)$ and V=0 occurs for both field orientations as a decreasing exponential function of field. This suggests, as in the crystal case, that the field projected into the CuO_2 layers is the only angular dependent dissipative mechanism in the textured thick film.

I-V curve measurements on the 76 μm thick sample demonstrate the nonohmic current dependence of the voltage. This is shown in figure 32. Observation of a nonohmic current dependence confirms an earlier statement concerning the presence of Josephson weak links in the lower branch resulting in a current dependence of the measured V_T.

An upward shift in the temperature at the peak, T_p, of the $d\rho/dT$ curve after the application of a magnetic field was

in a current dependence of the measured V_T.

An upward shift in the temperature at the peak, T_p, of the $d\rho/dT$ curve after the application of a magnetic field was observed in separate measurements of the resistivity on portions of the 76 μm and 120 μm branches. Since the thick films are also polycrystalline, this is consistent with the superposition of the *intergranular* and *intragranular* superconducting transition model discussed in the previous chapter.

The potentiometric ring technique has several advantages when the variation of parameters on a sample is to be considered. First, the technique is sensitive to differences in T_c and critical current between the two branches, particularly in the critical region. Secondly, only one sample is considered and, therefore, problems of experimental control associated with more than one sample are avoided. Specifically, it may be difficult to avoid different conditions for sample preparation and different experimental conditions for the same measurement on different samples. In our experiment for example, only the parameter of thickness of the bismuth slurry was varied. This technique could be carried out on thin films before and after radiation damage had been performed on one of the branches.

E. CONCLUSION

In summary; measurements of the temperature dependence of the transverse voltage of a textured thick film ring indicated a negative voltage minimum and change of voltage sign in the critical region of the sample's bulk superconducting transition. The application of a magnetic field shifted this negative voltage minimum to lower temperatures and reduced its magnitude. Anisotropy in the temperature dependence of the transverse voltage between a field oriented parallel to the substrate normal and one oriented perpendicular to it, was observed. These results were consistent with a higher T_c and greater texturing in the thinner branch of the ring as determined by separate resistivity measurements, x-ray diffraction and scanning electron micrographs of portions of the branches.

CHAPTER VIII

GENERAL CONCLUSION

The resistance in magnetic fields up to 1.7 T of members of the family of bismuth based high temperature superconductors was investigated for current densities between 0.03 A/cm^2 and 3.0 A/cm^2. The samples included two $Bi_2Sr_2CaCu_2O_x$ single crystals, two Sn doped and two Sb doped BiPbSrCaCuO polycrystalline samples and a diffusion grown $Bi_2Sr_2CaCu_2O_x$ thick film patterned into a ring with branches 120 μm and 76 μm thick.

The resistivity of the $Bi_2Sr_2CaCu_2O_x$ single crystals below T_c was described by the thermally activated flux flow of two dimensional vortices. The thermally activated flux flow expression $\rho=\rho_o U/T \exp(-U/T)$ was fit to the data applying a temperature dependence for the activation energy, U with the form $U=U_o(1-(T/T_c)^2)^{3/2}$ as suggested by Malozemoff *et al.* (1989). The activation energy depended on the projected field $H_\perp=H\sin\theta$, $U\propto(H\sin\theta)^{-\alpha}$ where $\alpha\approx1/3$. The prefactor was consistent with the Bardeen Stephen result for flux flow resistivity due to motion of vortices in an applied magnetic field and also demonstrated a projected field dependence. These results show that dissipation in $Bi_2Sr_2CaCu_2O_x$ single crystals in a magnetic field results from the motion of two-

dimensional vortices whose density is given by $H_{\perp}$, in the CuO_2 planes. Furthermore, the activation energies associated with thermally activated flow of these vortices also have a projected field dependence.

The intergranular superconducting transition due to the presence of weak links was investigated in two Sn-doped and two Sb-doped $Bi_{1.7}Pb_{0.3}Sr_2Ca_2Cu_3O_y$ samples by the measurement of the resistivity and current dependent resistivity in an applied magnetic field. A comparison of the magnitude of their zero field resistive tails and T_c^0, the temperature at which the resistivity went to zero, determined a range of weak link strengths that characterized each sample. Samples with a larger resistive tail and lower T_c^0 were characterized as having weak links with lower critical currents and critical temperatures in the transport current path. These samples also demonstrated greater broadening in a magnetic field. An analysis of the $d\rho/dT$ curve in a magnetic field identified a broad maximum or hump in the polycrystalline results that was not present in a single crystal $d\rho/dT$ curve in a magnetic field. This broad hump or maximum was identified with the presence of an *intergranular* superconducting transition superimposed upon the *intragranular* superconducting transition. The feature attributed to the intergranular transition was found to be strongly suppressed with the

application of a magnetic field. Samples with lower T_c and I_c weak link characteristics demonstrated a suppression to lower temperatures of this feature in agreement with the greater broadening of the resistive transition in a magnetic field observed in these samples. The current dependence of the resistivity, associated with the presence of weak links, was confirmed with the samples for which resistivity as a function of current was measured. An investigation of $d\rho/dJ$ as a function of temperature in zero field demonstrated the presence of a range of weak link strengths. A similar distribution was observed in the current dependent resistivity as a function of magnetic field at 77 K. This provided further evidence for the presence of an intergranular transition in an applied magnetic field, with smaller applied fields required to decouple superconducting grains in samples characterized by lower T_c and I_c weak link characteristics.

In the potentiometric ring experiment, measurements were performed to elucidate results that could be obtained from the measurement of a transverse voltage in the critical region of an inhomogeneous sample. The transverse voltage, the voltage in the centre of one 120 μm thick branch with respect to the voltage in the centre of the other 76 μm thick branch was measured in magnetic fields ranging from 0 to 1.6 T applied parallel and perpendicular to the sample surface. Below the critical temperature results indicated a transverse

voltage that was negative with respect to its value in the normal state. The transverse voltage displayed a negative voltage minimum in the critical region of the superconducting transition. The application of a magnetic field suppressed the voltage minimum in temperature and reduced its magnitude. This suppression was stronger for the field oriented parallel to the substrate surface than perpendicular to it. These results were consistent with separate resistivity measurements in zero field that indicated a $d\rho/dT$ peak temperature, T_p of 77.7±0.2 K in the 120 μm thick branch compared with a T_p of 80.7±0.1 K in the 76 μm thick branch and were also consistent with x-ray and scanning electron micrography that demonstrated that the 76 μm branch had greater texturing and larger grains.

BIBLIOGRAPHY

Anderson, P. W., Phys. Rev. Lett. 9, 309 (1962).

Anderson, P.W., and Kim, Y.B., Rev. Mod. Phys. 36, 39 (1964).

Antognazza, L., Brunner, O., Mieville, L., Triscone, J.-M., and Fischer, O., Physica C, 185-189, 2081 (1991).

Bardeen, J., and Stephen, M.J., Phys. Rev. 140, A1197 (1965).

Batlogg, B., Palstra, T.T.M., Schneemeyer, L.F., Dover, R.B. van, and Cava, R. J., Physica C, 153-155, 1062 (1988).

Beek, C. J. van der, and Kes, P. H., Phys. Rev. B, 43, 13032 (1991).

Beyers, R., and Shaw, T. M., in *Solid State Physics Vol. 42, The structure of* $Y_1Ba_2Cu_3O_{7-\delta}$, edited by Ehrenreich, H. and Turnbull, D., (Academic Press, Boston, 1989), p. 135.

Bolle, C. A., Gammel, P. L., Grier, D. G., Murray, C. A., and Bishop, D. J., Phys. Rev. Lett. 66, 112 (1991).

Brandt, E.H., Int. J. Mod. Phys., B5, 751 (1991).

Briceno, G., Crommie, M. F., and Zettl, A., Phys. Rev. Lett. 66, 2164 (1991).

Chu, C. W., Bechtold, J., Gao, L., Hor, P. H., Huang, Z. J., Meng, R. L., Sun, Y. Y., Wang, Y. Q., and Xue, Y. Y., Phys. Rev. Lett. 60, 941 (1988).

Clem, J. R., Phys. Rev. B 43, 7837 (1991).

Deutscher, G., Physica C 153-155, 15 (1988).

Deutscher, G., Y. Imry and L. Gunther, Phys. Rev. B 10, 4598, (1974).

Dew-Hughes, D., Cryogenics, 28, 674 (1988).

Dimos, D., Chaudhari, P., and Mannhart, J., Phys. Rev. B 41, 4038 (1990).

Ekin, J. W., Braginski, A. I., Panson, A. J., Janocko, M. A., Capone II, D. W., Zaluzec, N. J., Flandermeyer, B., Lima, de O. F., Hong, M., Kwo, J., and Liou, S. H., J. Appl. Phys. 62, 4821 (1987).

Farrell, D. E., Bonham, S., Foster, J., Chang, Y. C., Jiang, P. Z., Vandervoort, K. G., and Kogan, D. J., Phys. Rev. Lett. 63, 782 (1989).

Fehrenbacher, R., Geshkenbein V. B., and Blatter, G., Phys. Rev. B 45, 5450 (1992).

Geshkenbein, V., Larkin, A., Feigel'man, M., and Vinokur, V., Physica C, 162-164, 239 (1989).

Goldschmidt, D., Phys. Rev. B, 39, 2372 (1989).

Gor'kov, L. P., and Kopnin, N. B., Sov. Phys. Usp. 18, 496 (1976).

Gridin, V. V., Krause T. W., and Datars, W. R., J. Appl. Phys. 68, 675 (1990).

Gridin, V. V., and Datars, W. R., Phys. Rev. B 43, 3675 (1991).

Guo, S. J., Easterling, K. E., Dou, S. X., and Liu, H. K., J. Crys. Growth, 100, 303 (1990).

Huang, Y. T., Shei, C. Y., Wang, W. N., Chiang C. K., and Lee, W. H., Physica C 169, 76 (1990).

Imry, Y., in *Inhomogeneous Superconductors - 1979, AIP Conference Proceedings No. 58, The Phase Transition in Josephson Junction Arrays, edited by Gubser, D. U., Francavilla, T. L., Wolf, S. A. and Leibowitz, J. R.,* (American Institute of Physics, New York, 1980), p. 141.

Iye, Y., Nakamura, S., and Tamegai, T., Physica C, 159, 616 (1989).

Jin, S., Tiefel, T. H., Sherwood, R. C., Davis, M. E., Dover, R. B. van, Kammlott, G. W., Fastnacht, R. A., and Klien, H. D., Appl. Phys. Lett., 52, 2074 (1988).

Jones, E. C., Christen D. K., Klabunde, C. E., Thompson, J. R., Norton, Feenstra, R., Lowndes, D. H., and Budai, J. D., Appl. Phys. Lett. 59, 3183 (1991).

Kes, P. H., Physica C, 185-189, 288 (1991).

Kes, P. H., Aarts, J., Berg, J. van den, Beek C. J. van der, and Mydosh, J. A., Supercond. Sci. Technol. 1, 242 (1989).

Kes, P. H., Aarts, J., Vinokur, V. M., and Beek, C. J. van der, Phys. Rev. Lett. 64, 1063 (1990).

Kes, P. H., and Berg, J. van den, in *Studies of High Temperature Superconductors Vol. 15, Flux Pinning and Thermally Activated Depinning in Single Crystals of High Temperature Superconductors*, edited by Narilakar, A., (Nova Science Publishers, New York, 1990), p. 83.

Kim, D. H., Gray, K. E., Kampwirth, R. T., Smith, J. C., Richeson, D. S., Marks, T. J., Kang, J. H., Talvacchio, J., and Eddy, M., Physica C, 177, 431 (1991).

Klee, M., Vries, J.W.C. De, and Brand, W., Physica C, 156, 641 (1988).

Koshelev, A. E., Logvenov, G. Y., Larkin, V. A., Ryazanov, V. V. and Soifer, K. Y., Physica C, 177, 129 (1991).

Kosterlitz J.M. and Thouless D. J., J. Phys. C 6, 1181 (1973).

Kumakura, H., Togano, K., Maeda, H., and Yanagisawa, E., Physica C 162-164, 685 (1989).

Li, J.N., Kadowaki, K., Menken, M.J.V., Huang, Y.K., Bakker, K., Menovski, A.A., and Franse, J.J.M., Appl. Phys. A 48, 193 (1989).

Likharev, K. K., Rev. Mod. Phys. 51, 101 (1979).

Maeda, M., Tanaka, Y., Fukutomi, M., and Asano, A., Jpn. J. Appl. Phys. 27, L209 (1988).

Malozemoff, A. P., Worthington, T. K., Zeldov, E., Yeh, N. C., McElfresh, M. W., and Holtzberg, F., in *Strong Correlation and Superconductivity, Fluc Creep and the Crossover to Flux Flow in the Resistivity of High-T_c Superconductors*, edited by Fukuyama H., Maekawa, S., and Malozemoff, A. P., (Springer-Verlag, Berlin, 1989), p.349.

Mandal, P., Poddar, A., Das, A. N., Ghosh B., and Choudhury, P., Physica C, 169, 43 (1990).

Martin S., Fiory A. T., Flemming R. M., Espinosa G. P., and Cooper A. S. Phys. Rev. Lett. 62, 677 (1989).

Maury, R., Fert, A. R., Redoules, J. P., Ayache, J., Sabras, J., and Monty, C., Physica C 167, 591 (1990).

Michel, C., Herieu, M., Borel, M. M., Grandin, A., Deslandes, F., Provost, J., and Raveau B., Z. Phys. B 68, 421 (1987).

Nkum R. K., private communication

Nkum R. K., and Datars, W. R., Phys. Rev. B 44, 12516 (1991).

Nkum R. K., and Datars W. R., Physica C 190, 465 (1992).

Okuda, K., Kawamata, S., Noguchi, S., Itoh, N. and Kadowaki, K., J. Phys. Soc. Jap. 60, 3226 (1991).

Palstra, T. T. M., Batlogg, B., Schneemeyer, L. F., and Waszczak, J. V., Phys. Rev. Lett. 61, 1662 (1988).

Palstra, T. T. M., Batlogg, B., Dover, R. B. van, Schneemeyer, L. F., and Waszczak, J. V., Phys. Rev. Lett. 63, 1511 (1989); T. T. M.

Pellam, G., Dousselin, G., Cortes, H., and Rosenblatt, J., Solid State Comm. 11, 427 (1972).

Pureur, P., Schaf, J., Gusmão M. A. and Kunzler, J. V., 176, 357 (1991).

Ramesh, R., Thomas, G., Green, S.M., Mei, Y., Jiang, C., and Luo, H.L., Appl. Phys. Lett. 53, 1759 (1988).

Svoboda, P., Vašek, P., Smrčková, O., and Sýkorová, D., Physica C, 167, 188 (1990).

Tachikawa, K., Watanabe, T., and Inone, T., Supercond. Sci. Techno. 3, 180 (1990).

Tarascon, J. M., McKinnon, W. R., Barboux, P., Hwang, D. M., Bagley, B. G., Greene, L. H., Hull, G. W., and LePage, Y., Phys. Rev. B, 38, 8885 (1988).

Tinkham, M., *Introduction to Superconductivity*, (McGraw-Hill, NewYork, 1975) (reprinted by Krieger, Malabar, FL, 1980).

Tinkham, M., Phys. Rev. Lett. 61, 1658 (1988).

Tinkham M., and Lobb, C. J., *Solid State Physics Vol. 42, Physical Properties of the New Superconductors*, edited by Ehrenreich, H. and Turnbull, D., (Academic Press, Boston, 1989), p. 91.

Thuneberg, E. V., Cryogenics, 29, 236 (1989).

Ummat, P. K., Krause, T. W., and Datars, W. R., J. Appl. Phys. 69, 4017 (1991).

Yeshurun, Y., and Malozemoff, A. P., Phys. Rev. Lett. 60, 2202 (1988).